E-787 TN-XXX
January 29, 2002

1998 $\pi\nu\bar{\nu}(1)$ Data Analysis

Paul Bergbusch, Shaomin Chen, Jingliang Hu,
Akira Konaka, Joseph Mildenberger

TRIUMF
4004 Wesbrook Mall, Vancouver, B.C., Canada, V6T 2A3

Abstract

The current state of the 1998 data analysis is summarized, including descriptions of the cuts, background levels, and acceptance based on analyses of the "1/3" data sample. The estimated total backgrounds for the 1998 data set are found to be as low or lower in all areas as the combined 1995–97 data, which is of comparable size.

Contents

Abstract **1**

Table of Contents **3**

List of Figures **5**

List of Tables **8**

1 Correction for kinematic variables **9**
- 1.1 Variation of momentum measurement . . . 9
- 1.2 Magnetic field measurement . . . 9
- 1.3 Pion kinetic energy deficit . . . 10
- 1.4 Monte Carlo simulation . . . 12
- 1.5 Dip angle correction . . . 13

2 Kinematic background estimate from 2/3 1998 data **16**
- 2.1 The application of safety cuts . . . 16
  - 2.1.1 UTC-RSSC matching . . . 16
  - 2.1.2 UTC xy hits . . . 16
  - 2.1.3 Track overlapping in UTC . . . 16
- 2.2 $K_{\mu 2}$ background . . . 17
  - 2.2.1 Anomaly of $K_{\mu 2}$ background in 2/3 sample . . . 17
  - 2.2.2 $K_{\mu 2}$ background estimate . . . 17
- 2.3 $K_{\pi 2}$ background estimate . . . 19

3 $K_{\mu 2}$ background function for 1998 **19**
- 3.1 $K_{\mu 2}$ tail function . . . 21
- 3.2 $K_{\mu 2}$ band function . . . 23

4 $K_{\pi 2}$ background function for 1998 **25**

5 Outside-The-Box Studies **27**
- 5.1 Correlation Studies . . . 27
  - 5.1.1 $K_{\pi 2}$ Correlation Study . . . 27
- 5.2 $K_{\mu 2}$ Range-Tail Correlation Study . . . 30
- 5.3 Muon-Band Correlation Study . . . 32
- 5.4 Beam Correlation Study . . . 34
- 5.5 Search for Single-Cut Failures . . . 34
  - 5.5.1 PV . . . 37
  - 5.5.2 $K_{\pi 2}$ Kinematics . . . 38
  - 5.5.3 TD . . . 38
  - 5.5.4 $K_{\mu 2}$ Kinematics . . . 39
  - 5.5.5 Beam . . . 39

6 Opening the BOX **40**

7 The candidate event **42**
7.1 Event display 42
7.2 TD pion identification 42
7.3 E/P/R calibrations in the vicinity of the candidate event 42
7.4 Basic information about this candidate 42
7.5 Scalers 42
7.6 Probability of signal 42
7.6.1 Reconstruction quantities 46
7.6.2 Kaon identification 47
7.6.3 Pion identification 47
7.6.4 Single particle identification 47
7.6.5 Probability of signal 47
7.7 Possibility of being a CEX background 58
7.8 Kinematic variable positions inside the BOX 58

8 K_{Blive} of 1998 **63**

9 Acceptance of 1998 data **63**
9.1 $K_{\mu 2}$-based acceptance 63
9.2 $K_{\pi 2}$-based acceptance 65
9.3 π_{scat}-based kinematic acceptance 65
9.4 π_{scat}-based TD acceptance 67
9.5 μ-veto accidental loss 67
9.6 $T \cdot 2$ efficiency 70
9.7 UMC based acceptance 71

10 f_s measurement **71**

11 Measurement of the $K_{\pi 2}$ branching ratio **73**

12 Sensitivity of 1998 data **73**

13 $\pi^+\nu\bar{\nu}$ Acceptance for the paper **78**

14 $K^+ \to \pi^+ f$ branching ratio **78**

15 Statistical Analysis of the $K^+ \to \pi^+\nu\bar{\nu}$ Branching Ratio **80**
15.1 Definition of Signal/Noise Cells 80
15.2 Likelihood Estimator and Analysis 83

List of Figures

1 a) Variation of the average magnetic field in every eight runs as a function of run number in 1998 data. b) The pion momentum with $B_0 = 10\ k$G in the UTC reconstruction as a function of actual magnetic field in 1998 $K_{\pi2}$ data. 10
2 a) The magnetic field variation as a function of run number. b) The magnetic field variation as a function of spill record in a problematic run. 11
3 Left: The pion momentum as a function of recorded magnetic field in 1998 $K_{\pi2}$ monitor data. The momentum drift in smaller magnetic fields comes from the fake $\mathbf{B}_0$ measurement. A slight increase of momentum is also observed in the larger magnetic field, indicating a necessary fine calibration. Right: The pion momentum using the final calibrated magnetic field in 1998 $K_{\pi2}$ monitor data. No correlation between the momentum and the actual magnetic field is observed since the field variation is absorbed in deriving the momentum. . . 11
4 Comparisons of momentum, range and kinetic energy between $K_{\pi2}(1)$ data and Monte Carlo. Samples are selected by applying cuts given in Table 2. . 14
5 The pion momentum resolution as a function of used xy hits in the first super layer (left), the second super layer (middle) and third super layer (right). . 17
6 Event display with an additional track (indicated by green color circles) very close to the studied one (displayed by red color circles). 18
7 The ratio of N(obs.) over N(RP) Rej(E) are shown at the top of plots. Comparison between the expected and observed $K_{\pi2}$ background is shown at the bottom of plots in linear and logarithmic scales separately. 20
8 Momentum distribution for $K_{\mu2}$ tail events with no scattering cuts but with the χ_{rm} cut and the upper ERBOX cuts (histogram). $K_{\mu2}$ peak events with no scattering cuts but with a cut on range greater than 50 cm (black dots). 21
9 χ_{rm} distribution for $K_{\mu2}$ band events with all cuts applied except for the **RS_LIKE, RS_DEDX, RS_CHIMAX** and upper RBOX cuts (histogram) and with all cuts applied except for the upper RBOX cut (black dots). . . . 23
10 Range vs. kinetic energy distribution for 1998 $K^+ \rightarrow \pi^+\nu\bar{\nu}$ data set with all cuts applied except for the cuts on range and kinetic energy. The box enclosing the signal region contains a single candidate event. 41
11 Event display in xy and z views 43
12 Event display: TDC(left) and ADC(right) 44
13 Event display: target plot(left) and RS plot(right) 44
14 TD pulse shapes and fitting in the stopping counter. 45
15 Kinetic energy, range and momentum for $K_{\mu2}$ monitor and skim1 $K_{\pi2}$ events in RUN 37443. 45
16 KB, Teff and CK scaler distributions. 47
17 Quantities related to the timing consistency. 48
18 Quantities related to target kaon reconstruction. 49
19 Quantities related to target/IC pion reconstruction. 50
20 Quantities related to UTC/target reconstruction. 51
21 Quantities related to Range Stack reconstruction. 52
22 Quantities related to kaon particle identification. 53
23 Quantities related to pion particle identification from kinematic variables. . . 54

24 Quantities related to pion particle identification from TD variables. 55
25 Quantities related to the detection of photon activities. 56
26 Quantities related to single beam detection. 57
27 Probability of signal. 59
28 Examination of the possibility being a CEX background. 60
29 The scatter plots for the kinematic variable deviations from the $K_{\pi 2}$ peaks. Lower box cut positions are indicated by the solid lines. 61
30 The scatter plots for the kinematic variables. Upper box positions are indicated by the solid lines. 62
31 The pion lifetime spectrum. The fit is performed with 1-parameter N_A fit (top) and 2-parameter t_π and N_A fit (bottom) separately. 70

List of Tables

1 The measured muon and pion momenta from $K_{\mu 2}$ and $K_{\pi 2}$ monitor data in different years. Since the dip angle cut applied reduces the longitude momentum contribution, the momenta in this table are regarded as full transverse momenta and the expected magnetic field for different years are obtained by comparing to the known momentum values. 9
2 Selection criteria for $K_{\pi 2}(1)$ monitor data and Monte Carlo sample separately. 13
3 The peak positions and sigmas of momentum, range and kinetic energy for both $K_{\pi 2}(1)$ data and Monte Carlo, as also shown in Fig. 4. 13
4 Dip angle (cos3d) dependence of the peak positions and sigmas for range, kinetic energy and momentum. Correction are applied for data and MC sample separately. For data, the first order correction is from $K_{\pi 2}(1)$ monitor sample, and the second order correction is from skim1 sample. 15
5 $K_{\mu 2}$ background estimate. 19
6 $K_{\mu 2}$ tail function obtained from first bifurcation sample (outside the BOX) and from second bifurcation sample (inside the BOX). The background level has been normalized to the departure point. 22
7 $K_{\mu 2}$ band function obtained from first bifurcation with loose scattering cuts. The background level has been normalized to the departure point. 24
8 $K_{\pi 2}$ background function. The background level has been normalized to the departure point. 26
9 Complete listing of cuts applied in the analysis, (except the pileup and UTC safety cuts), divided into cut classes. 27
10 Predicted and observed numbers of $K_{\pi 2}$ background events in the 2/3 1998 data sample. 28
11 Events observed in the $K_{\pi 2}$ correlation study. 29
12 Predicted and observed numbers of $K_{\mu 2}$ range-tail background events in the 2/3 1998 data sample. 31
13 Events observed in the $K_{\mu 2}$ range-tail correlation study. 32
14 Predicted and observed numbers of muon-band background events in the 2/3 1998 data sample. 33
15 Events observed in the muon-band correlation study. 33
16 Predicted and observed numbers of beam background events in the 2/3 1998 data sample. 35
17 Events observed in the single-beam kaon-entering correlation study. 36
18 Events observed in the single-beam pion-entering correlation study. 36
19 Basic information about this candidate 46
20 The total K_{Blive} values for $\pi\nu\bar{\nu}$, $K_{\mu 2}$ and $K_{\pi 2}$. 63
21 $K_{\mu 2}$-based acceptances for the $\pi\nu\bar{\nu}$ analysis. All setup cuts are defined in Table 22. DELCO2 is defined as a 2ns delay conincidence. 64
22 Setup cuts used in the $K_{\mu 2}$-based acceptance measurement shown in Table 22. PV(noBV) is the pass3 PV for all detector subsystems except for BV. KM2PBOX is a 2σ cut on the $K_{\mu 2}$ momentum. 65

23 $K_{\pi 2}$-based acceptances for the $\pi^+\nu\bar{\nu}$ analysis. OPSCUT_LKB is not applied to the 1995 data. SETUP$_{ops}$ includes BAD_RUN, BAD_STC, TRIGGER, pass1 reconstruction, beam and kinematic cuts (except those whose acceptances are being measured here), photon energy in BV+EC+RD> 200 MeV, all TD cuts except TDECON, TDVEL and those which require electron information ($K_{\pi 2}(2)$ monitors do not have extended TD time information), and a 2σ cut on the $K_{\pi 2}(2)$ range, energy and momentum. SETUP_tgkin is SETUP_ops plus OPSVETO, OPSVETO_LKB and TGPVCUT. 66

24 π_{scat}-based kinematic acceptances for the $\pi\nu\bar{\nu}$ analysis. Acceptances from both fixed cuts and neutral network cut are presented. Errors are statistical only. SETUP_PISCAT includes BAD_RUN, BAD_STC, all pass1 cuts, b4abm2 < 1.3, $\mid t_\pi - t_{rs} \mid < 5$ ns, ICBIT, $\mid t_{IC} - t_{RS} \mid < 5$ ns, TARGF, DTGTTP, RTDIF, TGQUALT, TGZFOOL, BHTRS, CKTRS, CKTAIL, photon veto in the stack only, all TD cuts, cos3d and LAYV4. The final box is defined by Rdev > 2.7, range < 40 cm, Edev > 2.35, kinetic energy < 135 MeV Pdev > 2.5 and momentum < 229 MeV/c. "Small" box is defined by Rdev > 4.0, range < 38.8 cm, Edev > 3.0, kinetic energy < 131 MeV, Pdev > 5.0 and momentum < 222.2 MeV/c. "Large" box is defined by Rdev > 2.0, range < 41.2 cm, Edev > 1.0, kinetic energy < 139 MeV, Pdev $> 0.$ and momentum < 235.8 MeV/c. 68

25 π_{scat}-based TD acceptances for the $\pi^+\nu\bar{\nu}1$ analysis. A_TD is an average of A_TD_1 and A_TD_2, in which A_TD_2 is scaled by a factor of 1.014 to account for pion absorption and decay-in-flight. The final A_TD include statistical error (100% correlated) and systematic error (use the difference between A_TD_1 and A_TD_2 and divide it by two). The total TD acceptance includes the FITPI acceptance as calculated in the counting method. SETUP_TD_1 is the same as SETUP$_{\pi_{scat}}$ in Table 24, with BOX, LAYV4, RNGMOM, ZFRF, ZUTOUT LAYER14 and EICKIN, but without the TD cuts. SETUP_TD_2 is SETUP_TD_1 with CL_RSDEDX, CHIMAX PR_RF and PR_RFZ1 also applied. 69

26 Accidental induced acceptance of the trigger muon veto. 69

27 $T \cdot 2$ efficiencies for $K_{\mu 2}$, $K_{\pi 2}$, $\pi^+\nu\bar{\nu}$ and $\pi^+ f$. 70

28 UMC $K_{\mu 2}$ acceptance of cuts applied in the f_s analysis. 71

29 UMC $K_{\pi 2}$ acceptance of cuts applied in the $K_{\pi 2}$ branching ratio analysis. . 72

30 The $\pi\nu\bar{\nu}$ and πf trigger acceptances in 1998 data. 72

31 The $\pi\nu\bar{\nu}$ and πf fiducial acceptances in 1998 data. For $\pi\nu\bar{\nu}$, BOX 1 is defined as the upper BOX cut and BOX 2 is defined as the lower BOX cut. For πf, BOX 1 is defined as both lower and upper BOX cuts and BOX 2 is defined by requiring $35.5 \leq$ range ≤ 40 cm, $120 \leq$ kinetic energy ≤ 135 MeV and $221 \leq$ momentum ≤ 229 MeV. 73

32 Cuts applied in the f_s analysis. RTOT40 requires range > 40 cm to remove some $K_{\pi 2}$ and radiative $K_{\mu 2}$ not removed by PV(noBV). 74

33 $K_{\mu 2}$-based acceptances of cuts applied in the f_s analysis. The SETUP cuts are defined in Table 22. SETUP_BAD is ICBIT. 75

34 Cuts applied in the $K_{\pi2}$ BR analysis. KP2BOX is a 3σ cut on the KPI2 range, energy and momentum. KP2STOP requires the stopping layer to be between layers 8 and 15 inclusive. 76
35 $K_{\pi2}$-based acceptances of cuts applied in the Kp2 BR analysis. The FITPI acceptance is measured using piscat (counting method) similar to the pi nu nubar measurement of FITPI acceptance, except that here the piscat are selected using KP2BOX and KP2STOP instead of BOX and LAYV4. The SETUP are defined in Table 22, except that all SETUP here include the requirement of at least 200 MeV of photon energy in BV+EC; $120 \leq erd \leq 150$ MeV is replaced by $75 \leq erd \leq 105$ MeV; PV(noBV) is not applied; and KM2PBOX is replaced by KP2BOX, KP2STOP and FITPI. SETUP$_{bad}$ is ICBIT. 77
36 $\pi^+\nu\bar{\nu}$ and $\pi^+ f$ acceptance and sensitivity of the 1998 analysis. 78
37 Definitions for the acceptance categories for the paper. 79
38 $K^+ \to \pi^+\nu\bar{\nu}$ branching ratio limits in different confidence level intervals. . . 86
39 $K^+ \to \pi^+\nu\bar{\nu}$ branching ratio central values, and probabilities that the observed events are due solely to background processes. 86
40 Numbers of observed events and numbers of dA/dN cells used in various calculations of the $K^+ \to \pi^+\nu\bar{\nu}$ branching ratio. 87
41 Number of background events expected in the $\pi^+\nu\bar{\nu}(1)$ signal region. 87
42 $K^+ \to \pi^+\nu\bar{\nu}$ single-event sensitivities of the 1995-7 and 1998 analyses. 87

1 Correction for kinematic variables

1.1 Variation of momentum measurement

From a study of $K_{\mu 2}$ and $K_{\pi 2}$ monitor data, the momentum peak positions are found to increase every year (see Table 1, in which a requirement of $\mid cos3d \mid \leq 0.1$ is imposed to reduce contribution from longitude momentum). Both $K_{\mu 2}$ and $K_{\pi 2}$ monitor data show a consistent increasing trend, which coincide with the decrease of magnetic field observed online. In E787, the magnetic field affects only the transverse momentum as indicated by expression (1)

$$\mathbf{P}_{\perp} = \mathbf{0.29979} \times \mathbf{B_0} \times \mathbf{R}. \tag{1}$$

Where, $\mathbf{R}$ is the radius of charged track curvature in centimeter unit and $\mathbf{B}_0$ is the magnetic field in kG unit. When the magnetic field decreases, the radius $\mathbf{R}$ will increase. A constant $\mathbf{B}_0$ input under this circusmastance will result in an upward variation of momentum measurement. Since the online DAQ system records the magnetic field value for each spill, the recorded decreasing magnetic field should be used as an input. This will compensate the increasing radius $\mathbf{R}$ and resolve the problem of momentum variation.

1.2 Magnetic field measurement

In E787, the magnetic field value is continuously read out for each spill from two Hall probes installed inside the detector. They are both mounted on the inside face of the magnet end plate on the downstream at a radial position close to the barrel photon veto system. The power supply to the magnet is regulated through a shunt in the output current path and is usually subject to temperature and aging effects. It has been noticed that the Hall probes readout drifted downward slowly over the years to about a few per mill lower than the 10 kG designed value. In 1998, the variation of uncalibrated magnetic field shows a clear periodic behavior: gently decreasing from 36030 to 38983 run and quickly jumping up in the rest runs (see Fig. 1). The online log book indicates that there was a power dip occurring in run 38893 which corresponds to the date of October 6, 1998. All high power crates and all magnets tripped at that time. When the power supply was resumed, the magnetic field was observed to have a 0.3% variation (also see Fig. 1.a). A further investigation is also performed to check the coherence between the measured magnetic field and the track momentum reconstructed with a constant 10 kG magnetic field input. Figure 1.b) shows

Year	P_{μ} (MeV/c)	P_{π} (MeV/c)	$B_{exp.}$ (kG)
1995	235.3	205.2	10.002
1996	235.3	205.2	10.002
1997	236.0	205.7	9.975
1998	236.3	206.3	9.954

Table 1: The measured muon and pion momenta from $K_{\mu 2}$ and $K_{\pi 2}$ monitor data in different years. Since the dip angle cut applied reduces the longitude momentum contribution, the momenta in this table are regarded as full transverse momenta and the expected magnetic field for different years are obtained by comparing to the known momentum values.

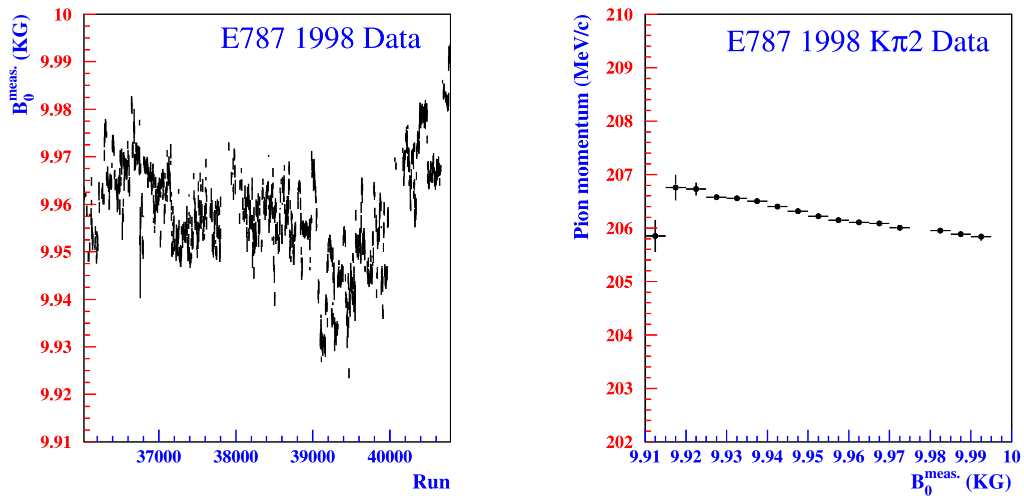

Figure 1: a) Variation of the average magnetic field in every eight runs as a function of run number in 1998 data. b) The pion momentum with $B_0 = 10$ kG in the UTC reconstruction as a function of actual magnetic field in 1998 $K_{\pi 2}$ data.

both an offset and a descent trend of momentum associated with the increasing magnetic field. In present $\pi^+\nu\bar{\nu}$ analysis, online calibrated magnetic field is used in UTC charged track reconstruction. It is seen that the magnetic field recorded may occasionally give a very low value for some spills as shown in Fig. 2.a). Also noted is magnetic field can also vary in a single run (see Fig. 2.b)). In the first order correction, the online uncalibrated magnetic field measurement is first converted in kilo Gauss unit by a factor of 5.071×10^{-3}, which is obtained from the study momentum peak positions in $K_{\pi 2}$ and $K_{\mu 2}$ monitor data. Figure 3.a) shows the pion momentum peak position using measured $\mathbf{B}_0$ as a function of the magnetic field. An improvement is seen. A fine correction is also performed taking into account of the possibility of fake $\mathbf{B}_0$ measurement and the slight dependence between the conversion factor given above and the $\mathbf{B}_0$ measurement. In this analysis, if $\mathbf{B}_0$ measurement deviates from 10 kG by 0.8%, a constant 10 kG is assigned. The correlation between the conversion factor and $\mathbf{B}_0$ is obtained by a linear fit and is applied to the correction. After being applied with all corrections discussed above, the pion momentum is seen nearly independent of the actual magnetic field variation (see Fig. 3).

1.3 Pion kinetic energy deficit

The kinetic energy measurement 105.73 MeV from $K_{\pi 2}$ monitor sample shows about 3 MeV deficit than the expected 108.54 MeV. In previous analysis, this deficit is simply scaled by using both $K_{\pi 2}$ and $K_{\mu 2}$ monitor samples, and this correction is incorrect. New correction is therefore introduced.

In E787, the kinetic energy measurement includes contributions from target (E_{tg}), I-counter (E_{IC}), UTC material (E_{DC}) and Range Stack (E_{RS}), in which E_{DC} is completely from the estimate of UTC inactive material scaled by the dip angle. Majority of E_{RS} is from the sum of ADC from each hit counter, taking into account of the saturation of energy-

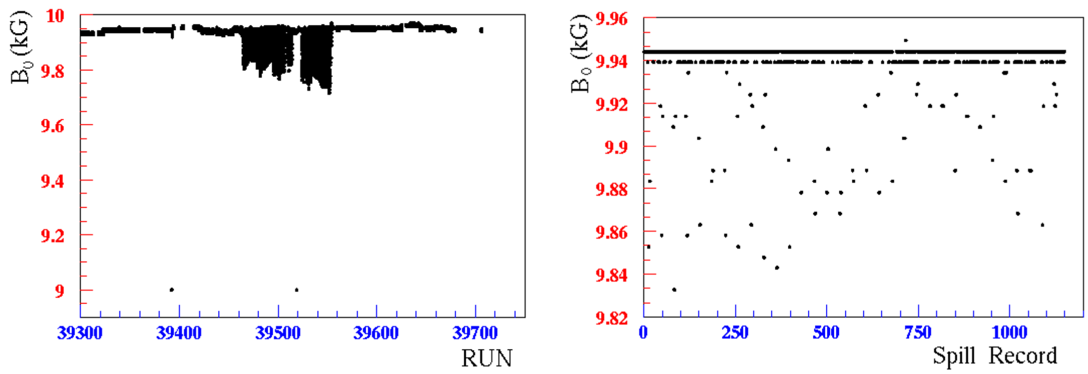

Figure 2: a) The magnetic field variation as a function of run number. b) The magnetic field variation as a function of spill record in a problematic run.

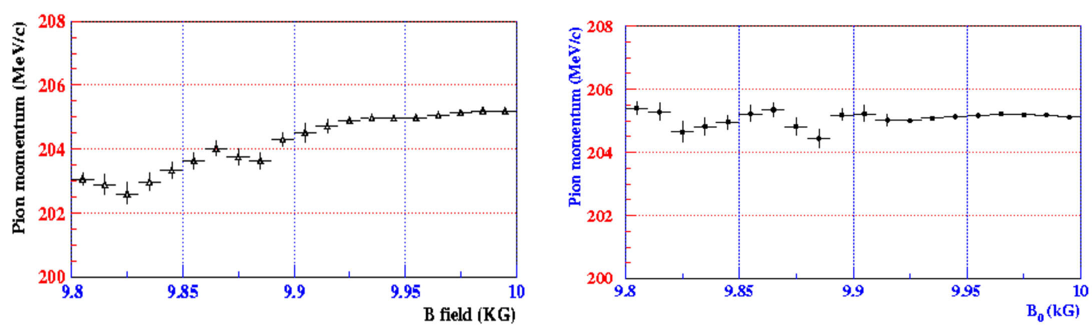

Figure 3: Left: The pion momentum as a function of recorded magnetic field in 1998 $K_{\pi 2}$ monitor data. The momentum drift in smaller magnetic fields comes from the fake $\mathbf{B}_0$ measurement. A slight increase of momentum is also observed in the larger magnetic field, indicating a necessary fine calibration. Right: The pion momentum using the final calibrated magnetic field in 1998 $K_{\pi 2}$ monitor data. No correlation between the momentum and the actual magnetic field is observed since the field variation is absorbed in deriving the momentum.

light relation in the scintillator. Energy loss in inactive Range Stack material is from an estimate of the effective path length. Muon energy from pion decay in the last counter is subtracted. For E_{tg} and E_{IC}, they are directly from measurement of scintillators. There was no correction for pion or muon energy deposit in the kaon stopping fiber, the target edge fibers and inactive material in previous analysis.

To find out the reason why pion kinetic energy has a deficit, a study is conduct to check if the deficit is from target or Range Stack. Theoretically, for $K_{\mu 2}$ and $K_{\pi 2}$ monitor samples, the energy loss before and after UTC is calculable

$$E_{tg+IC}^{theo} = \sqrt{M^2 + P^2} - \sqrt{M^2 + P_{DC}^2}, \tag{2}$$

and

$$E_{RS}^{theo} = \sqrt{M^2 + P_{DC}^2} - M \tag{3}$$

where M is either pion or muon invariant mass, P is the pion or muon momentum when kaon decays at rest and is known to be either 205.14 or 235.53 MeV/c. P_{DC} is the momentum measured by UTC. Tiny UTC inactive material contribution (about 0.2 MeV) is neglected above. Comparisons between the present kinetic energy measurement and the expected values is performed. Since energy measured by the target edge fiber is available, it can be added onto the present E_{tg} measurement if the timing of the corresponding edge fiber is consistent with t_π within 10 ns and the energy is less than 2 MeV.

It is observed that both $K_{\mu 2}$ and $K_{\pi 2}$ samples have about 2 MeV kinetic energy deficit in the target. However, in Range Stack, $K_{\mu 2}$ sample shows a 2 MeV kinetic energy excess, while $K_{\pi 2}$ yields no or very little energy offset, leading to a "correct" full kinetic energy measurement for $K_{\mu 2}$ but a 2 MeV deficit energy measurement for $K_{\pi 2}$. Same energy deficit effect is also seen in Monte Carlo sample. The previous total kinetic energy correction obtained from both $K_{\mu 2}$ and $K_{\pi 2}$ assumes that the energy measurement tends to be correct when the energy going up. This assumption contradicts with the above study and therefore is incorrect. In this analysis, The final total kinetic energy is corrected by adding edge fiber energy and a constant 1.96 MeV for average pion energy deposit in kaon fiber(s). From a study of π_{scat} sample, this correction can make the computed pion mass from momentum and kinetic energy come out at the right position when the kinetic energy is within the $\pi^+\nu\bar{\nu}1$ region.

1.4 Monte Carlo simulation

Monte Carlo simulation adopts the modified UMC version 6.0 with three major changes. First, the UTC wire position resolutions are directly from the UTC calibration file in stead of using a constant 150 μm. Second, the magnetic field value is scaled so that the value at the center of UTC is 10 kG, making the $K_{\mu 2}$ and $K_{\pi 2}$ momentum peaks come out at the right position. And third, a bug existing in previous UMC version 6.0 causing a dip angle dependence is found to be due to a straight line extrapolation whenever a charged particle crosses a boundary between media and regions.

To check the consistency between data and Monte Carlo, $K_{\pi 2}(1)$ is employed with selection criteria listed in Table 2. The comparisons of momentum, range and kinetic energy between data and Monte Carlo are shown in Fig. 3, and the results are listed in Table 4. An initial correction to the dip angle dependence as discussed in the next section has already

Sample	cuts
Data	B4DEDX, BWTRS, CERENKOV, BHTRS, TGQUALT, $t_\pi - t_K > 3$ ns, TGZFOOL, TARGF, DTGTTP, RTDIF, KIC, TGGEO, PIGAP, TGLIKE, LAYV4, LAYER14, COS3D, UTCQUAL, $\chi_{rm} < 3$ and TDCUT
M.C.	UFATE, USTMED and USTOP_HEX, TGQUALT, $t_\pi - t_K > 3$ ns, TGZFOOL, TARGF, DTGTTP, RTDIF, KIC, TGGEO, PIGAP, TGLIKE, LAYV4, LAYER14, COS3D, UTCQUAL, $\chi_{rm} < 3$

Table 2: Selection criteria for $K_{\pi 2}(1)$ monitor data and Monte Carlo sample separately.

	Peak (data)	Peak (M.C.)	Sigma (data)	M.C. (M.C.)
P (MeV/c)	205.08±0.02	205.13±0.01	2.27±0.01	2.33±0.03
R (cm)	30.40±0.01	30.32±0.01	0.94±0.01	1.08±0.01
E (MeV)	108.37±0.02	108.53±0.01	3.39±0.04	3.37±0.02

Table 3: The peak positions and sigmas of momentum, range and kinetic energy for both $K_{\pi 2}(1)$ data and Monte Carlo, as also shown in Fig. 4.

been applied. In Monte Carlo, after the kinetic energy is corrected as detailed in preceding section, it is smeared by a normal distribution with a resolution of 3.04 MeV in order to match data. All quantities for the three measureables are in good agreement except for the resolution of range. This difference is also seen in 1995-1997 $\pi^+\nu\bar{\nu}1$ analysis. The reason is still unknown. To evaluate the possible impact on the BOX acceptance, the UMC range resolution is smeared by 0.53cm, the same amount of the difference between data and UMC, the BOX acceptance is observed to have merely 0.4% change. This tiny change is due to the fact that the range distribution around the range cut position is very flat and the range resolution effect gives the same amount events exchange below and above the range cut position.

1.5 Dip angle correction

Dip angle dependence observed in momentum measurement has been a long standing problem in E787. This effect is seen in both $K_{\mu 2}$ and $K_{\pi 2}$ samples. Historically, it was thought to be due to either trigger effect or resolution effect, or incorrect UTC strip geometrical input, or something wrong in converting the target energy loss into the momentum, or non-uniform magnetic field. The first two are turn down by Monte Carlo simulation study. From a study on $\mathbf{B_0 = 0}$ cosmic ray, the edge of I-counter and T-counter turn out to be correct, negating the third possibility. Also, there is no evidence showing that the dip angle dependence varies as a function target range and it is therefore unlikely from an incorrect conversion from the target energy loss into the momentum. Since the present magnetic field map cannot be measured, one cannot exclude that the observed dip angle dependence is from the non-uniform magnetic field. In Monte Carlo sample, current non-uniform magnetic field does produce small dip angle dependence in momentum, but the magnitude is smaller than that observed in data (see Table 4). In 1998 data analysis, the dip angle effect observed in

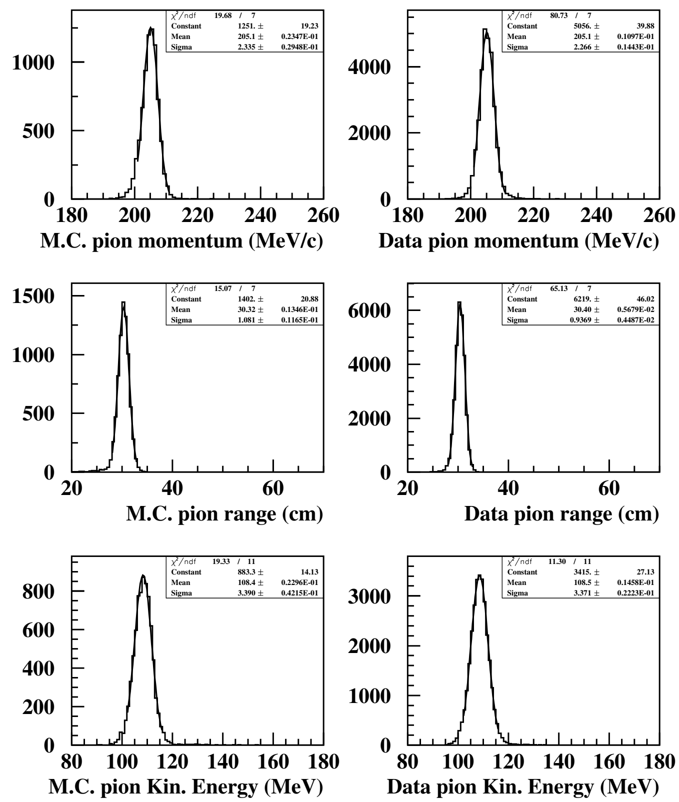

Figure 4: Comparisons of momentum, range and kinetic energy between $K_{\pi 2}(1)$ data and Monte Carlo. Samples are selected by applying cuts given in Table 2.

	P0	P1	P2
R(peak) (cm) from $K_{\pi 2}(1)$	30.52	-0.1034	0.9501
R(peak) (cm) from skim1	30.31	0.0363	-0.3741
R(peak) (cm) from MC $K_{\pi 2}(1)$	30.20	0.0646	0.9700
E(peak) (MeV) from $K_{\pi 2}(1)$	108.30	0.0889	4.2618
E(peak) (MeV) from skim1	108.41	-0.1775	-1.2285
E(peak) (MeV) from MC	108.35	-0.0411	-0.9621
P(peak) (MeV/c) from $K_{\pi 2}(1)$	205.47	0.6139	5.3626
P(peak) (MeV/c) from skim1	205.17	-0.1369	-1.1713
P(peak) (MeV/c) from MC $K_{\pi 2}(1)$	205.32	0.7711	3.2885
R(sigma) (cm) from skim1	0.8608	0.0249	0.7955
R(sigma) (cm) from MC $K_{\pi 2}(1)$	0.9031	-	-
E(sigma) (MeV) from skim1	3.3845	-	-
E(sigma) (MeV) from MC $K_{\pi 2}(1)$	3.3898	-	-
P(sigma) (MeV/c) from skim1	2.1877	0.0376	1.7232
P(sigma) (MeV/c) from MC $K_{\pi 2}(1)$	2.3104	-	-

Table 4: Dip angle (cos3d) dependence of the peak positions and sigmas for range, kinetic energy and momentum. Correction are applied for data and MC sample separately. For data, the first order correction is from $K_{\pi 2}(1)$ monitor sample, and the second order correction is from skim1 sample.

momentum, range and kinetic energy are corrected using $K_{\pi 2}(1)$ sample for data and Monte Carlo sample separately by means of

$$X_{new} = X_{old} \cdot X_{peak} / (P0 + P1 \cdot cos3d + P2 \cdot cos3d^2). \tag{4}$$

Where X stands for either range or kinetic energy or momentum. X_{peak} of $K_{\pi 2}$ is 30.37 cm for range, 108.55 MeV for kinetic energy and 205.14 MeV/c for momentum. The correction (see Table 4) obtained from $K_{\pi 2}(1)$ sample are applied first in PASS2 cut. The final correction factors (see Table 4) are directly from $K_{\pi 2}$ in skim1 sample. It is seen that the correction factors obtained from $K_{\pi 2}$ sample can be well applied to $K_{\mu 2}$ sample. Also observed is the dip angle dependence on the resolutions of range and momentum. Since cuts on rejecting $K_{\pi 2}$ background rely on the deviations of range, kinetic energy and momentum from the $K_{\pi 2}$ peak positions, the final deviations are computed according to

$$X_{dev} = (X_{new} - X_{peak}) / (P0 + P1 \cdot cos3d + P2 \cdot cos3d^2). \tag{5}$$

Where $P0$, $P1$ and $P2$ are determined by $K_{\pi 2}$ from skim1 sample (also see Table 4). Through out 1998 analysis, all range, kinetic energy and momentum measurements are corrected by the factors given in Table 4.

2 Kinematic background estimate from 2/3 1998 data

Final kinematic background estimate will be based on the 2/3 1998 data, because the cuts set for 1/3 1998 data should not have any bias for 2/3 sample. There are two major differences between the background estimate from 1/3 and 2/3 1998 data. In 1/3 $K_{\mu 2}$ background analysis, PASS1 FITPI cut is ignored, while it is applied in 2/3 data analysis. Also, both fixed and NN scattering cuts are applied to the 2/3 data. To be more conservative, safety cuts are not applied in the central value of the background.

2.1 The application of safety cuts

Differing from the 1/3 background study, three safety cuts are applied to remove events with poor track quality in 2/3 background analysis. Of these three safety cuts, the cut on UTC-RSSC matching was used in 1995-1997 $\pi^+\nu\bar{\nu}1$ analysis but was ignored in 1/3 background study. Two new cuts are developed to ensure a good momentum resolution.

2.1.1 UTC-RSSC matching

In 2/3 skim2 analysis, 3 out of 16 events (with no PASS1 FITPI cut) show a clear feature of UTC mis-fitting in r-z plane. The track finding in UTC reconstruction picks up noises in the foil layers, incorrectly pulling the track back to the barrel, leading to a wrong momentum measurement. Also known is that there is no corresponding straw chamber hit recorded in these 3 events. In previous Princeton analysis, there is an afterburner cut on events with a UTC-RSSC matching problem, rejecting any event with not only less than 4 Z hits but also **PR_RFZ1** $< 10^{-7}$ or **PR_RFZ2** < 0.05. This cuts causes about 0.6% acceptance loss.

2.1.2 UTC xy hits

A further investigation is also done for checking the number of xy hits used in track fitting. In UTC xy track reconstruction, all the xy hits associated to the same cluster are first used in the fit. If any xy hit causes a worse χ^2, then this hit will be removed. The final momentum resolution strongly depends on how many xy hits are used in the fit. To get a cut on the minimum number of xy hits in each super layer, a $K_{\pi 2}(1)$ monitor sample is used for study. The pion momentum resolution is seen as a function of used xy hits in all three super layers (see Fig. 5). Based on all these figures, cuts on the minimum number of xy hits are set at 1 for the first two super layers and 2 for the third super layer to ensure a good momentum resolution at a cost of 1.5% acceptance loss.

2.1.3 Track overlapping in UTC

A new feature of track overlapping in UTC is observed in 1998 data. This attributes to the condition of high kaon rate during the data acquisition of 1998 data. 3 out of 16 events (with no PASS1 FITPI cut) are found to have a track very close or overlapping with the final track in UTC (see Fig. 6 for example). This additional track can cause a confusion either in UTC or in Range Stack track reconstruction. The number of un-used xy hits are checked along the studied track within two cells (for the first two super layers) and three cells (for the third

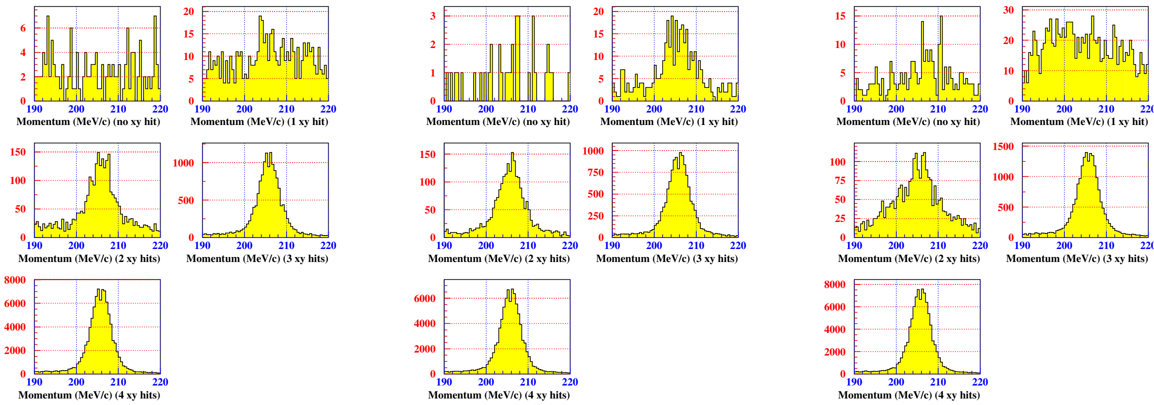

Figure 5: The pion momentum resolution as a function of used xy hits in the first super layer (left), the second super layer (middle) and third super layer (right).

super layer). A cut is designed to require no more than 9 un-used xy hits for signal event. The acceptance loss is estimated to be about 1.5%.

2.2 $K_{\mu 2}$ background

2.2.1 Anomaly of $K_{\mu 2}$ background in 2/3 sample

Applying all the kinematic cuts obtained from 1/3 1998 data analysis, 8 events are found in the fixed scattering cut method, while 16 events are found in the NN scattering cut method and 8 out of 16 events are the same as found in the fixed scattering cut method. Second bifurcation predicts 2.7 ± 1.0 and 4.8 ± 1.1 for both methods. They are a factor of 3 less than those actually observed. The PASS1 FITPI cut reduces the numbers to 5 and 10 and yields a factor of 1.6 rejection. This factor remains stable throughout the analysis. To gain more statistics in finding out the reason for the difference between 1/3 and 2/3 $K_{\mu 2}$ background estimates, The PASS1 FITPI cut is kept unused when studying this anomaly.

By examining the 16 events, one finds 5 events (2 in the fixed scattering cut method) fail the cut on UTC-RSSC matching. 5 events (4 in common with the above 5 events) cannot pass the cut on the number of used xy hits in three super layers. Also, 3 events (1 in common with the above 5 events) are rejected by the cut on two-track overlapping. In total, 8 out of 16 events (or 3 out of 8 events in the fixed scattering cut method) are found to have a problem in UTC tracking, which was not spotted in 1/3 data sample. Final signal search will adopt the safety cuts, but the background estimate will not use them in order to be more conservatively.

2.2.2 $K_{\mu 2}$ background estimate

The final $K_{\mu 2}$ background estimate is from 2/3 skim2 sample, applying all the cuts including PASS1 FITPI and both the fixed and NN scattering cuts. Table 5 gives the $K_{\mu 2}$ background estimate computed by $\frac{N_{bkg}}{TD_{rej}-1}$. For the systematic uncertainty, it is evaluated from the difference between the result from the NN scattering method alone and the one obtained

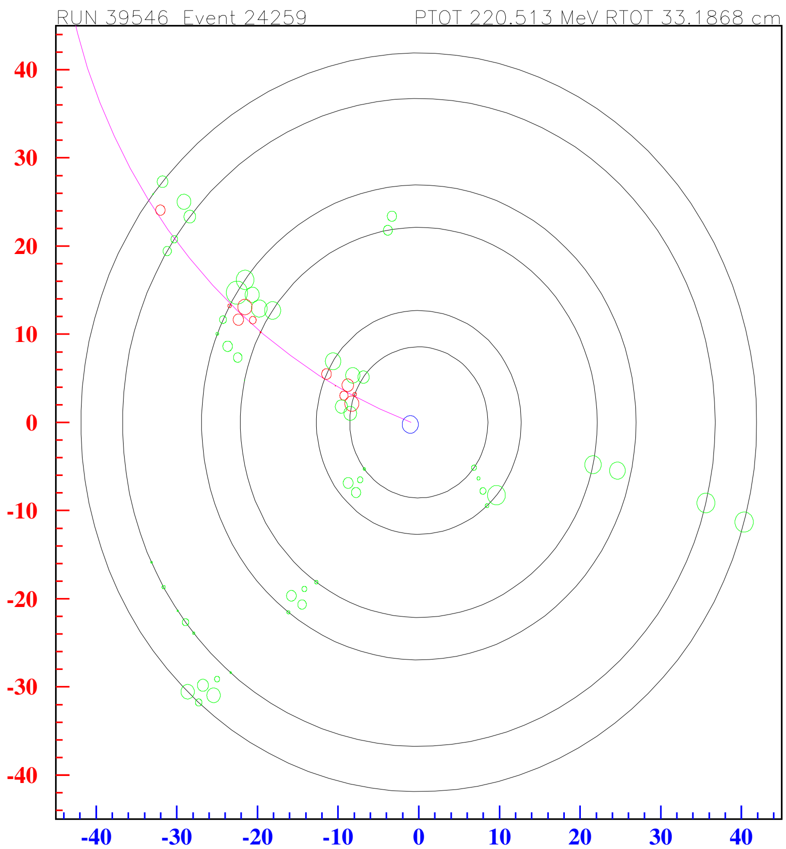

Figure 6: Event display with an additional track (indicated by green color circles) very close to the studied one (displayed by red color circles).

	Events	TD_{rej}	Bkg level in 1998
Band	2×1.5	326±51	0.0092±0.0067
Tail	3×1.5	185±51	0.0245±0.0155

Table 5: $K_{\mu 2}$ background estimate.

in Table 5. In the NN scattering method with PASS1 FITPI applied, 10 events left over. 4 out of 10 events are of momenta greater than 225 MeV/c. However, by scanning the 6 band events, 4 events are found to be tail events once a UTC refit is performed using proper Z hit information. Therefore, the NN scattering method gives 8 tail and 2 band events, which yields a background level of 0.074 with the TD rejection given in Table 5, leading to a difference of +0.041 for the background level. Since the final signal search uses the safety cuts, the background level can be reduced. Using the safety cuts gives 1 tail event and 2 band events, which makes the background reduce to 0.017, giving a difference of −0.017. They are all assigned to the systematic uncertainty. The final $K_{\mu 2}$ background estimate is

$$N_{K_{\mu 2}} = 0.034 \pm 0.017^{+0.040}_{-0.017}. \tag{6}$$

Where the first error is statistical and the second error is systematic.

2.3 $K_{\pi 2}$ background estimate

The method for the $K_{\mu 2}$ background estimate in 2/3 sample is almost the same as that used in 1/3 sample except both the fixed and NN scattering cuts are applied. 1 event is found inside the BOX in the first bifurcation. Since the background line shape from second bifurcation is found to agree with that from the first bifurcation (see Fig. 7) and has also sufficient statistics inside the BOX. The $K_{\pi 2}$ background estiamted will be based on the second bifurcation. The photon veto rejection is determined to be 43.9 ± 0.5. The final $K_{\pi 2}$ background estimate is obtained from $\frac{N_{bkg}}{PV_{rej}-1}$ and is given below

$$N_{K_{\pi 2}} = 0.012 \pm 0.003^{+0.001}_{-0.003}. \tag{7}$$

Where the first error is statistical and the second error is systematic. The systematic uncertainty includes the line shape difference between the first and second bifurcations and the effect due to the safety cuts.

3 $K_{\mu 2}$ background function for 1998

In this analysis, $K_{\mu 2}$ background function is split into $K_{\mu 2}$ tail and $K_{\mu 2}$ band functions. Full sample is exploited in constructing both background functions in order to gain more statistics. Since the final cuts include both fixed and NN scattering cuts and the safety cuts as well, the background functions are different from the ones presenting in the 1/3 1998 data analysis.

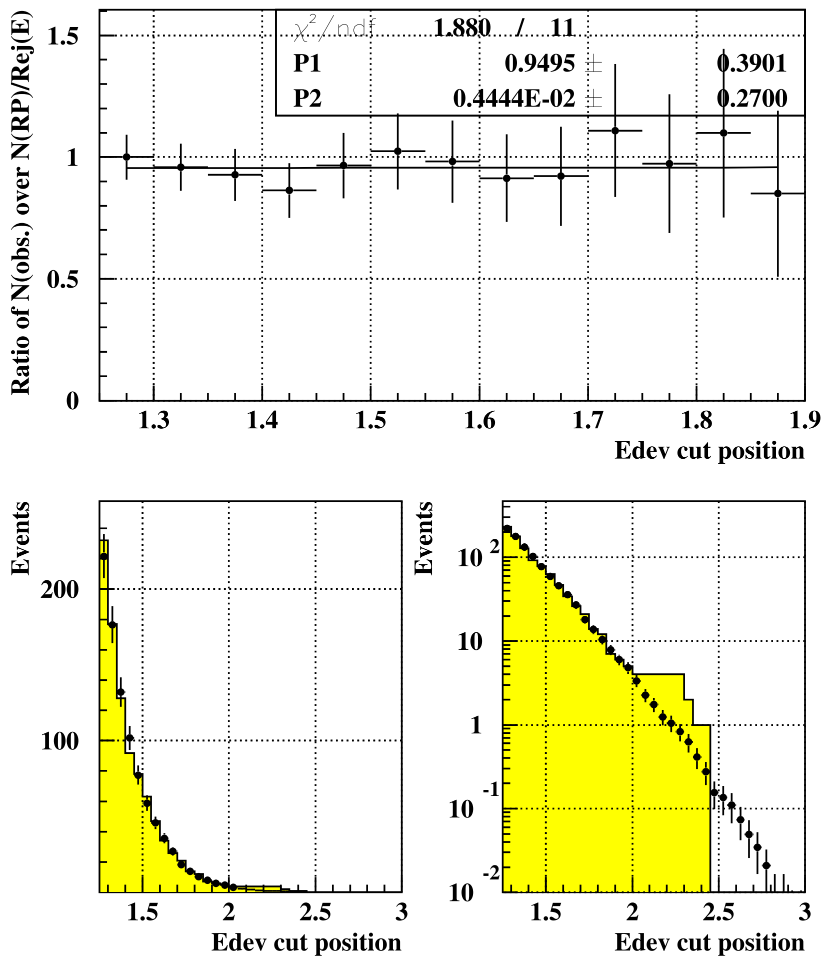

Figure 7: The ratio of N(obs.) over N(RP) Rej(E) are shown at the top of plots. Comparison between the expected and observed $K_{\pi 2}$ background is shown at the bottom of plots in linear and logarithmic scales separately.

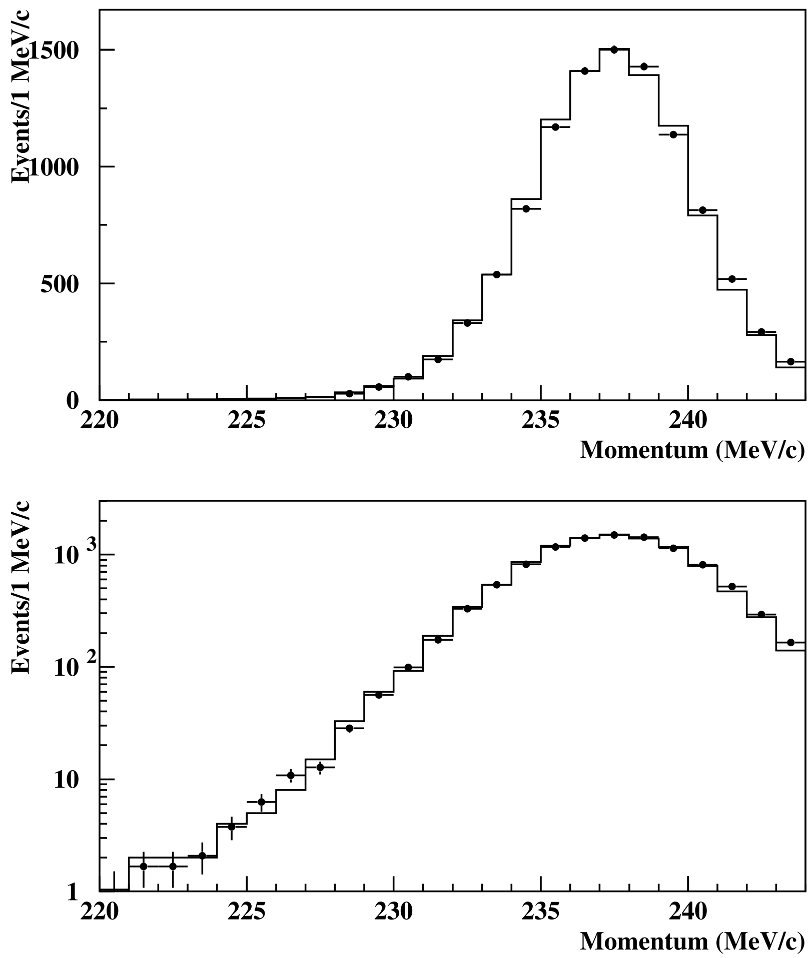

Figure 8: Momentum distribution for $K_{\mu 2}$ tail events with no scattering cuts but with the χ_{rm} cut and the upper ERBOX cuts (histogram). $K_{\mu 2}$ peak events with no scattering cuts but with a cut on range greater than 50 cm (black dots).

3.1 $K_{\mu 2}$ tail function

For $K_{\mu 2}$ tail function includes two parts. One is for the inside-the-BOX function and the other is the outside-the-BOX function. For the outside-the-BOX function, all cuts except for the upper PBOX cut are applied to both skim2 and skim5 samples. Sample from first bifurction is used to construct the outside-the-BOX function. For the inside-the-BOX function, all cuts except for the scattering cuts and the upper PBOX cut are applied to both skim2 and skim5 samples. To get rid of the band background contamination, events from second bifurction are selected with a cut on range greater than 50 cm and all cuts except for the χ_{rm} cut and the upper ERBOX cuts. Figure 8 shows that the momentum line shapes inside the BOX are almost the same for both samples. The final $K_{\mu 2}$ tail function is tabulated in Table 6.

p (MeV/c)	Acc.	Bkg. level
242	1.026	1.000000
241	1.026	0.966329
240	1.026	0.895622
239	1.026	0.794612
238	1.026	0.683501
237	1.026	0.572390
236	1.026	0.424242
235	1.026	0.276094
234	1.026	0.158249
233	1.025	0.090909
232	1.024	0.053872
231	1.022	0.037037
230	1.016	0.023569
229	**1.000**	**0.013468**
228	0.976	0.007405
227	0.944	0.004340
226	0.897	0.002975
225	0.838	0.001812
224	0.761	0.001140
223	0.684	0.000738
222	0.598	0.000514
221	0.511	0.000335
220	0.426	0.000156
219	0.346	0.000447

Table 6: $K_{\mu 2}$ tail function obtained from first bifurcation sample (outside the BOX) and from second bifurcation sample (inside the BOX). The background level has been normalized to the departure point.

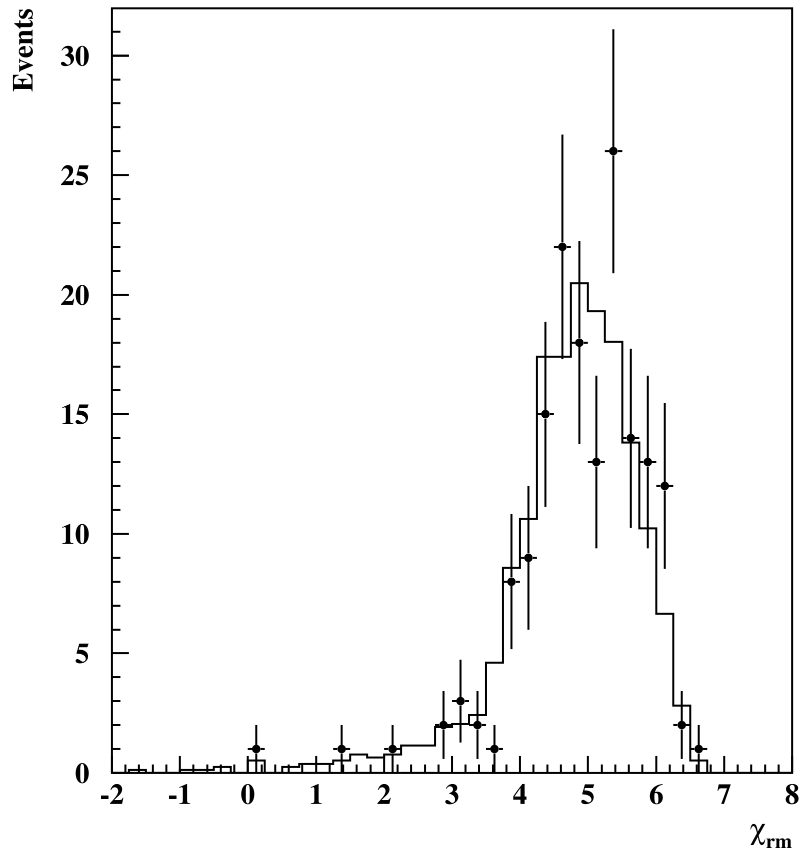

Figure 9: χ_{rm} distribution for $K_{\mu 2}$ band events with all cuts applied except for the **RS_LIKE, RS_DEDX, RS_CHIMAX** and upper RBOX cuts (histogram) and with all cuts applied except for the upper RBOX cut (black dots).

3.2 $K_{\mu 2}$ band function

The $K_{\mu 2}$ band events are defined for those with momentum less than 225 MeV/c. In 1/3 data analysis, the function was built from second bifurcation sample (photon veto inverted) with all cuts applied, leading to only one event inside the BOX. Even full statistics are used, the events left over are still not sufficient for giving a realiable band function inside the BOX. A detail study on the events sneaking into the BOX region shows that the χ_{rm} tail is independence of the scattering cuts. Figure 9 shows the comparision between the skim2 and skim5 samples with all cuts applied except for the upper RBOX cut and the same samples with all cuts applied except for the **RS_LIKE, RS_DEDX, RS_CHIMAX** and upper RBOX cuts. Both χ_{rm} distributions are in good agreement. The $K_{\mu 2}$ band background function is then constructed using the one with loose scattering cuts. Table 7 list the numberical value for the band function.

χ_{rm}	Acc.	Bkg. level
6.50	1.015	1.000000
6.25	1.015	0.996880
6.00	1.014	0.979719
5.75	1.014	0.939157
5.50	1.014	0.876755
5.25	1.014	0.792512
5.00	1.014	0.682528
4.75	1.014	0.564743
4.50	1.014	0.439938
4.25	1.014	0.333854
4.00	1.014	0.227770
3.75	1.014	0.163027
3.50	1.014	0.110765
3.25	1.014	0.082683
3.00	1.013	0.067862
2.75	1.012	0.055382
2.50	1.010	0.043681
2.25	1.007	0.036661
2.00	**1.000**	**0.029641**
1.75	0.988	0.024961
1.50	0.966	0.021060
1.25	0.923	0.016380
1.00	0.860	0.013260
0.75	0.772	0.010920
0.50	0.670	0.008580
0.25	0.541	0.007020
0.00	0.406	0.007020
-0.25	0.279	0.003900
-0.50	0.179	0.003900
-0.75	0.105	0.002340
-1.00	0.053	0.001560
-1.25	0.025	0.000780

Table 7: $K_{\mu 2}$ band function obtained from first bifurcation with loose scattering cuts. The background level has been normalized to the departure point.

4 $K_{\pi 2}$ background function for 1998

Comparing to the 1/3 1998 data analysis, the determination of $K_{\pi 2}$ background function has no significant change except both fixed and NN scattering cuts together with safety cuts are applied now. Table 8 gives the $K_{\pi 2}$ background function obtained from full statistics.

Rdev	Edev	Pdev	Acc.	Bkg. level
1.600	1.250	1.400	1.350	1.00000
1.650	1.300	1.450	1.336	0.79457
1.700	1.350	1.500	1.320	0.59360
1.750	1.400	1.550	1.307	0.45791
1.800	1.450	1.600	1.293	0.34057
1.850	1.500	1.650	1.276	0.25493
1.900	1.550	1.700	1.264	0.19455
1.950	1.600	1.750	1.251	0.14745
2.000	1.650	1.800	1.238	0.11058
2.050	1.700	1.850	1.224	0.07708
2.100	1.750	1.900	1.205	0.05960
2.150	1.800	1.950	1.190	0.04363
2.200	1.850	2.000	1.169	0.03282
2.250	1.900	2.050	1.151	0.02394
2.300	1.950	2.100	1.133	0.01928
2.350	2.000	2.150	1.117	0.01343
2.400	2.050	2.200	1.100	0.00909
2.450	2.100	2.250	1.086	0.00682
2.500	2.150	2.300	1.070	0.00486
2.550	2.200	2.350	1.051	0.00398
2.600	2.250	2.400	1.034	0.00300
2.650	2.300	2.450	1.017	0.00205
2.700	**2.350**	**2.500**	**1.000**	**0.00147**
2.750	2.400	2.550	0.984	0.00110
2.800	2.450	2.600	0.969	0.00065
2.850	2.500	2.650	0.951	0.00055
2.900	2.550	2.700	0.935	0.00045
2.950	2.600	2.750	0.918	0.00031
3.000	2.650	2.800	0.902	0.00021
3.050	2.700	2.850	0.888	0.00014
3.100	2.750	2.900	0.870	0.00010
3.150	2.800	2.950	0.852	0.00006
3.200	2.850	3.000	0.835	0.00004
3.250	2.900	3.050	0.818	0.00003
3.300	2.950	3.100	0.802	0.00002

Table 8: $K_{\pi 2}$ background function. The background level has been normalized to the departure point.

	cut class	cut members
1.	pv	PV function
2.	kp2	$K_{\pi2}$ kinematic function (lower limits on R, E, and P)
3.	td	TD function (FITPI, EV5, ELVETO, TDFOOL, TD neural net)
4.	km2	$K_{\mu2}$ kinematic functions (upper limits on R and E; upper limit on P [range-tail function]; RNGMOM [muon-band function])
5.	bmfn	DELC, BWTRS, CKTRS, CKTAIL, CPITRS, CPITAIL, PBNRS, B4DEDX, B4TRS, B4TD
6.	fiducial	LAYV4, COS3D, ZFRF, ZUTOUT, LAY14
7.	scatfix	Fixed scattering cuts (CHIMAX_RSDEDX, CL_RSDEDX, RSLIKE, PR_RF, PRRFZ1_N), plus PR_RF_AB, PR_RFZ2, UTCQUAL
8.	scatnn	Neural net scattering cut, plus PR_RF_AB, PR_RFZ2, UTCQUAL
9.	scatboth	Fixed and neural net scattering cuts, plus PR_RF_AB, PR_RFZ2, UTCQUAL
10.	tgdedx	TGDEDX, PIGAP, TGLIKE, TGB4
11.	tgepi	TGCCDPF, EPITG, EPIMAXK, PHIVTX, OPSVETO, TGEDGE
12.	tgtrack	TGER, TARGF, DTGTTP, RTDIF, DRP, TGQUALT
13.	timcon	TIMCON, TIC, TGCCD
14.	ic	EIC, KIC, TGGEO
15.	b4ekz	B4EKZ, TGZFOOL
16.	bhtrs	BHTRS

Table 9: Complete listing of cuts applied in the analysis, (except the pileup and UTC safety cuts), divided into cut classes. Classes $6-16$ are the “pathology cut classes”, which are turned off one by one in the outside-the-box correlation study. Classes $1-16$ are used in the single-class-failure study.

5 Outside-The-Box Studies

The outside-the-box studies are described in the 1/3 1998 analysis note, and in E787 TN365. As before, there are two parts to this study: a correlation study and a single-cut failure study.

5.1 Correlation Studies

The correlation studies consist of performing the bifurcated background measurements at loose cut positions, and comparing with the observed numbers of events in these regions (after masking out the box). This is performed 12 times, once with all other cuts applied, and once for each of 11 pathology cut classes turned off (in order to investigate potential correlations between bifurcated cuts). The 11 pathology cut classes are described in Table 9, along with the 5 cut classes that are loosened in (a) the $K_{\pi2}$ correlation study (PV and $K_{\pi2}$ kinematics); (b) the $K_{\mu2}$ correlation study (TD and $K_{\mu2}$ kinematics); and (c) the beam correlation study (beam function cuts). These 16 cut classes, along with the pileup and UTC safety cuts, are a complete listing of all cuts in the analysis (the pileup and UTC safety cuts are not applied as part of this study, because they require additional information which was not available in the summary ntuple at the time of this study).

5.1.1 $K_{\pi2}$ Correlation Study

The results of the 2/3 1998 $K_{\pi2}$ correlation study are shown in Table 10. Predicted background is consistent with observed background in all cases, though one could perhaps argue that there is a factor of 2 correlation (twice as many events observed than predicted) in the 10×10 box. This was also perhaps apparent in the 20×20 box for 1/3 1998.

cuts turned off		$K_{\pi 2}$: PV $\times$ kin. 10×10	20×20	50×50	50×315
none	predict:	1.18	4.74	33.00	225.00
	observe:	3	5	36	233
fiducial	predict:	1.63	6.37	43.00	259.00
	observe:	4	6	46	267
scatfix	predict:	1.86	6.40	46.00	281.00
	observe:	4	8	50	290
scatnn	predict:	1.40	5.57	38.00	241.00
	observe:	3	6	41	249
scatboth	predict:	3.48	11.08	68.00	347.00
	observe:	10	18	73	359
tgdedx	predict:	2.12	6.46	48.00	277.00
	observe:	5	8	51	287
tgepi	predict:	2.03	7.76	46.00	286.00
	observe:	3	8	49	295
tgtrack	predict:	1.18	4.74	33.00	229.00
	observe:	3	5	36	237
timcon	predict:	1.18	4.75	34.00	231.00
	observe:	3	5	37	241
ic	predict:	1.88	6.94	41.00	269.00
	observe:	4	9	44	277
b4ekz	predict:	1.41	5.18	34.00	235.00
	observe:	4	6	37	243
bhtrs	predict:	1.18	4.74	33.00	225.00
	observe:	3	5	36	233

Table 10: Predicted and observed numbers of $K_{\pi 2}$ background events in the 2/3 1998 data sample, obtained by loosening the PV and $K_{\pi 2}$ kinematic function cuts by the factors shown. Background predictions and observations are made with various pathology cuts, grouped into classes (see Table 9), turned off.

run	event	R	E	P	$bgpv$	$bgtd$
37520	164572	38.0220	117.656	226.300	6.96496	0.616839
37761	142498	32.7228	116.117	223.516	1.35515	0.
39171	80123	32.6496	129.890	210.769	3.35124	0.0251771
39180	85391	33.1624	121.026	210.110	7.27628	0.
39773	16286	33.1136	116.117	210.549	0.262483	0.386049
40262	16892	32.8938	125.128	210.183	0.201441	0.0251771
40312	19258	32.6984	116.777	211.062	0.860701	0.
40579	44887	34.0171	125.348	221.905	1.01941	0.
40640	22691	33.2112	116.557	212.161	8.68026	0.
40654	114665	33.0891	128.938	209.744	8.13698	0.
*38904	65881	32.2344	115.751	210.256	12.9716	0.
*40643	184840	32.2833	114.872	209.890	6.75131	0.

Table 11: Events observed in the $K_{\pi 2}$ correlation study. See the text for more details.

The 10 $K_{\pi 2}$ "scatboth" events in the 10×10 box, plus the 2 additional "none" events in the 20×20 box, are listed in Table 11. The 3 "none" events in the 10×10 box are denoted by *. The 2 additional "none" events in the 20×20 box are denoted by **.

All events in Table 11 are clearly $K_{\pi 2}$, except perhaps for the 1st, 2nd, and 8th events listed, which all have large P and $bgpv > 1$, so these could be radiative $K_{\mu 2}$. All of the events not denoted by * or ** are rejected by at least one of the scattering cuts. Note that none of the listed events belong to the famous 16-event $K_{\mu 2}$ sample, because they all pass the TD cut.

The 1st event has large R, P, and $bgpv$, non-zero $bgtd$, and it fails the RSDEDX confidence level cut, so it could be a radiative $K_{\mu 2}$ event. The pion decay time for this event is small ($tmuav = 8.5$), but 2 pulses are clearly visible in the stopping counter. There is 25 MeV of "missing" energy (as implied by momentum), which is at the peak of the ^{12}C giant dipole resonance cross section, so perhaps the second pulse in the stopping counter is coming from a GDR-emitted neutron (which is expected to come at small $tmuav$).

The 2nd event listed (which is 1 of the 3 in the 10×10 box) is close to the box in PV and kinematics, has perfect TD quantities, and is very far from the muon band. Furthermore, this type of event seems to preferentially have good TD quantities. That is, if we loosen the TD cuts and re-make Table 11, we don't increase the number of $K_{\mu 2}$ events by the appropriate loosening factor (if we loosen TD by a factor of 10, we get one additional $K_{\mu 2}$ event; if we loosen TD by a factor of 80, we get 17 additional $K_{\mu 2}$ events). So, if this event is $K_{\mu 2}$, it may represent a long tail on the muon band, which correlates TD and kinematics. However, this event fails the UTC safety cuts (the only event in Table 11 to do so) because there are only 2 (used) xy hits in the 3rd superlayer. There are 2 unused xy hits in the 3rd superlayer which are very close to the used hits and which, if used, downshift the measured momentum into the $K_{\pi 2}$ peak. George re-fit this event (by forcing the fitter to set the L/R ambifuity to the "left", or larger ϕ), and found that P was shifted into the $K_{\pi 2}$ peak, with only a small change in the χ^2/d.o.f. (went to 3.73 from 3.19). So this event is indeed $K_{\pi 2}$, with a momentum mis-fit much like several of the $K_{\mu 2}$ events found in the famous 16-event $K_{\mu 2}$ sample. Therefore, the safety cut seems to be doing its job, and this $K_{\pi 2}$ background event is well understood.

The 8th event listed in Table 10 has a large scatter in z early in the range stack, which downshifts R. E is also small (by 15 MeV as implied by momentum) perhaps because the track enters the spider web (the scattered track goes far upstream in the range stack). Also, the second pulse in the stopping counter ($tmuav = 27$ ns) could be coming from an accidental which is largely hidden in the spider web. Finally, the event fails the fixed scattering cuts (PRRFZ1_N) as well as the well as the Princeton safety cut (PR_RF_AB), so it is likely a radiative $K_{\mu 2}$ event.

If one eliminates these 3 events from the $K_{\pi 2}$ 10×10 outside-the-box region, any PV-kinematic correlation becomes even less apparent. However, even with 3 fewer observed events in the 10×10 "scatboth" region, there are still about twice as many events observed than predicted. But this is perhaps expected, because the scattering cuts are sensitive to photons lying on the track, which can simultaneously shift $K_{\pi 2}$ events up in R and E, and reduce the PV rejection.

One can use the 2 $K_{\mu 2}$ events observed here to estimate the $K_{\mu 2}$ background in the box. These 2 events pass everything except scattering cuts and PV. "Scattering" muons are best represented by a sample of $K_{\mu 2}$ range-tail events, so to get the rejection of the scattering cuts, we can compare the numbers of observed events in the "none" and "scatboth" rows of the $K_{\mu 2}$ range-tail Table (see the next section): the rejection factor is about 50. Here, in the $K_{\pi 2}$ 10×10 box, we have loosened PV by a factor of 10. We know that the PV rejection in the muon band is about 2.3, so we expect the PV enhancement of muon-band events in the $K_{\pi 2}$ 10×10 box to be about 2. One of these 2 $K_{\mu 2}$ events has $P > 225$; the other has $P < 225$, so according to the usual definition, one is "range tail" and one is "band". So the range-tail background in the box in 1998 is estimated to be $1/50/2 \cdot 1.5 = 0.015$ events, and the muon-band background is estimated to be $1/50/2 \cdot 1.5 = 0.015$ events, which are consistent with the standard bifurcated estimates of 0.024 and 0.009, respectively.

Note that when one compares the 1/3 and 2/3 1998 $K_{\pi 2}$ correlation study Tables, the predicted and observed background numbers scale up by 2 (as they should) except in the 10×10 box. For exmaple, for the "tgdedx" 10×10 prediction, there are 2 events in the normalization in the 1/3 data, so we expect 4 in the 2/3 data, but we see 9, so the "predict" number goes up by almost a factor of 5. Similarly, in the "scatboth" 10×10 box, there are 0 events observed in 1/3 1998, but 10 events (7 if we omit $K_{\mu 2}$ and mis-fit $K_{\pi 2}$) observed in 2/3. This again could be a statistical fluctuation.

So the only concern here (other than the above-mentioned statistical fluctuations) is perhaps the appearance of a suspected radiative $K_{\mu 2}$-GDR background event, which correlates TD and kinematics. We expect GDR events to appear when the scattering cuts are turned off, but from the $K_{\mu 2}$ range-tail Tables (see the next section), there is no apparent TD-kinematic correlation, even when scattering cuts are turned off. So we expect that this type of event has been accounted-for in the background estimates.

5.2 $K_{\mu 2}$ Range-Tail Correlation Study

The results of the 2/3 1998 $K_{\mu 2}$ range-tail correlation study are shown in Table 12. Predicted background is consistent with observed background in all cases. Therefore, any TD-kinematic correlations are expected to be small.

The 12 range-tail "none" events in the 352×10 box are listed in Table 13. The 2 events

cuts turned off		$K_{\mu 2}$ range tail: TD × kin.								
		10 × 10	73 × 73	134 × 120	352 × 120	10 × 73	10 × 120	73 × 10	134 × 10	352 × 10
none	predict:	0.33	23.67	66.44	204.00	3.30	5.61	2.37	3.91	12.00
	observe:	0	30	66	205	3	5	2	4	12
fiducial	predict:	3.26	101.64	279.34	968.00	14.61	21.34	22.69	42.71	148.00
	observe:	3	109	274	969	13	21	15	35	148
scatfix	predict:	0.55	40.96	108.01	325.00	3.61	5.79	6.26	10.30	31.00
	observe:	0	49	109	326	3	5	4	10	31
scatnn	predict:	0.89	40.98	116.34	329.00	6.73	10.49	5.44	9.90	28.00
	observe:	0	48	115	330	7	10	6	12	28
scatboth	predict:	27.79	1605.00	4089.50	10755.00	196.54	312.33	226.95	363.89	957.00
	observe:	25	1750	4093	10794	205	312	231	380	963
tgdedx	predict:	0.37	25.73	75.95	237.00	3.15	5.49	3.03	5.13	16.00
	observe:	0	33	77	238	3	5	2	4	16
tgepi	predict:	0.35	26.07	72.76	222.00	3.88	6.53	2.37	3.93	12.00
	observe:	0	33	73	224	4	6	2	4	12
tgtrack	predict:	0.32	25.02	68.42	209.00	3.34	5.62	2.42	3.93	12.00
	observe:	0	31	68	210	3	5	2	4	12
timcon	predict:	0.38	24.91	69.38	210.00	3.32	5.62	2.81	4.62	14.00
	observe:	0	31	69	211	3	5	3	5	14
ic	predict:	0.55	25.58	71.09	217.00	4.45	7.48	3.17	5.24	16.00
	observe:	1	32	71	218	4	7	4	6	16
b4ekz	predict:	0.33	23.65	67.42	206.00	3.30	5.62	2.35	3.93	12.00
	observe:	0	30	67	207	3	5	2	4	12
bhtrs	predict:	0.33	23.67	66.44	204.00	3.30	5.61	2.37	3.91	12.00
	observe:	0	30	66	205	3	5	2	4	12

Table 12: Predicted and observed numbers of $K_{\mu 2}$ range-tail background events in the 2/3 1998 data sample, obtained by loosening the TD and $K_{\mu 2}$ range-tail kinematic function cuts by the factors shown. Background predictions and observations are made with various pathology cuts, grouped into classes (see Table 9), turned off.

run	event	R	E	P	$rngmom\_val$	$bgpv$	$bgtd$
36971	33193	39.56	130.11	231.87	-0.0684	0.1648	351.821
37409	78031	37.09	121.54	229.45	-0.7328	0.7325	351.821
38308	42536	39.90	132.53	232.97	0.0684	0.2381	133.64
38645	185171	38.10	122.34	232.16	-0.6546	0.3540	351.821
38689	2291	38.14	122.13	225.13	0.6155	0.3540	133.64
38710	21502	37.68	124.18	230.18	-0.5178	0.0549	42.2304
38926	64163	33.77	124.03	230.99	-3.4880	0.1892	351.821
38940	193735	36.48	118.24	229.45	-1.0649	0.1892	68.4859
39879	98536	38.90	124.03	230.92	-0.2052	0.3540	351.821
39956	33971	35.58	119.93	228.94	-1.8075	0.0488	351.821
40433	69302	36.78	123.00	232.97	-1.6903	0.1343	351.821
40591	42545	38.46	125.64	232.89	-0.6546	0.2808	351.821

Table 13: Events observed in the $K_{\mu 2}$ range-tail correlation study. See the text for more details.

in the 73×10 box, the 2 further events in the 134×10 box, and the remaining 8 events in the 352×10 box, are easily found from their $bgtd$ values ($bgtd < 1$ is the box cut position). Only 1 of these 12 events fails the UTC safety cuts, denoted in the Table by *. All of the events in Table 13 look like $K_{\mu 2}$ momentum-peak events, except perhaps for the 5th event listed. The 5th and 10th events are also those that show up in the 2/3 1998 16-event sample, by virtue of the fact that they pass the $K_{\mu 2}$ kinematic functions ($P < 229$). The 5th event is the only event which fails the UTC safety cuts: it has a L/R ambiguity, and when re-fit it migrates well into the muon band. The 10th event fails EV5, and is likely a range-tail event.

Note that when the scattering cuts are turned off, the $K_{\mu 2}$ muon-band kinematic function (which is histogrammed in order to make the background predictions in the next section) is not flat: there is a large spike at inside-the-box function values. This spike vanishes with application of the scattering cuts (PRRFZ1_N and UTCQUAL are very effective). This implies that UTC-fitting is responsible for a long tail on the $K_{\mu 2}$ momentum peak, which shifts events into the "muon band" ($P < 225$). The $K_{\mu 2}$ range-tail kinematic function also has a spike at inside-the-box values in the 2/3 1998 data, especially when fiducial cuts are turned off. This spike is suppressed by fiducial and UTC safety cuts. Note that the background estimates in the outside-the-box Tables appear too good to be true (e.g., in the 2/3 1998 $K_{\mu 2}$ range-tail 10×10 box, the prediction is 0.33 events, which implies $0.0033 \cdot 1.5 = 0.005$ in the final box, whereas the final $K_{\mu 2}$ range-tail background estimate is 0.024 events). This is due to a combination of poor statistics, and the fact that small spikes remain in the functions because UTC safety cuts are not applied in this study. These spikes cause the number of background events to increase by less than a factor of 10 when the function cut is loosened by a factor of 10.

5.3 Muon-Band Correlation Study

The results of the 2/3 1998 muon-band correlation study are shown in Table 14. Predicted background is consistent with observed background in all cases. Therefore, any TD-

cuts turned off		$K_{\mu 2}$ muon band: TD × kin. 10 × 10	58 × 58	134 × 146	352 × 305	10 × 58	10 × 146	10 × 305	58 × 10	134 × 10	352 × 10
none	predict:	0.21	5.64	32.82	118.00	0.94	2.73	5.04	1.28	2.56	5.00
	observe:	1	7	36	118	1	4	6	3	3	5
fiducial	predict:	0.81	12.93	52.78	181.00	2.10	4.45	7.32	4.97	9.60	20.00
	observe:	1	14	55	182	2	5	8	5	8	20
scatfix	predict:	1.17	11.27	50.74	167.00	2.26	4.93	7.85	5.87	12.08	25.00
	observe:	2	11	51	167	3	7	9	6	10	25
scatnn	predict:	0.56	8.09	44.94	155.00	1.53	4.03	7.19	2.94	6.20	12.00
	observe:	1	10	50	155	2	5	8	5	7	12
scatboth	predict:	4.87	51.45	198.84	634.00	9.24	16.44	24.30	27.11	58.87	127.00
	observe:	3	37	190	635	7	14	24	19	47	127
tgdedx	predict:	0.31	7.25	40.00	162.00	1.27	3.50	7.09	1.75	3.50	7.00
	observe:	1	8	45	162	1	4	8	3	3	7
tgepi	predict:	0.22	5.45	36.29	136.00	0.85	2.63	5.04	1.42	3.07	6.00
	observe:	1	7	41	136	1	4	6	3	4	6
tgtrack	predict:	0.25	6.10	33.54	123.00	0.98	2.70	5.04	1.52	3.05	6.00
	observe:	1	7	36	123	1	4	6	3	3	6
timcon	predict:	0.24	5.54	34.32	124.00	1.07	3.27	6.05	1.26	2.56	5.00
	observe:	1	7	38	124	1	5	7	3	3	5
ic	predict:	0.20	6.05	33.23	124.00	0.98	2.72	5.04	1.26	2.48	5.00
	observe:	1	7	36	124	1	4	6	3	3	5
b4ekz	predict:	0.21	5.59	33.08	119.00	0.93	2.71	5.04	1.27	2.58	5.00
	observe:	1	7	36	119	1	4	6	3	3	5
bhtrs	predict:	0.21	5.64	32.82	118.00	0.94	2.73	5.04	1.28	2.56	5.00
	observe:	1	7	36	118	1	4	6	3	3	5

Table 14: Predicted and observed numbers of muon-band background events in the 2/3 1998 data sample, obtained by loosening the TD and muon-band kinematic function cuts by the factors shown. Background predictions and observations are made with various pathology cuts, grouped into classes (see Table 9), turned off.

kinematic correlations are expected to be small.

The 5 muon-band "none" events in the 352×10 box are listed in Table 15. The 1 event in the 10×10 box, the 2 additional events in the 59×10 box, and the remaining 2 events in the 352×10 box are easily found from their *bgtd* values (*bgtd* < 1 is the box cut position). None of these events fail the UTC safety cuts. The 1st, 4th, and 5th events are clearly muon-band events, given their large *rngmom_val*. The 2nd event is also likely a muon-band event, given that *rngmom_val* > 1. The 3rd event is a "perfect" event except that it has *bgtd* just outside the box: this could be a candidate event which contaminates the $K_{\mu 2}$ data sample.

Comparing the 1/3 and 2/3 1998 muon-band correlation study Tables, we see that the

run	event	R	E	P	*rngmom_val*	*bgpv*	*bgtd*
38484	146162	36.41	119.19	214.29	2.18	0.281	351.821
39120	180802	35.82	123.52	215.82	1.358	0.092	22.2314
39180	56327	37.05	125.50	224.91	0.088	0.134	3.10098
40391	36733	37.53	130.84	214.80	2.882	0.433	351.821
40484	133829	38.22	125.57	216.78	2.824	0.586	59.4096

Table 15: Events observed in the muon-band correlation study. See the text for more details.

predicted and observed numbers of muon-band background events do not scale up by a factor of 2 when going from 1/3 to 2/3; the numbers scale by a factor of about 2.5 (far from the box) up to about 4 (near the box), except when the scattering cuts are turned off; then the factor of 2 holds everywhere. This is also somewhat true when comparing the range-tail Tables. In other words, the scattering cuts have more rejection on the 1/3 1998 data than they do on the 2/3 1998 data. The final cut positions of the scattering cuts (both fixed and neural net) were set using small statistics (e.g., trying to reduce 6 events to 1 event on the 1/3 1998 data), so the $1/3 - 2/3$ scaling discrepancy in $K_{\mu 2}$ background observed here is likely due to bias in the scattering cuts, in particular, with respect to their rejection of muon-band events ($P < 225$), which is where the UTC mis-fit events show up. The bias may be as large as a factor of about $4/2 = 2$ in $K_{\mu 2}$ background suppression on the 1/3 1998 data.

5.4 Beam Correlation Study

The results of the 2/3 1998 beam correlation study are shown in Table 16. Predicted background is not consistent with observed background for the single-beam kaon- and pion-entering backgrounds. Specifically, there appear to be correlations in the bifurcations far from the box, and perhaps also close to the box (it's difficult to tell due to statistics). This was not apparent in 1/3 1998. For the double-beam kaon- and pion-entering backgrounds however, predicted and observed numbers of events are consistent.

The 17 single-beam kaon-entering events in the 2/3 1998 "loose3" box with "tgepi" turned off are listed in Table 17. The 2 "none" events in the "loose2" box are denoted by *; the 6 additional "none" events in the "loose3" box are denoted by **. Most of the events look like $K_{\pi 2}$ decay-in-flight, given that *bgtd* is usually 0 and $bgpv > 0$. (Note that run 38570, event 2446 is written down twice, due to duplication in the ntuples).

The 10 single-beam pion-entering events in the 2/3 1998 "loose3" box with "tgepi" turned off are listed in Table 18. The 2 "none" events in the "loose2" box are denoted by *; the 4 additional "none" events in the "loose3" box are denoted by **. Note that all of these events, except the 8th event listed, are also included in the single-beam kaon-entering list of events in Table 17. So these 9 events are those which (with "tgepi" turned off) pass CKTRS and CPITRS, and fail DELC only (and they fail it badly). This may be the source of the correlation: these events are counted twice as both kaon- and pion-entering background. Combining the single-beam kaon- and pion-entering results in Table 16, we see that we predict $9.6 + 4.1 = 13.7$ single-beam background events in the "loose3" box with "tgepi" turned off. We observe $17 + 10 = 27$, but only $16 + 1 = 17$ of these are "unique". So the real prediction is 13.7, and the real observation is 17, which is perhaps consistent. Similarly, we predict $4.2 + 1.9 = 6.1$ in the "loose3" box with "none" turned off, and we observe $8 + 6 = 14$ events, but only 8 of these are unique. 6.1 vs. 8 is again consistent.

5.5 Search for Single-Cut Failures

In the 2/3 1998 data, there are no events which fail a single "pathology" class of cuts (unlike the 1/3 1998 data, where an event was found which just failed the "fiducial" pathology cut class, and was determined to be a "pileup" double-beam background event, for which the "pileup" cut was designed). All of the events observed here in the 2/3 1998 sample fail one of

cuts turned off		single-beam kaon-entering loose1	loose2	loose3	single-beam pion-entering loose1	loose2	loose3
none	predict:	0.029	0.578	4.188	0.026	0.353	1.880
	observe:	0	2	8	0	2	6
fiducial	predict:	0.029	0.578	4.188	0.026	0.353	1.880
	observe:	0	2	10	0	2	6
scatfix	predict:	0.042	0.799	5.846	0.035	0.442	2.283
	observe:	0	3	10	0	2	6
scatnn	predict:	0.035	0.660	4.877	0.030	0.392	2.119
	observe:	0	2	8	0	2	6
scatboth	predict:	0.044	0.899	7.230	0.035	0.466	2.489
	observe:	0	3	10	0	2	6
tgdedx	predict:	0.029	0.578	4.188	0.026	0.353	1.880
	observe:	0	2	12	0	2	9
tgepi	predict:	0.097	1.331	9.622	0.086	0.877	4.119
	observe:	0	4	17	0	3	10
tgtrack	predict:	0.030	0.605	4.250	0.026	0.362	1.861
	observe:	0	2	8	0	2	6
timcon	predict:	0.118	1.380	9.406	0.103	0.871	4.280
	observe:	0	3	16	0	3	10
ic	predict:	0.051	0.838	5.712	0.040	0.428	2.140
	observe:	0	3	9	0	2	6
b4ekz	predict:	0.128	2.479	18.263	0.122	1.686	8.979
	observe:	0	5	19	0	4	9
bhtrs	predict:	0.032	0.587	4.195	0.028	0.352	1.871
	observe:	0	2	8	0	2	6
cuts turned off		double-beam kaon-entering loose1	loose2	loose3	double-beam pion-entering loose1	loose2	loose3
none	predict:	0.007	0.059	0.398	0.023	0.130	0.709
	observe:	0	0	0	0	0	1
fiducial	predict:	0.007	0.059	0.398	0.023	0.130	0.709
	observe:	0	0	0	0	0	1
scatfix	predict:	0.007	0.056	0.389	0.023	0.129	0.700
	observe:	0	0	0	0	0	1
scatnn	predict:	0.008	0.059	0.398	0.023	0.129	0.709
	observe:	0	0	0	0	0	1
scatboth	predict:	0.008	0.062	0.411	0.028	0.259	1.617
	observe:	0	0	0	0	0	2
tgdedx	predict:	0.007	0.059	0.395	0.021	0.128	0.706
	observe:	0	0	0	0	0	3
tgepi	predict:	0.008	0.066	0.446	0.039	0.497	3.362
	observe:	0	0	0	0	0	1
tgtrack	predict:	0.007	0.058	0.392	0.024	0.169	1.000
	observe:	0	0	0	0	0	1
timcon	predict:	0.008	0.058	0.412	0.026	0.176	1.030
	observe:	0	0	0	0	0	1
ic	predict:	0.009	0.065	0.426	0.028	0.251	1.577
	observe:	0	0	1	0	0	1
b4ekz	predict:	0.046	0.362	2.424	0.151	1.082	6.574
	observe:	0	0	1	0	0	10
bhtrs	predict:	0.008	0.061	0.398	0.026	0.138	0.713
	observe:	0	0	0	0	0	1

Table 16: Predicted and observed numbers of beam background events in the 2/3 1998 data sample, obtained by simulataneously loosening the bifurcated beam function cuts. The particular beam function cuts which are loosened, as well as the meanings of "loose1", "loose2", and "loose3" in the head of the Table, are described in the 1/3 1998 analysis note. Background predictions and observations are made with various pathology cuts, grouped into classes (see Table 9), turned off.

run	event	R	E	P	$bgpv$	$bgtd$	$t_\pi - t_K$
*37412	61504	33.19	120.00	211.36	0.946	0.	0.948
37591	11840	36.73	123.30	219.12	0.159	0.	0.499
*37677	58928	38.41	129.52	227.77	0.177	0.692	0.538
38228	62030	36.43	122.78	216.04	0.354	0.130	1.193
38392	65042	33.97	120.29	218.10	0.610	0.206	0.645
38443	4556	34.70	123.59	218.17	0.134	0.	1.603
38470	165821	38.83	123.44	224.32	0.861	0.	0.919
38570	2446	34.60	119.19	214.51	0.702	0.	1.056
38570	2446	34.60	119.19	214.51	0.702	0.	1.056
38834	44801	36.39	121.32	220.22	0.427	0.	0.665
*39156	199501	36.90	128.06	221.98	0.690	0.130	0.929
*39172	264604	34.73	118.68	218.46	0.537	0.	0.929
*39250	191824	33.94	117.29	215.02	0.537	0.	0.821
*39515	92044	38.36	120.44	222.64	0.348	0.025	0.283
39642	100646	35.21	119.71	219.19	0.690	0.	0.792
*40493	166453	36.21	120.29	223.37	0.134	0.	0.411
40590	101923	32.75	116.78	214.95	0.885	0.	1.046

Table 17: Events observed in the single-beam kaon-entering correlation study. See the text for more details.

run	event	R	E	P	$bgpv$	$bgtd$	$t_\pi - t_K$
*37412	61504	33.19	120.00	211.36	0.946160	0.	0.948
38443	4556	34.70	123.59	218.17	0.134294	0.	1.603
38470	165821	38.83	123.44	224.32	0.860701	0.	0.919
38570	2446	34.60	119.19	214.51	0.701990	0.	1.056
38570	2446	34.60	119.19	214.51	0.701990	0.	1.056
*39172	264604	34.73	118.68	218.46	0.537175	0.	0.929
*39250	191824	33.94	117.29	215.02	0.537175	0.	0.821
39592	166106	36.21	127.18	219.85	0.518862	0.	0.811
*39642	100646	35.21	119.71	219.19	0.689781	0.	0.792
*40493	166453	36.21	120.29	223.37	0.134294	0.	0.411

Table 18: Events observed in the single-beam pion-entering correlation study. See the text for more details.

the "function" cuts (PV, $K_{\pi 2}$ kinematic, TD, $K_{\mu 2}$ kinematic (range-tail or band), and beam). The fixed scattering cuts and Princeton safety cut are included in this study; the UTC safety cuts and the pileup cut are not (they were not in the summary ntuple at the time this study was performed). The only strange events observed here are the $K_{\mu 2}$ (and "signal") events which were already seen in the 16-event $K_{\mu 2}$ sample and in the outside-the-box correlation tests.

At the time this study was performed, the final function cut positions were at

- PV: $bgpv < 1$
- $K_{\pi 2}$ kinematic: $bgkp2 < 0.00318$
- TD: $bgtd < 1$
- $K_{\mu 2}$ range tail kinematic: $bgkm2t < 0.008405$
- muon-band kinematic: $bgkm2b < 0.003284$

and the final background levels (as measured on 2/3 1998, after fixed scattering cuts were applied) were

- $K_{\pi 2}$: 0.035 (single bifurcation, based on 1 event)
- $K_{\mu 2}$ range tail: 0.024 (single bifurcation, based on 3 events)
- muon band: 0.008 (single bifurcation, based on 2 events)
- single beam: 0.0025
- double beam: 0.00005
- CEX: 0.0122

These numbers are used in the following subsections.

5.5.1 PV

There is 1 event in the 2/3 1998 data sample which fails just the PV function cut. This event is

run	event	R	E	P	$bgpv$	$bgkp2$	$bgtd$	$bgkm2t$	$bgkmtb$
40640	22691	33.23	116.76	212.19	8.68	0.0019	0.00	0.0000	0.0030

This event has R, E, and P consistent with $K_{\pi 2}$ resolution tail. The $K_{\pi 2}$ background for 1998 is 0.035, and the PV rejection is about 50, so we expect $0.035 \cdot 50 \cdot 2/3 = 1.2$ events to fail just the PV, which is consistent with the 1 event observed.

5.5.2 $K_{\pi 2}$ Kinematics

There are 4111 events in the 2/3 1998 data sample which fail just the $K_{\pi 2}$ kinematic function. 2 of these fail only EBOX, and one fails only PBOX, but these 3 events fail so badly that they are outside the range of calibrated function values:

run	event	R	E	P	*bgpv*	*bgkp*2	*bgtd*	*bgkm2t*	*bgkmtb*
37082	172507	33.34	106.91	214.99	0.75	999.0000	0.00	0.0000	0.0000
37230	134809	32.80	101.84	212.04	0.10	999.0000	0.00	0.0000	0.0029
40657	185794	33.11	117.53	206.17	0.35	999.0000	0.00	0.0000	0.0033

There are 8 events which have $K_{\pi 2}$ kinematic function values within the range of calibrated values:

run	event	R	E	P	*bgpv*	*bgkp*2	*bgtd*	*bgkm2t*	*bgkmtb*
37524	37084	31.98	113.40	209.96	0.89	0.4084	0.00	0.0000	0.0030
37542	99037	32.21	118.73	208.60	0.52	0.4565	0.62	0.0000	0.0030
39228	119009	32.14	113.14	209.84	0.95	0.6143	0.00	0.0000	0.0030
39501	104692	32.16	114.14	209.21	0.54	0.1762	0.00	0.0000	0.0030
39773	16286	33.20	116.34	210.62	0.26	0.0131	0.39	0.0000	0.0031
40314	139348	32.01	115.76	208.58	0.82	0.4999	0.03	0.0000	0.0030
40645	192839	33.50	114.19	210.97	0.35	0.1116	0.33	0.0000	0.0031
40736	91328	32.40	114.96	209.90	0.44	0.0977	0.00	0.0000	0.0030

All of these events are clearly $K_{\pi 2}$. The $K_{\pi 2}$ background for 1998 is 0.035; the final $K_{\pi 2}$ kinematic function cut position is at $bgkp2 < 0.00318$; and the range of calibrated $K_{\pi 2}$ kinematic function values is $[0, 1]$; so we expect $0.035 \cdot 1/0.00318 \cdot 2/3 = 7.3$ events to fail just the $K_{\pi 2}$ kinematic function, which is consistent with the 8 observed.

5.5.3 TD

There are 6 events in the 2/3 1998 data sample which fail just the TD cuts: 2 fail FITPI (and so don't have meaningful 2nd-pulse quantities in the stopping counter, $bgtd = 1099$), 1 fails just ELVETO ($bgtd = 134$), 2 fail just the TD function ($bgtd = 3.1, 22.2$), and 1 fails both EV5 and ELVETO ($bgtd = 352$):

run	event	R	E	P	*bgpv*	*bgkp*2	*bgtd*	*bgkm2t*	*bgkmtb*
37400	51443	38.60	128.15	228.06	0.67	0.0000	1099.00	0.0058	0.0030
38689	2291	38.16	122.21	225.05	0.35	0.0000	133.64	0.0017	0.0030
39120	180802	35.95	123.80	215.94	0.09	0.0000	22.23	0.0000	0.0032
39180	56327	37.07	125.58	224.83	0.13	0.0000	3.10	0.0015	0.0029
39956	33971	35.66	120.11	228.97	0.05	0.0000	351.82	0.0083	0.0000
40571	126287	37.68	125.09	228.72	0.62	0.0000	1099.00	0.0076	0.0000

All 6 of these events show up in the 16-event $K_{\mu 2}$ sample. Events 1, 5, and 6 are range-tail events; events 2 and 3 are muon-band events (event 2 has the L/R ambiguity in the UTC, and migrates into the muon band after re-fit). Event 4 is the suspected signal event which fails TD due to its small $\pi \to \mu$ decay time ($tmuav = 11$ ns).

The $K_{\mu 2}$ range-tail and muon-band backgrounds for 1998 are 0.024 and 0.008 (including the "signal" event as a muon-band event). The final TD cut position is at $bgtd < 1$; the range of calibrated TD function values is $[0, 352]$; and because we know that the TD rejection in the range tail is roughly half that in the muon band after scattering cuts are applied, we expect $0.024 \cdot 352/2 \cdot 2/3 = 2.8$ range-tail events and $0.008 \cdot 352 \cdot 2/3 = 1.9$ muon-band events to fail just the TD cuts (excluding FITPI), which is consistent with the 1 range-tail event (after FITPI) and 3 muon-band events (including the "signal" event) observed.

5.5.4 $K_{\mu 2}$ Kinematics

There are 8 events in the 2/3 1998 data sample which fail just the $K_{\mu 2}$ kinematic functions: 1 fails just PBOX; 5 fail RBOX, EBOX, and RNGMOM; and 2 fail RBOX, EBOX, PBOX, and RNGMOM. Only 1 of these events has a function value within the range of calibrated values (the PBOX event):

run	event	R	E	P	$bgpv$	$bgkp2$	$bgtd$	$bgkm2t$	$bgkmtb$
36336	7099	38.65	119.84	237.20	0.43	0.0000	0.54	0.4957	0.0000

This event is a $K_{\mu 2}$ range-tail event. The $K_{\mu 2}$ range-tail and muon-band backgrounds for 1998 are 0.024 and 0.008 (including the "signal" event as a muon-band event). The final $K_{\mu 2}$ range-tail and muon-band kinematic function cut positions are at $bgkm2t < 0.008405$ and $bgkm2b < 0.003284$; and the range of calibrated function values is $[0, 1]$; so we expect $0.024 \cdot 1/0.008405 \cdot 2/3 = 1.9$ range-tail events and $0.008 \cdot 1/0.003284 \cdot 2/3 = 1.6$ muon-band events to fail just the $K_{\mu 2}$ kinematic functions, which is consistent with the 1 and 0 events observed.

5.5.5 Beam

There are 319 events which fail just the beam function cuts. 10 fail just the DELC cut. All of the rest (except 2) fail DELC and up to 6 other beam function cuts from other branches of the single- (and double-) beam background estimation structures. The 2 remaining events fail 4 and 5 beam function cuts, respectively. The 10 events which fail only DELC are

run	event	R	E	P	$bgpv$	$bgtd$	$rngmom\_val$	$t_\pi - t_K$
37412	61504	33.23	120.35	211.50	0.95	0.00	0.400586	0.948191
38470	165821	38.90	123.83	224.50	0.86	0.00	1.10405	0.918866
38891	93496	35.72	117.17	224.27	0.51	0.13	-0.713239	-0.439883
39172	264604	34.81	118.87	218.50	0.54	0.00	0.0683928	0.928642
39250	191824	33.95	117.38	214.95	0.54	0.00	0.283341	0.821115
39642	100646	35.22	119.79	219.12	0.69	0.00	0.0097704	0.791788
39656	119	37.58	126.45	227.60	0.21	0.03	-0.263801	0.244379
40308	116450	38.90	130.19	223.83	0.23	0.44	1.37763	-0.909091
40493	166453	36.27	120.41	223.34	0.13	0.00	-0.302882	0.410557
40775	43010	34.10	120.60	217.07	0.44	0.00	-0.302882	-0.596285

All of these events look like $K_{\pi 2}$ decay-in-flight or π_{scat} ($bgpv > 0$, $rngmom\_val \sim 0$), except perhaps for the 8th event listed which might be $K_{\mu 2}$ decay-in-flight ($bgtd > 0$, $rngmom\_val > 1$). The single-beam background in 1998 is 0.0025; the DELC rejection is about 4000, so we expect $0.0025 \cdot 4000 \cdot 2/3 = 6.7$ events to fail just the DELC cut, which is consistent with the 10 observed.

6 Opening the BOX

Fig. 10 shows a scatter plot of range vs. kinetic energy for events passing all other cuts in the analysis except for the cuts on range and kinetic energy. One event is observed in the signal region. This event comes from run 37443, event 176348 with range = 33.9 cm, kinetic energy = 117.4 MeV and momentum = 214.0 MeV/c.

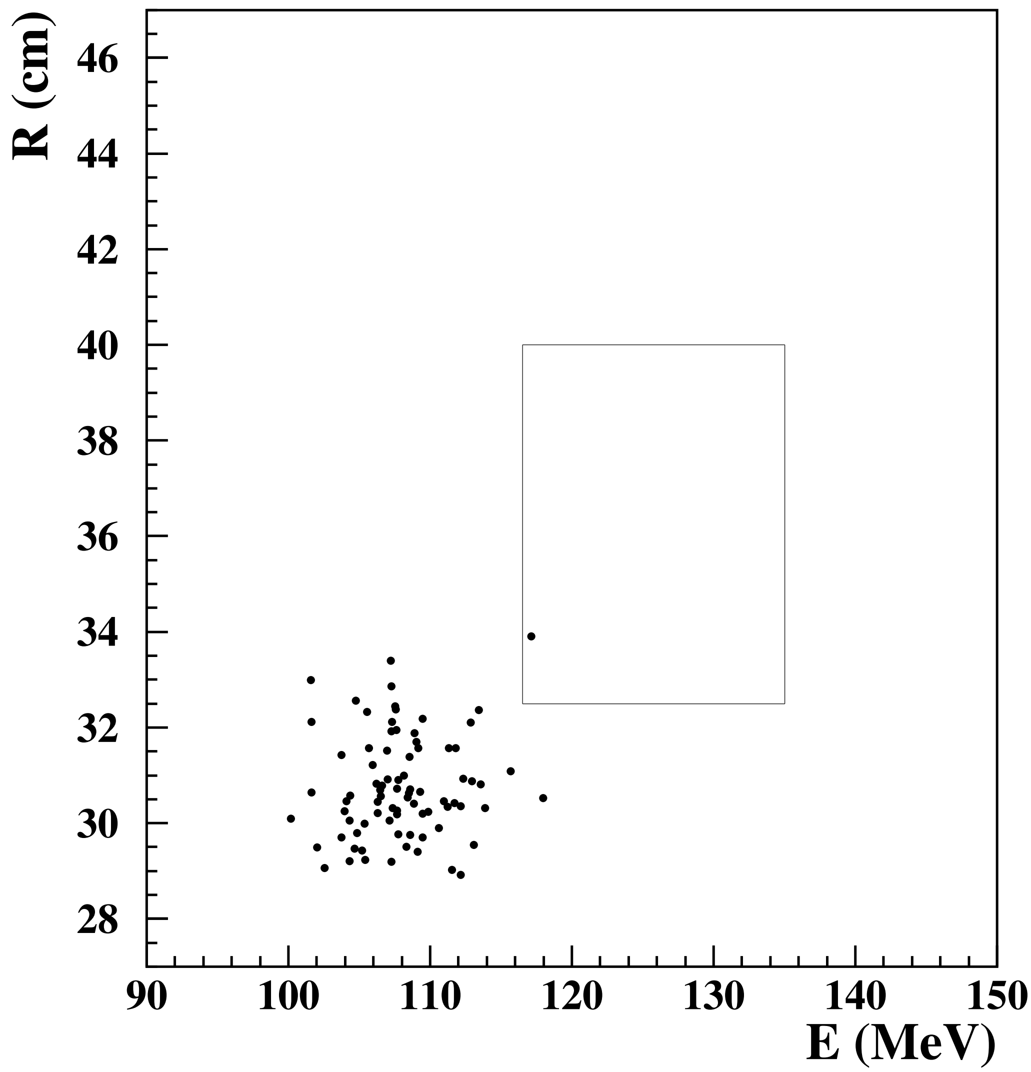

Figure 10: Range vs. kinetic energy distribution for 1998 $K^+ \to \pi^+ \nu \bar{\nu}$ data set with all cuts applied except for the cuts on range and kinetic energy. The box enclosing the signal region contains a single candidate event.

7 The candidate event

To verify this candidate event not to be a junk event or an background-like event, a detailed examination of this event is therefore conducted.

7.1 Event display

The event display for the candidate is shown in Fig. 11. The TDC and ADC plots in xy view are shown in Fig. 12. The reconstructions in target and UTC look clean and good. Hits from noise are far from the timing window. Target pattern recognition is performed well, and there is no ambiguity between kaon and pion fibers (see Fig. 13) since the pion fiber cluster is perpendicular to the kaon fiber cluster. The far end of kaon fiber matches the B4 hit position very well. Along the kaon fiber cluster, there is no other fiber or I-counter hit, indicating that the kaon doesn't stop at the edge of target or I-counter. The event has a nice UTC track fitting quality both in xy and rz views (see Fig. 11 and Fig. 13). The matching between UTC and Range Stack looks good and the track crosses two RSSC layers in xy plane, indicating a good measurement on both momentum and range. There are three extra well-isolated pion fiber hits in the target, the total energy is about 0.49 MeV, which is far below the 3.8 MeV threshold and can be treated as electronic noise.

7.2 TD pion identification

With regard to the pion particle identification, the TD pulse shapes (see Fig. 14) show a nice muon peak, which is well separated from the pion peak, indicating a very reliable pion signal.

7.3 E/P/R calibrations in the vicinity of the candidate event

Kinetic energy, range and momentum resolutions in that run measured by the $K_{\mu 2}$ monitor and skim1 $K_{\pi 2}$ events are found to be normal as shown in Fig. 15.

7.4 Basic information about this candidate

Some basic information about this event is given in Table 19.

7.5 Scalers

Fig. 16 shows the KB, Teff(effective spill length) and CK scaler distributions. The arrow indicates the corresponding scaler value for this candidate. The end-of-spill record shows normal value in magnetic field (9.94945 kG).

7.6 Probability of signal

To verify the candidate to be a signal, a number of quantities are checked, all of which are classified into four categories, including event reconstruction quality, kaon identification quality, pion identification and single particle quality. Probability functions are based on the reference distributions from these quantities.

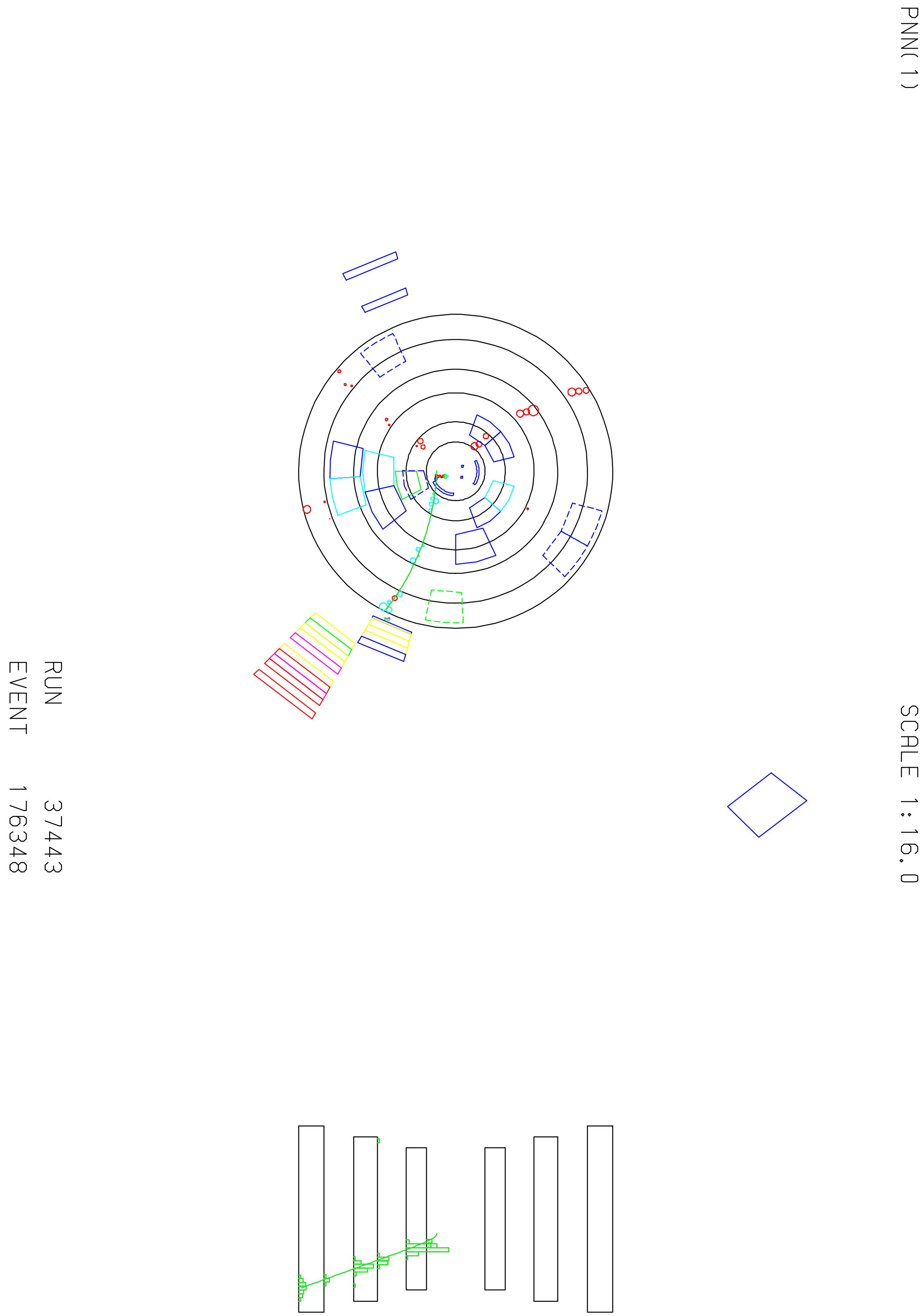

Figure 11: Event display in xy and z views

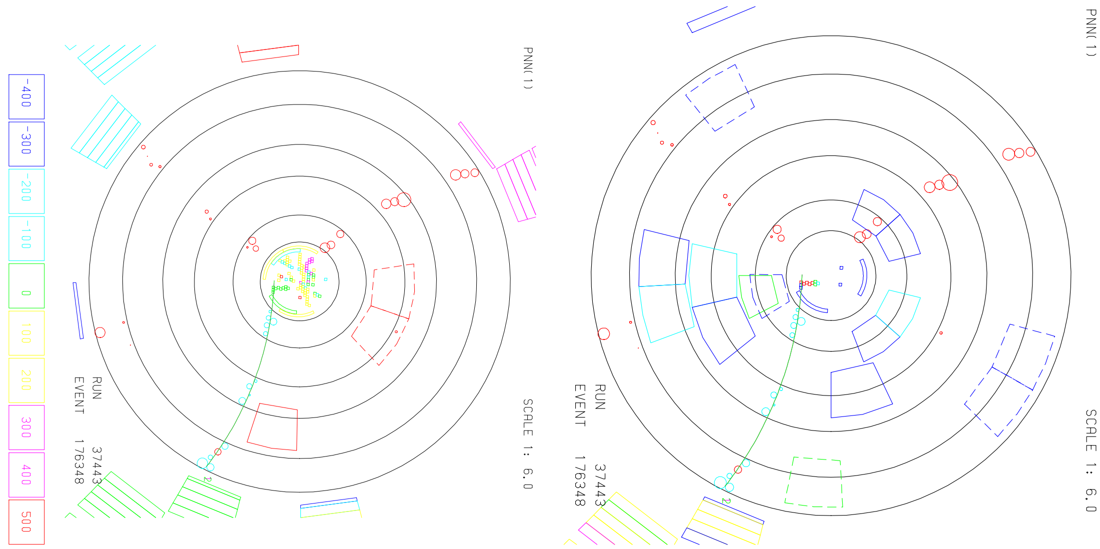

Figure 12: Event display: TDC(left) and ADC(right)

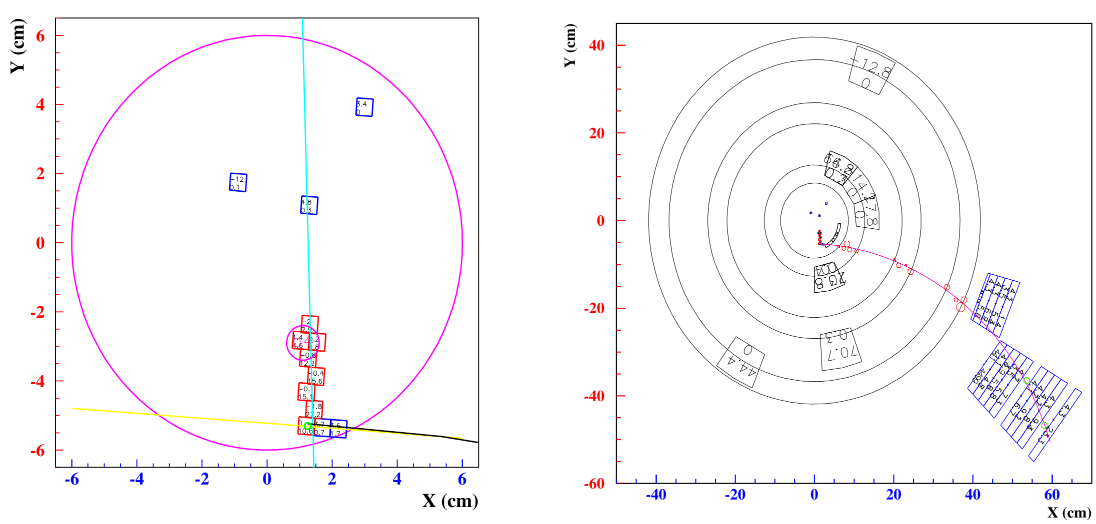

Figure 13: Event display: target plot(left) and RS plot(right)

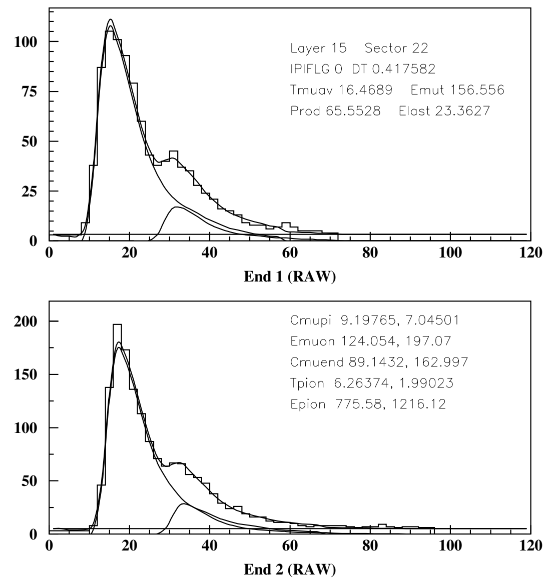

Figure 14: TD pulse shapes and fitting in the stopping counter.

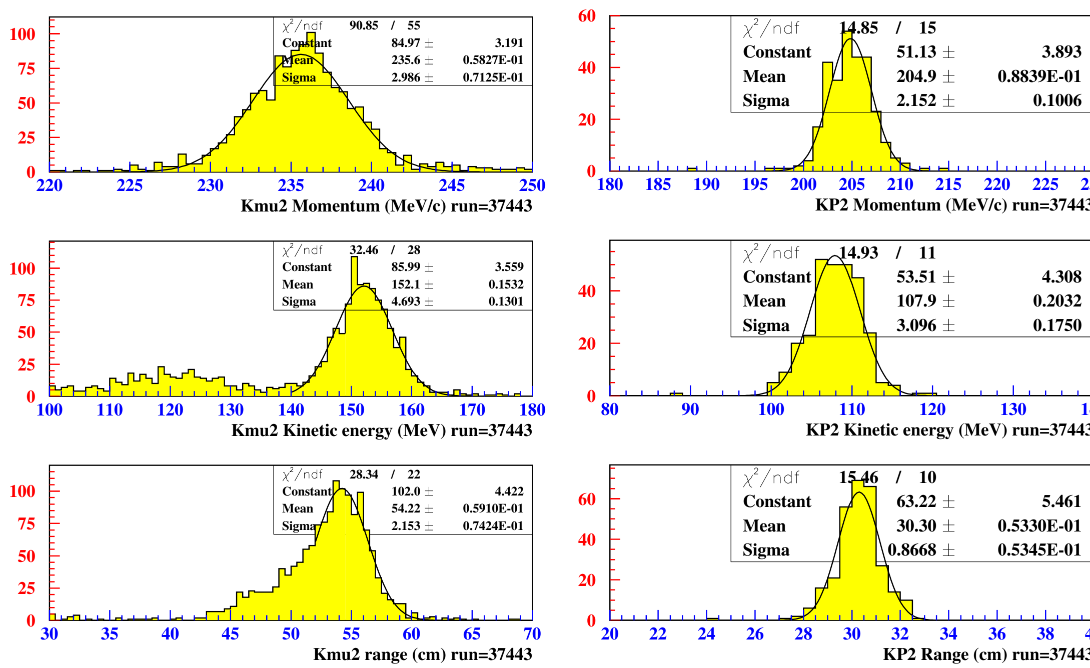

Figure 15: Kinetic energy, range and momentum for $K_{\mu 2}$ monitor and skim1 $K_{\pi 2}$ events in RUN 37443.

Run number	37443
Event number	176348
Tape number	22267.1.1
Data on which the event occurred	July 21, 1998
Pion stopping sector in RS	22
Pion stopping layer in RS	15
Kaon time in target (t_K)	-0.5 ns
Pion time in target (t_π)	3.7 ns
Pion time in RS (trs)	4.1 ns
Pion lifetime	16.5 ns
Muon energy	3.42 MeV
Muon time	41.8 ns
Electron time	5333.1 ns
Total momentum of pion track	214.0 MeV/c
Total range of pion track	33.9 cm
Total kinetic energy of pion track	117.4 MeV
Pdev of pion track from $K_{\pi2}$ peak	3.68
Edev of pion track from $K_{\pi2}$ peak	3.69
Rdev of pion track from $K_{\pi2}$ peak	2.61
Kaon energy in target	92.98 MeV
Pion energy in target	2.75 MeV
Pion range in target	1.9 cm
Cos3d of the pion track	0.34
Phi0 of the pion track	-0.06
z of kaon decay vertex	4.59 cm
(x, y) of kaon decay vertex	(1.25, -5.30) cm

Table 19: Basic information about this candidate

7.6.1 Reconstruction quantities

To make sure the candidate event is of good reconstruction quality, a number of reconstruction quantities involving all relevant sub-detectors are checked. The reconstruction quantities include the timing consistency (see Fig. 17), target kaon reconstruction (see Fig. 18), target/IC pion reconstruction (see Fig. 19), UTC/target reconstruction (see Fig. 20) and Range Stack reconstruction (see Fig. 21). $\pi^+\nu\bar{\nu}$ Monte Carlo is used for the **zf** and **zutout** distributions. Skim3 sample is used for producing **rsdedx_chimax**, **prrf**, **prrfz1**, **prrfz2**, sigma(tmean-trs), sigma(zdtiff-zutc), sigma(z(ADC)-zutc) and sigma(ef-eph), in which the sigma is defined as

$$sigma = \sqrt{\frac{\sum(\Delta x)^2}{ndof} - (\frac{\sum \Delta x}{ndof})^2}. \tag{8}$$

Where Δx is the difference between the expected and the measured. The arrows point to the location of the candidate event in corresponding histograms.

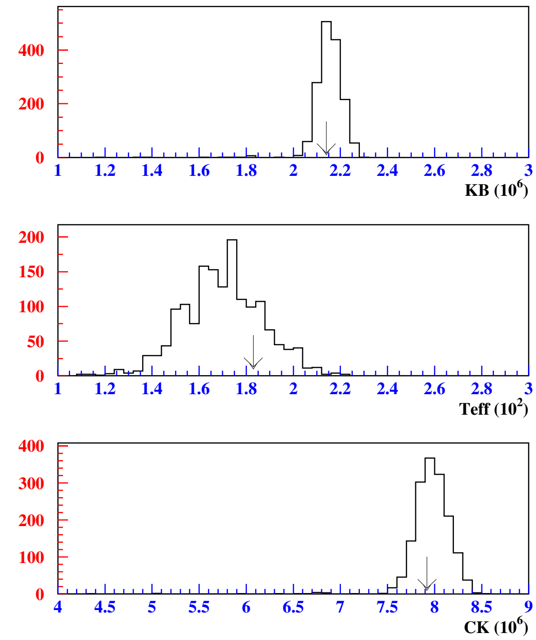

Figure 16: KB, Teff and CK scaler distributions.

7.6.2 Kaon identification

To check if the particle entering into target is a kaon, hits on Cerenkov counters, B4 counter and target are studied. Skim1 sample is used to produce the reference distributions with all cuts applied. Fig. 22 shows all relevant reference distributions and the corresponding candidate event positions.

7.6.3 Pion identification

In pion identification, two major informations need to be checked. One is the kinematic variables (see Fig. 23), the other is the Range Stack TD variables (see Fig. 24). The distributions of cos3d, momentum, range and kinetic energy are from $\pi^+\nu\bar{\nu}$ Monte Carlo. The rest variable distributions are from skim3 sample, which are dominated by π_{scat}.

7.6.4 Single particle identification

Single particle identification requires single kaon entering into the target and kaon decays into only one detectable particle. Therefore, no photon activity is detected and single beam is observed in the beam counters. The reference distributions for photon veto are obtained from $K_{\mu2}$ monitor, while those for single beam particle is from skim1 sample with all cuts applied. Fig. 25 and Fig. 26 show the quantities for single particle identification.

7.6.5 Probability of signal

Based on the reference distributions given above, probability for each quantity is computed for this candidate event (see Fig. 27). Depending on if the cut is on upper bound or on lower

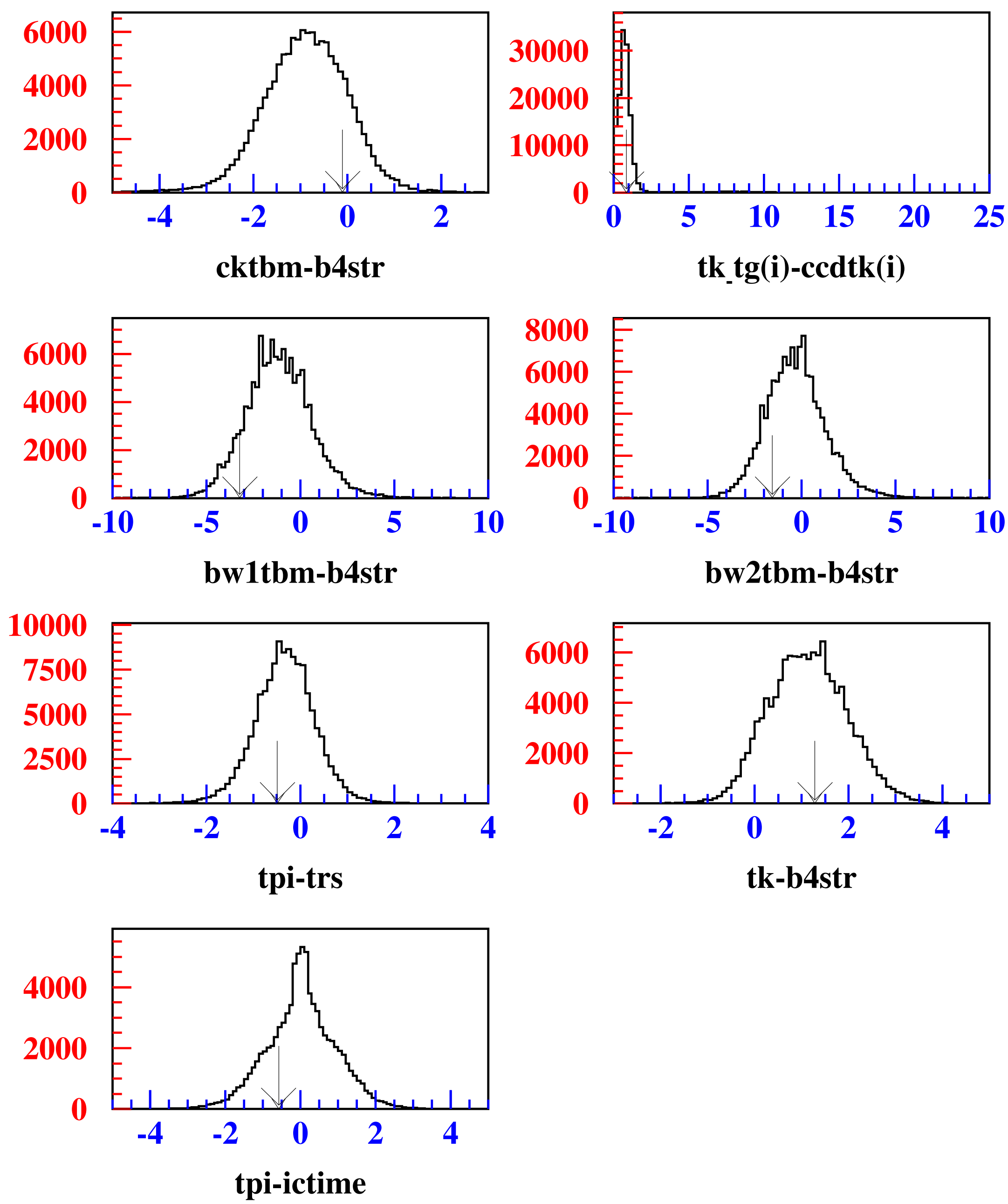

Figure 17: Quantities related to the timing consistency.

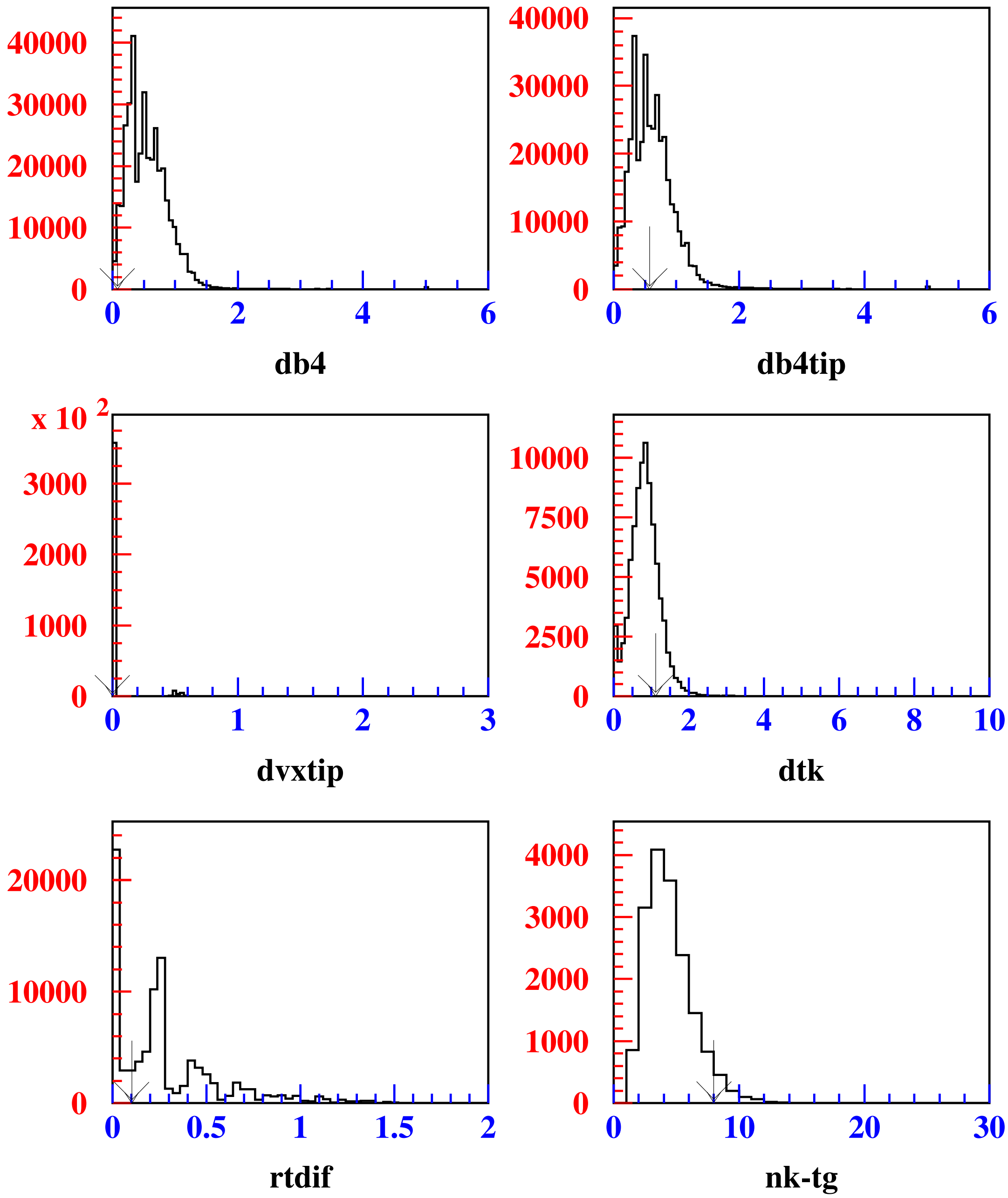

Figure 18: Quantities related to target kaon reconstruction.

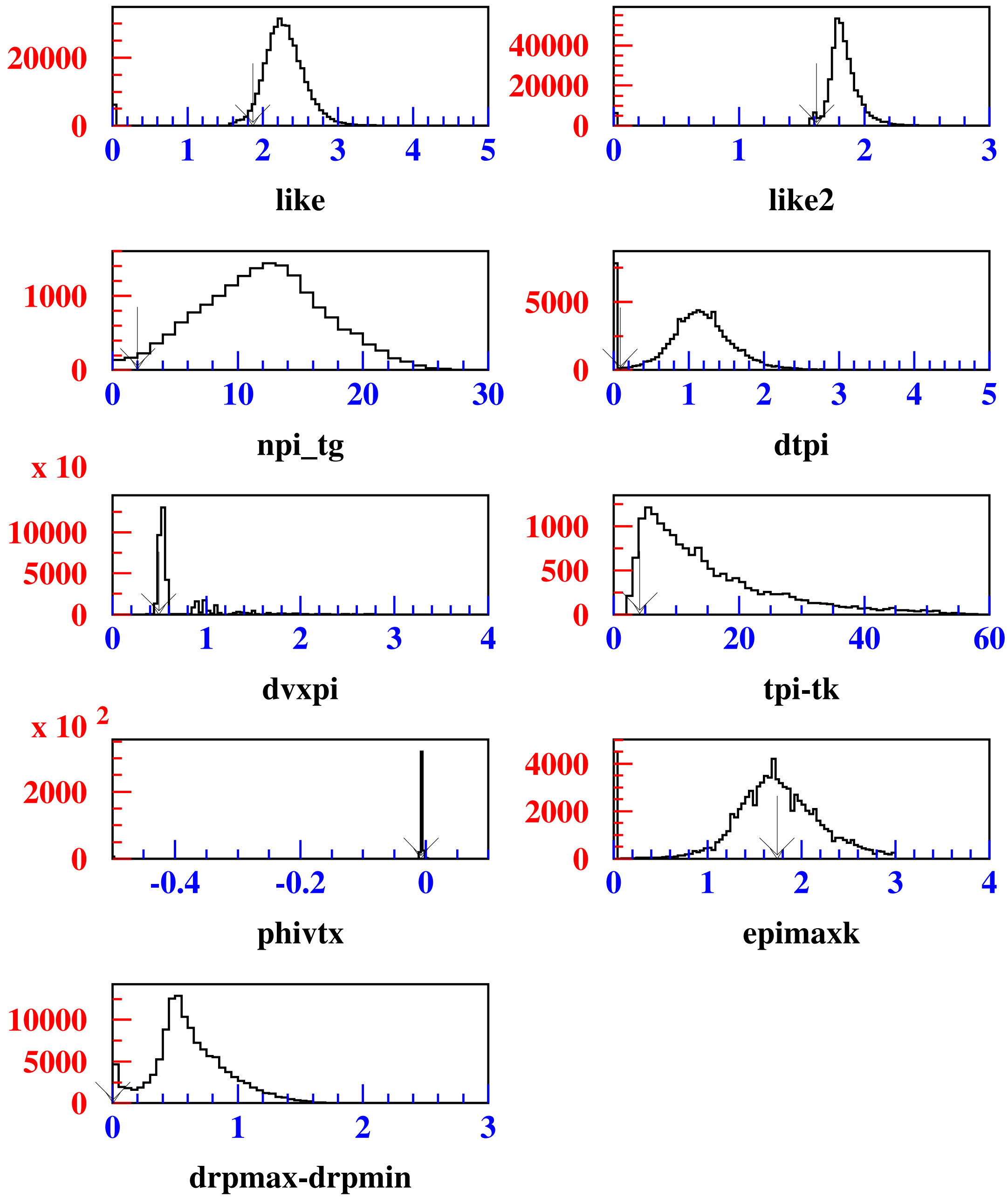

Figure 19: Quantities related to target/IC pion reconstruction.

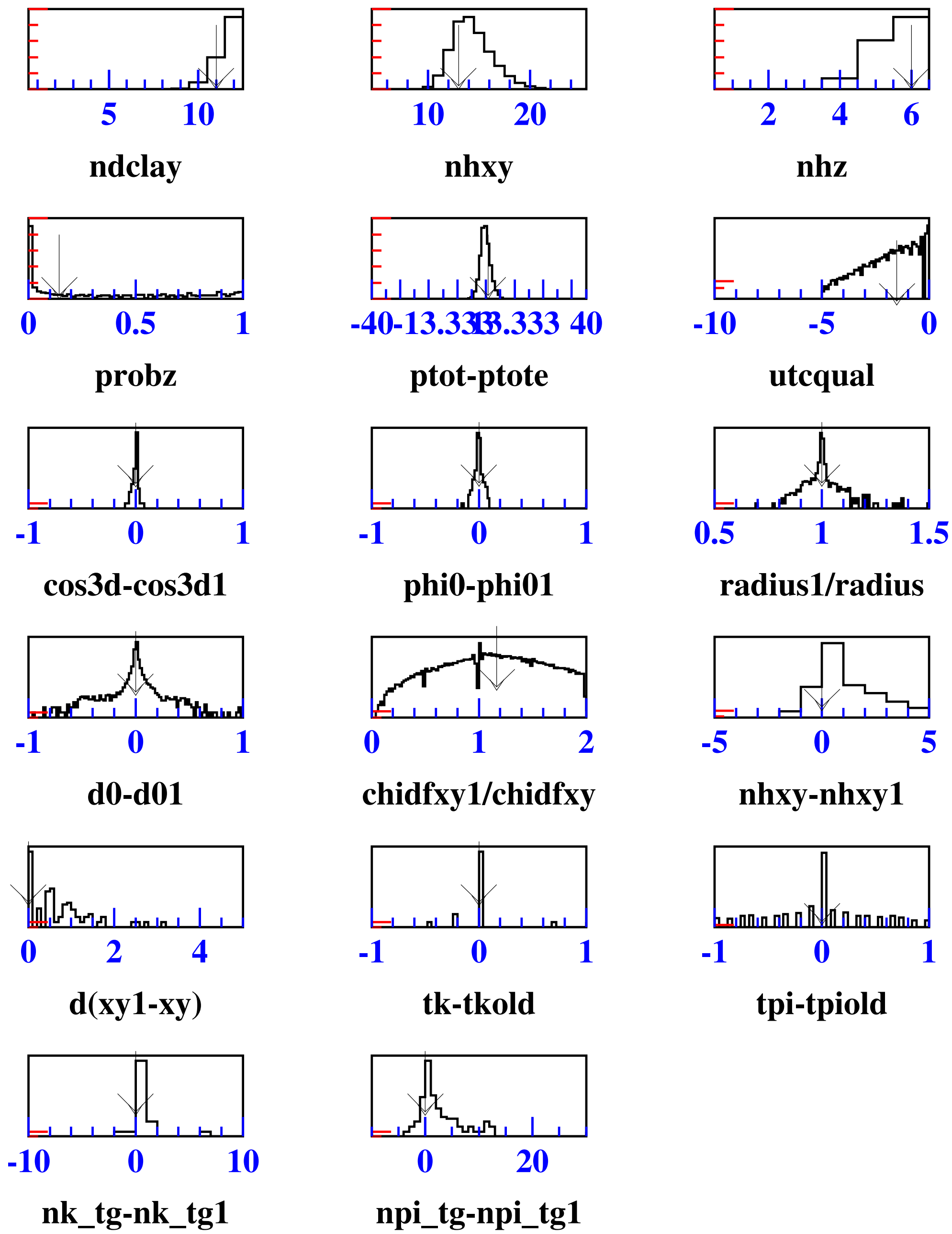

Figure 20: Quantities related to UTC/target reconstruction.

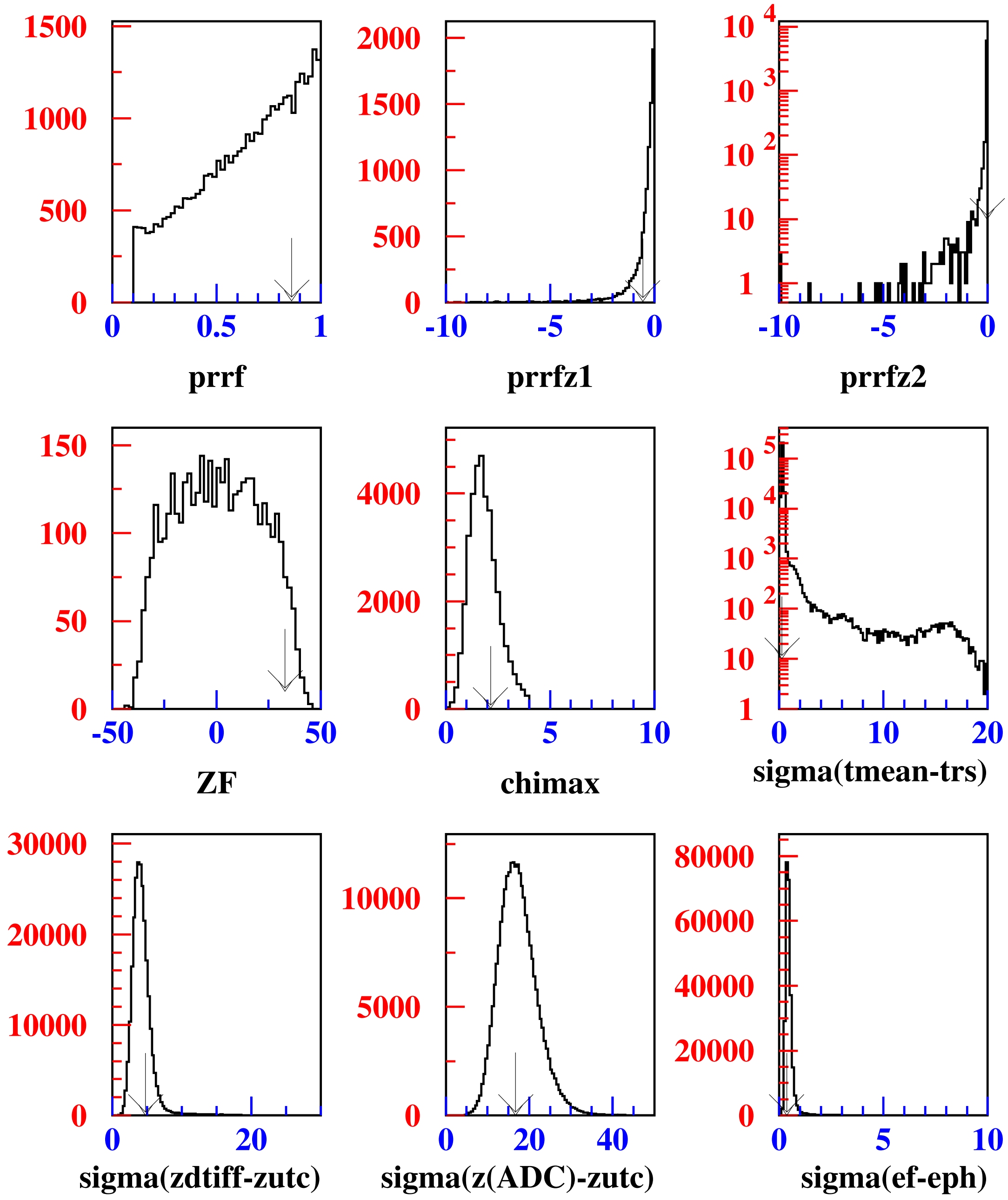

Figure 21: Quantities related to Range Stack reconstruction.

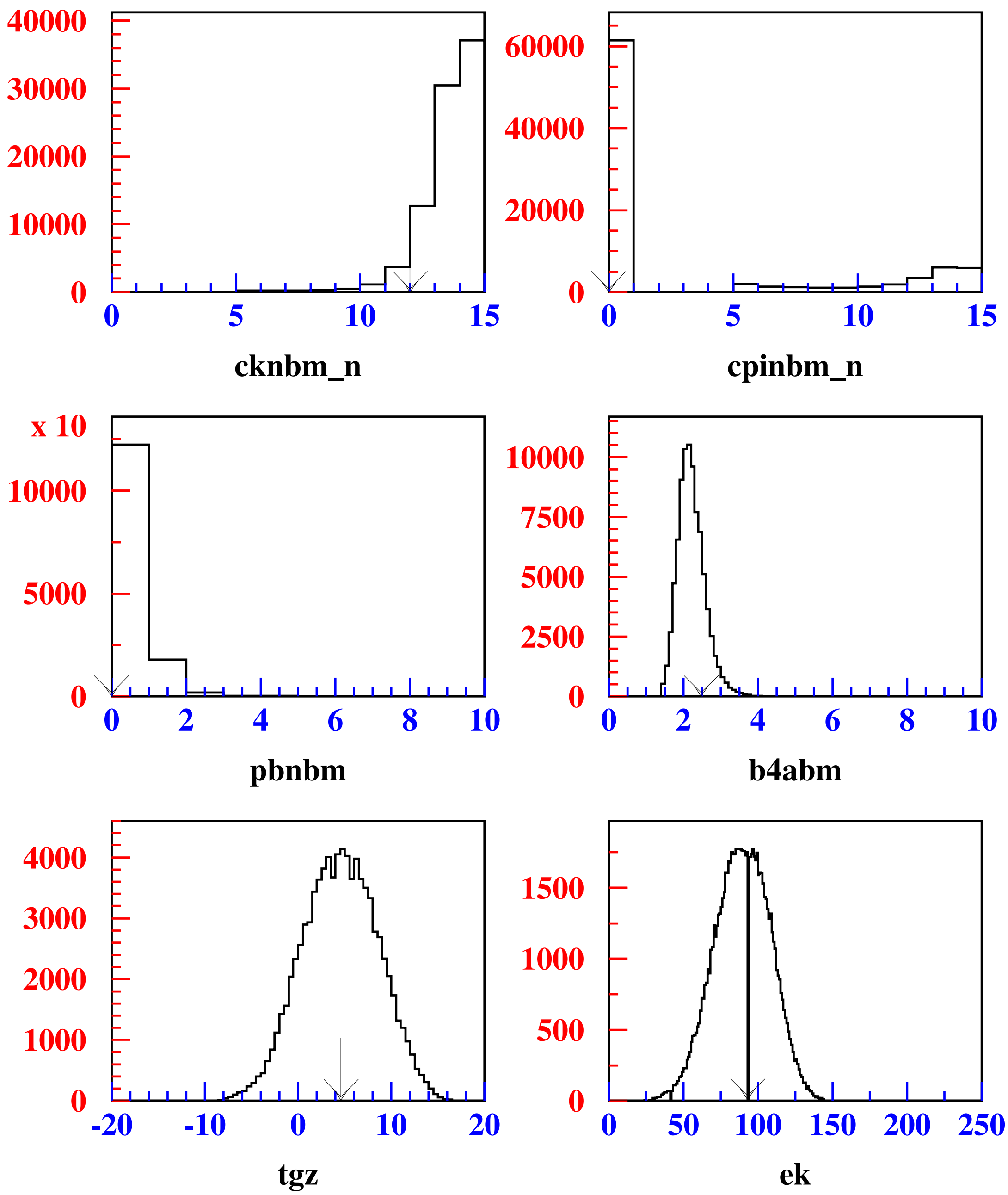

Figure 22: Quantities related to kaon particle identification.

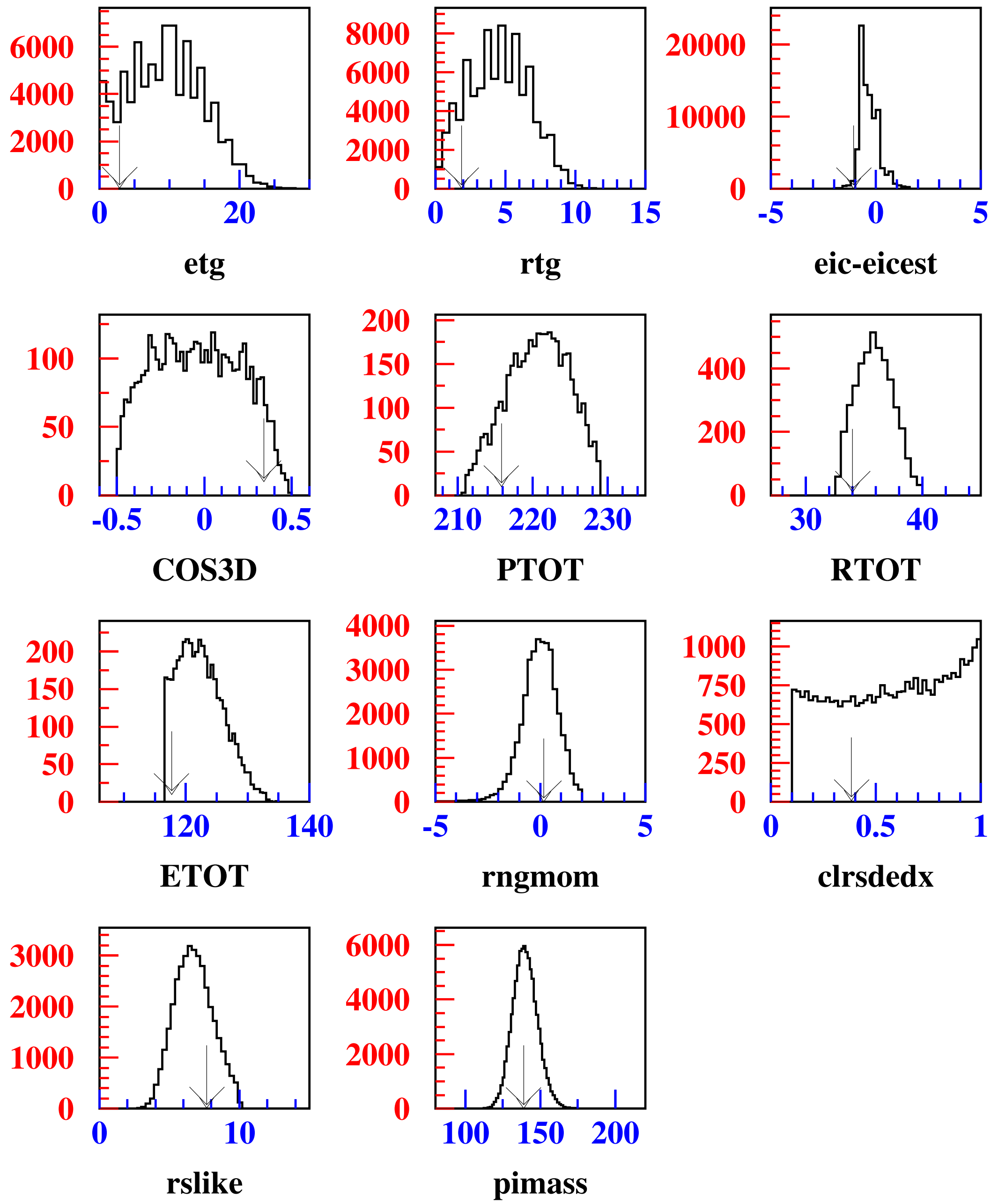

Figure 23: Quantities related to pion particle identification from kinematic variables.

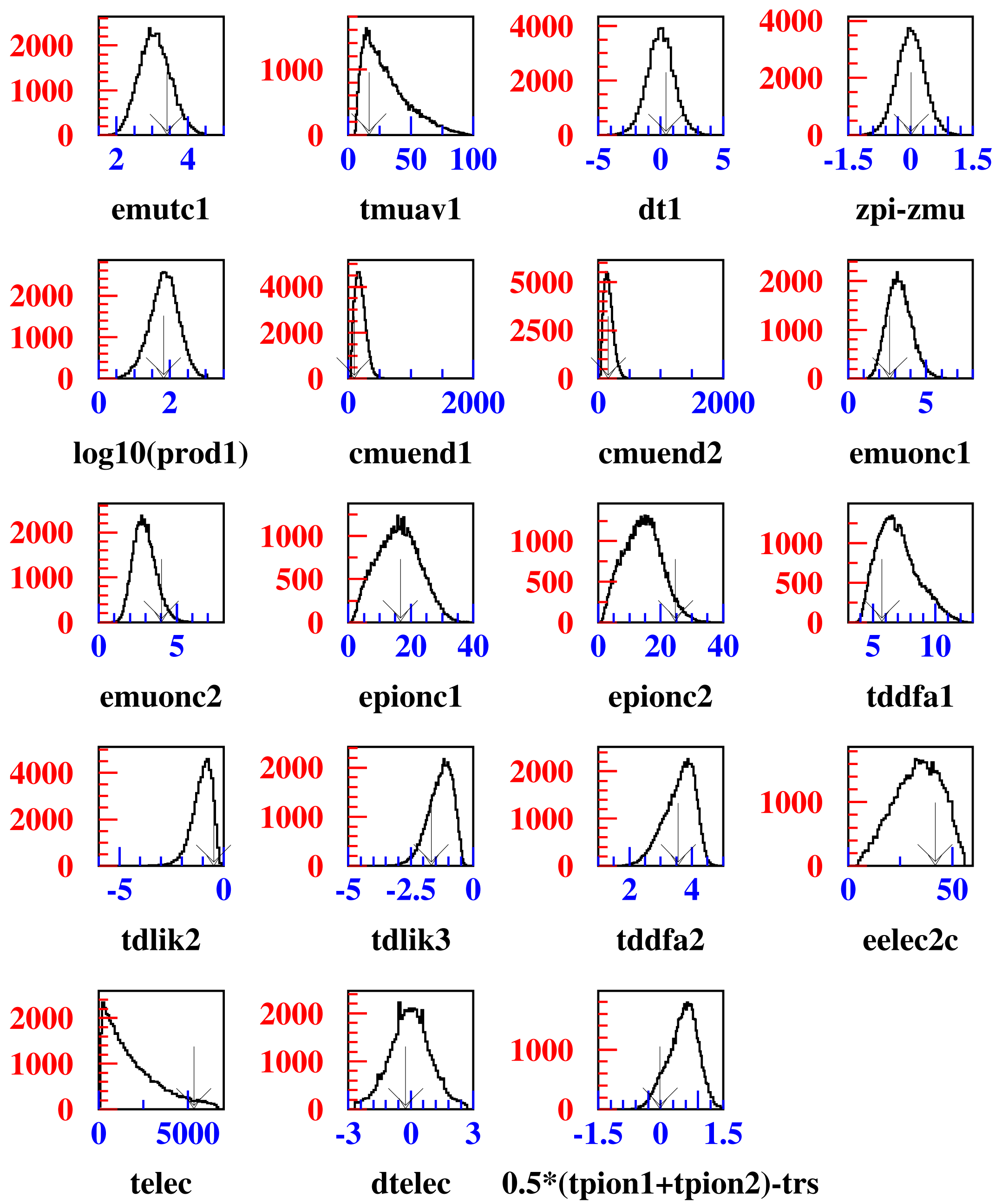

Figure 24: Quantities related to pion particle identification from TD variables.

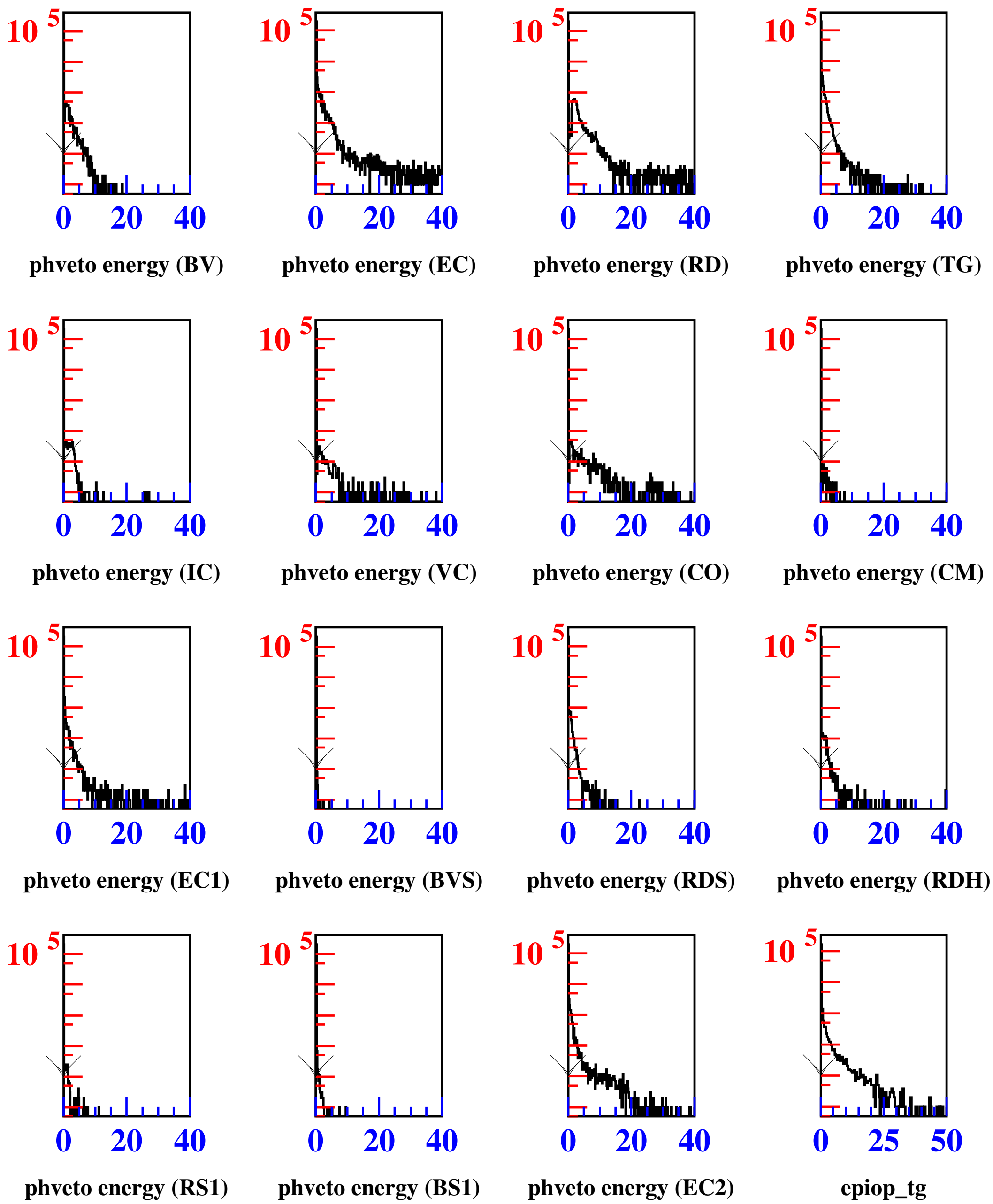

Figure 25: Quantities related to the detection of photon activities.

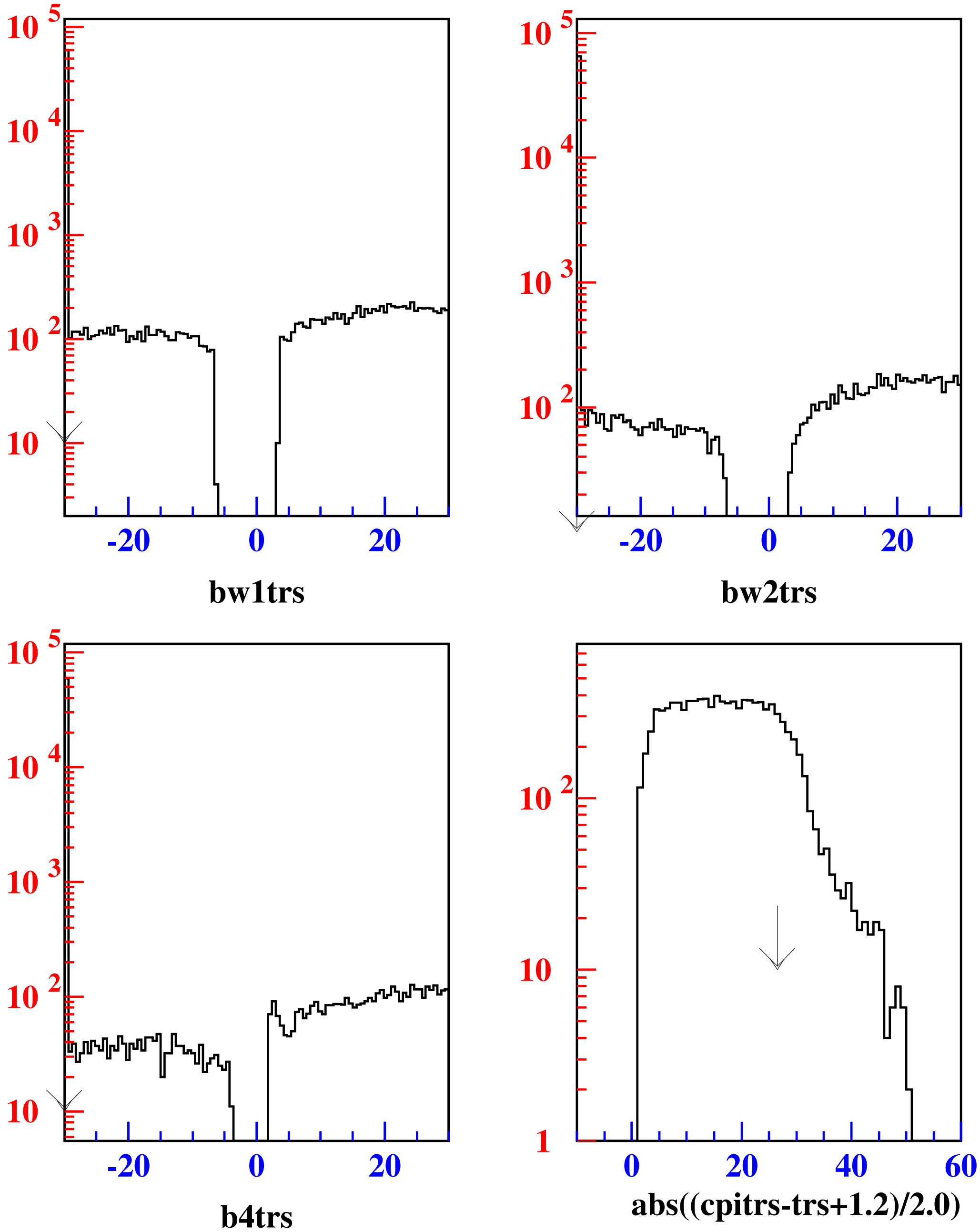

Figure 26: Quantities related to single beam detection.

bound or on both sides, the probability of each quantity is integrated to the location of the candidate event. By definition, background should distribute abound 0, while signal should be of flat distribution. The probabilities for reconstruction quality, kaon identification quality and pion identification quality do show a flat distribution, indicating that the candidate event is truly signal-like. However, for the distribution of single particle quality, there is a spike at 1, which is due to most of photon veto sub-detectors with no hit.

7.7 Possibility of being a CEX background

Since the $t_\pi - t_k$ is about $= 4.2$ ns, the possibility of being a CEX background is investigated. Based on the beam likelihood function and $t_\pi - t_k$, Monte Carlo CEX and $K_{\mu 2}$ monitor are used to constructed the NN functions. Fig. 28 shows the NN distributions for CEX and $K_{\mu 2}$ monitor, also shown is the NN location for the candidate. The NN distribution is flat for CEX background, while it peaks around 1.0 for $K_{\mu 2}$ monitor. The candidate event gives 0.95 NN value, which is still close to the peak position. Therefore, the possibility of being a CEX background is small, though one cannot totally exclude this possibility due to the small $t_\pi - t_k$.

7.8 Kinematic variable positions inside the BOX

In $\pi^+\nu\bar{\nu}$ analysis, the lower BOX position are defined as the deviations from the $K_{\pi 2}$ peaks. Fig. 29 shows the deviation position for the candidate event inside the BOX when all cuts are applied except for the one indicated in the plots. Since photon escapes from detection, the charged pion can pass all other cuts, resulting in a $K_{\pi 2}$ peak observed. This peak is strongly suppressed by lower BOX cut. In view of Pdev and Rdev, they are well separated from the $K_{\pi 2}$ background. A further checked is done by changing the lower BOX cuts to Rdev > 1.6, Edev > 1.25 and Pdev > 1.4, the departure positions given in the $K_{\pi 2}$ background function. 13 events are observed and scalled by 0.00147 for the $K_{\pi 2}$ background level at the standard lower BOX cut positions, yielding 0.019 $K_{\pi 2}$ background estimated inside the BOX. This value agrees with $0.012 \pm 0.003^{+0.001}_{-0.003}$ from the second bifurcation method.

Differing from the lower BOX cut, the upper BOX cut are directly set on the momentum, range and kinetic energy. Fig. 30 shows the kinematic position for the candidate event inside the BOX when all cuts are applied except for the one indicated in the plots. Apparently, one two $K_{\mu 2}$ tail events are observed outside the BOX. Since the upper momentum cut yield a rejection of about 50, leading to a 0.04 $K_{\mu 2}$ background estimated inside the BOX, which is consistent with $0.034 \pm 0.017^{+0.040}_{-0.017}$ from the second bifurcation method.

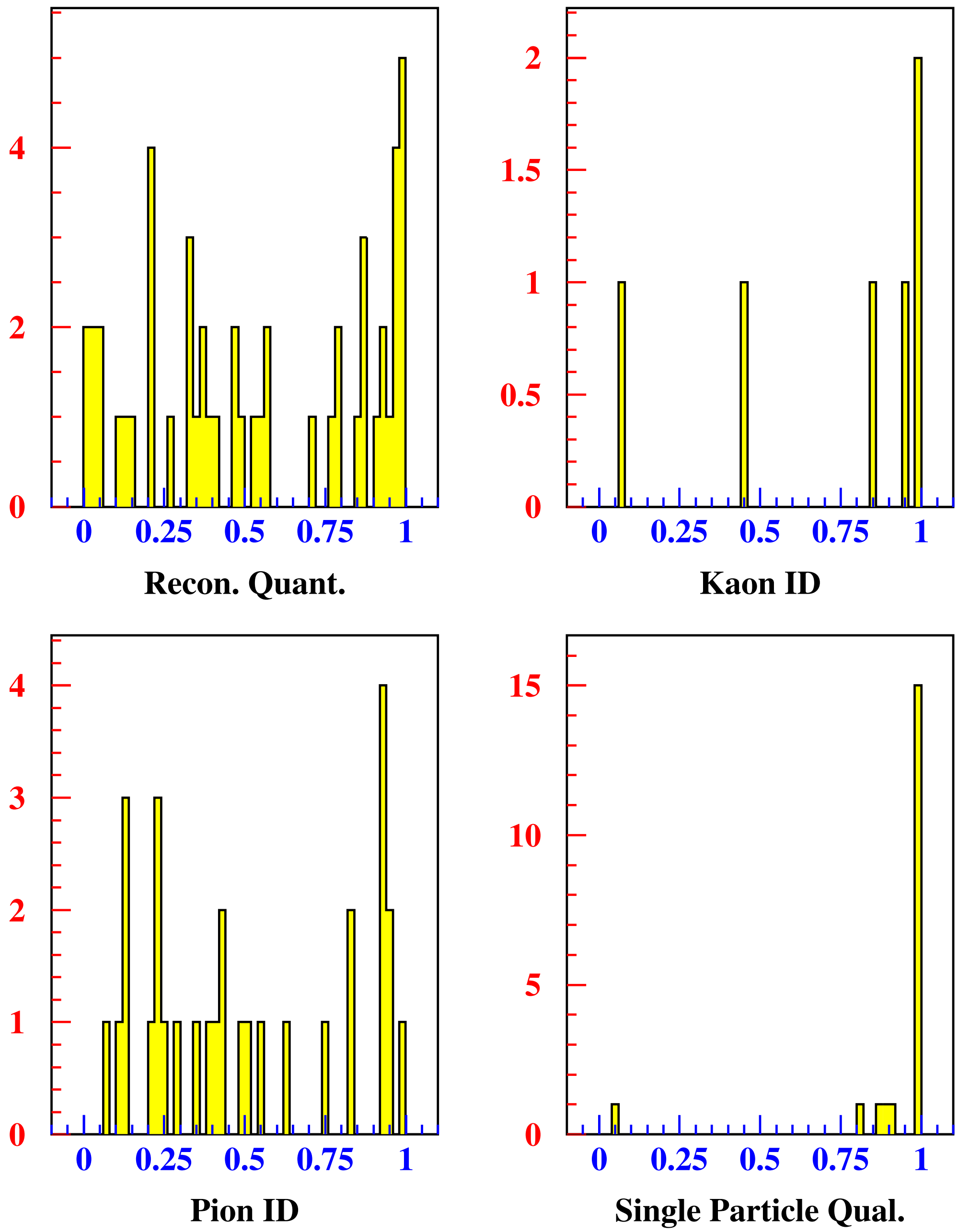

Figure 27: Probability of signal.

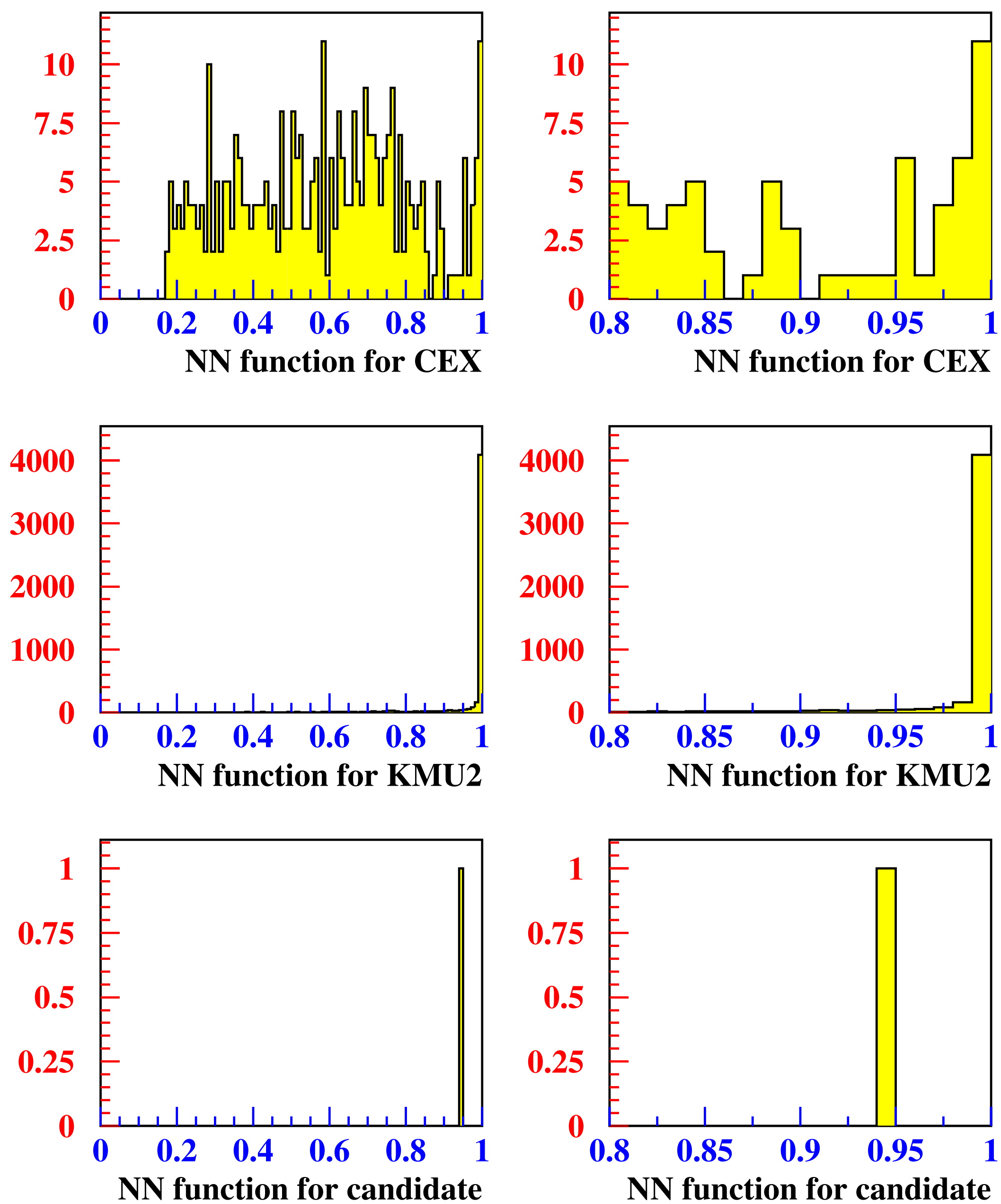

Figure 28: Examination of the possibility being a CEX background.

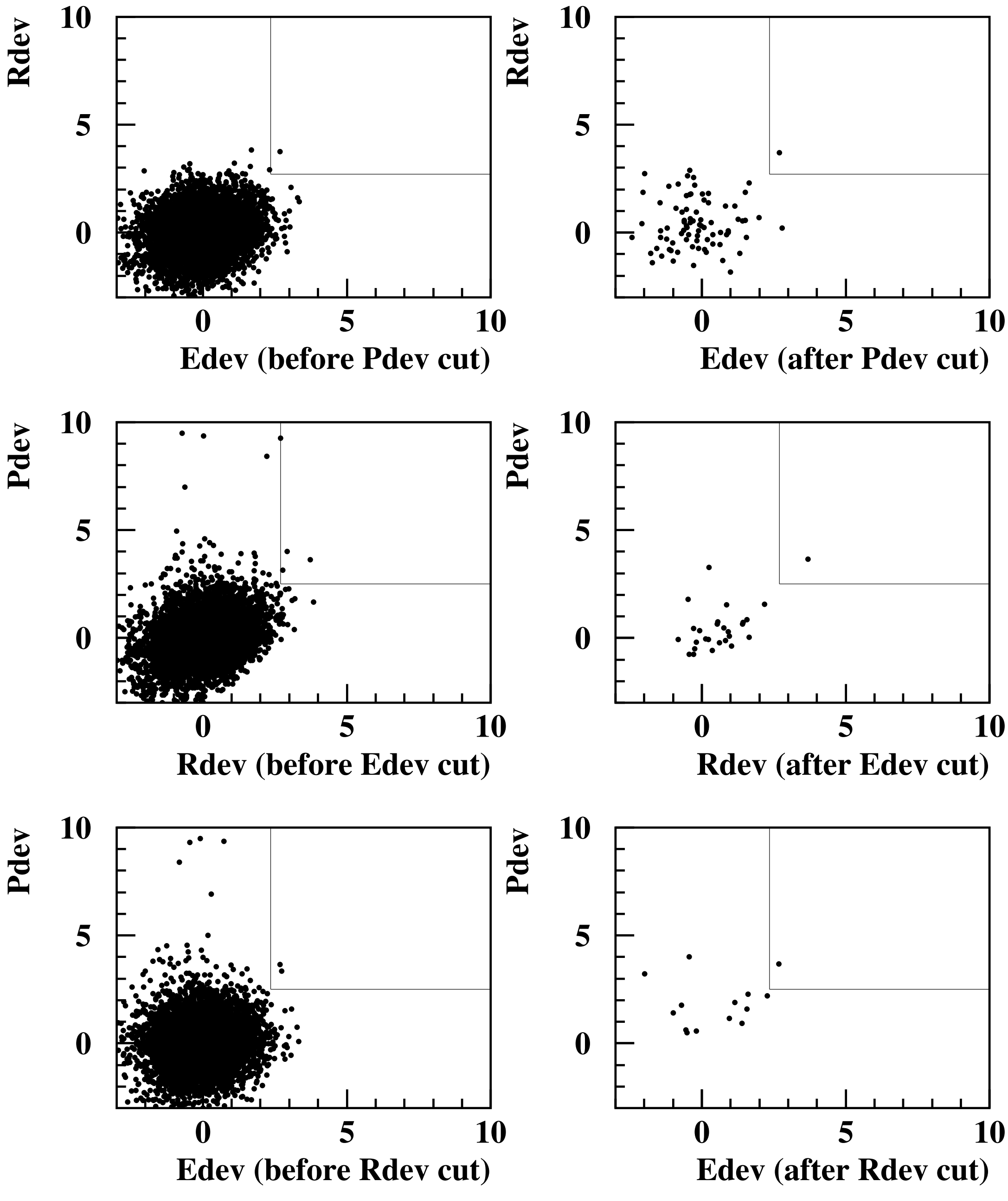

Figure 29: The scatter plots for the kinematic variable deviations from the $K_{\pi 2}$ peaks. Lower box cut positions are indicated by the solid lines.

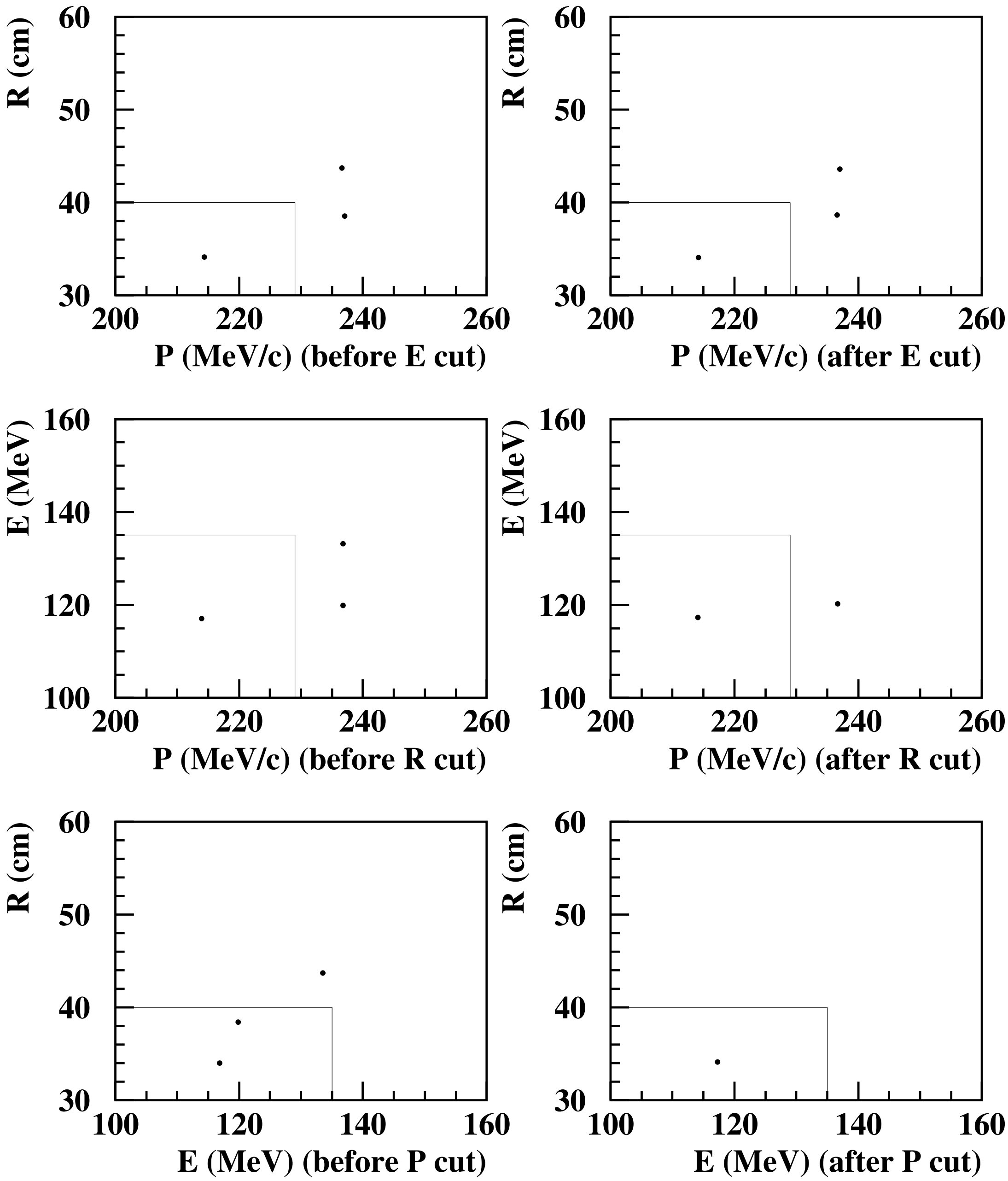

Figure 30: The scatter plots for the kinematic variables. Upper box positions are indicated by the solid lines.

Sample	$K_{Blive} \times 10^{12}$	Prescale (online)	Prescale (offline)	K_{Blive}^{eff}
$\pi^+\nu\bar{\nu}$	2.704	1	1	2.704 $\times 10^{12}$
$K_{\mu2}$	2.722	199888	1	1.362 $\times 10^{7}$
$K_{\pi2}$	2.724	140576	4	4.842 $\times 10^{6}$

Table 20: The total K_{Blive} values for $\pi\nu\bar{\nu}$, $K_{\mu2}$ and $K_{\pi2}$.

8 K_{Blive} of 1998

The quantity of K_{Blive} is defined as the number of kaons passing the KBeam trigger and entering the detector while each of them is still "live" or is not read out as a previous event. The total K_{Blive} are counted for $K_{\mu2}$, $K_{\pi2}$ and $\pi^+\nu\bar{\nu}$ respectively. In this procedure, bad runs are removed. For some unknown reasons, the run numbers in these three samples are different. In this analysis, the run numbers, which do not appearing in the $\pi\nu\bar{\nu}$ sample, are not used in getting the effective K_{Blive} (see Table 20). It is noted that there is a 0.8% difference between $(K_{Blive})_{\pi^+\nu\bar{\nu}}$ and $(K_{Blive})_{K_{\mu2}}$ or $(K_{Blive})_{K_{\pi2}}$, which is still unknown and will be treated as a systematic uncertainty for the total K_{Blive}. The final K_{Blive} used in estimating the sensitivity for $\pi^+\nu\bar{\nu}$ is

$$K_{Blive} = (2.70 \pm 0.02_{sys.}) \times 10^{12}. \tag{9}$$

Where statistic uncertainty is ignored.

9 Acceptance of 1998 data

The acceptance of 1998 data is measured in the same way as the 1995-1997 data analysis. The global measurement can be split into several studies on $K_{\mu2}$-based acceptance, $K_{\pi2}$-based acceptance, π_{scat}-based kinematic acceptance, π_{scat}-based TD acceptance, μ-veto acceptance due to accidental loss, T.2 efficiency, UMC-based acceptance and stopping fraction f_s evaluation.

9.1 $K_{\mu2}$-based acceptance

The structure and results of $K_{\mu2}$-based acceptance study are shown in Table 21. The acceptance is aimed at measuring pass1 reconstruction cuts; beam background cuts except those involving track energy in the target; kinematic pathology cuts except those involving track energy, scattering and fiducial region; online and offline photon veto cuts. The $K_{\mu2}(1)$ monitor sample is used for this measurement. All setup cuts are defined in Table 22. The final $K_{\mu2}$-based acceptance is

$$A_{K_{\mu2}} = 0.4191 \pm 0.0005_{stat.}. \tag{10}$$

Cut	1998 (acceptance)
SETUP$_{rd}$	1782053 (0.00000)
RD_TRK	1782053 (1.00000)
TRKTIM	1780981 (0.99940)
A$_{RD}$	0.9994 ± 0.0000
SETUP$_{recon}$	903807
UTC/RANGE	903807 (1.00000)
UTCQUAL	878005 (0.97146)
TARGET	876143 (0.99788)
A$_{recon}$	0.9694 ± 0.0002
SETUP$_{rest}$	1077148
ICBIT	1077148 (1.00000)
TIC	1068441 (0.99192)
TIMCON	1060353 (0.99243)
DCBIT	940988 (0.88743)
DELCO2	902381 (0.95897)
TGCCD	863232 (0.95662)
DELCO	788384 (0.91329)
CKTRS	783661 (0.99401)
CKTAIL	757567 (0.96670)
B4DEDX	746955 (0.98599)
CPITRS	745760 (0.99840)
CPITAIL	745537 (0.99970)
PSCUT	741692 (0.99484)
TARGF	716580 (0.96614)
DTGTTP	716514 (0.99991)
RTDIF	709064 (0.98960)
TGQUALT	709064 (1.00000)
PIGAP	702294 (0.99045)
TGB4	680991 (0.96967)
KIC	676712 (0.99372)
TGGEO	674666 (0.99698)
EIC	654021 (0.96940)
EICKIN	654021 (1.00000)
B4EKZ	640372 (0.97913)
B4EKZ_IC	640372 (1.00000)
TGZFOOL	640372 (1.00000)
TGCUT	640328 (0.99993)
BWTRS	627344 (0.97972)
BHTRS	625786 (0.99752)
B4TRS	623811 (0.99684)
B4TD	618093 (0.99083)
PBNRS	614836 (0.99473)
A$_{rest}$	0.5708 ± 0.0005
SETUP_PV	336531
HEX	315251 (0.93677)
ONLINE PV	306765 (0.97308)
STLAY	302696 (0.98674)
RSHEX	295125 (0.97499)
INTIME	294484 (0.99783)
PVCUT	291757 (0.99074)
TGPVCUT	290443 (0.99550)
TGPVTR	290443 (1.00000)
PASS3 PV	256678 (0.88375)
A$_{PV}$	0.7627 ± 0.0007
Full-Record	250203
LAYER14acc	248613 (0.99365)
A$_{L14}$	0.9937 ± 0.0002
A$_{K_{\mu 2}}$	0.4191 ± 0.0005

Table 21: $K_{\mu 2}$-based acceptances for the $\pi\nu\bar{\nu}$ analysis. All setup cuts are defined in Table 22. DELCO2 is defined as a 2ns delay conincidence.

$K_{\mu 2}$ SETUP	component cuts
SETUP$_{RD}$	BAD_RUN, BAD_STC, TRIGGER, ICBIT, $t_{IC} - t_{Ck} > 5$ ns, B4DEDX, UTC, TARGET
SETUP$_{recon}$	BAD_RUN, BAD_STC, TRIGGER, ICBIT, $t_{IC} - t_{Ck} > 5$ ns, B4DEDX, CPITRS, CPITAIL, CKTRS, CKTAIL, BWTRS, BHTRS, A$_{RD}$ cuts, $\mid t_{IC} - t_{Ck} \mid < 5$ ns, PV(noBV), $120 \leq Erd \leq 150$ MeV
SETUP$_{rest}$	BAD_RUN, BAD_STC, TRIGGER, ICBIT, A$_{RD}$ cuts, A$_{recon}$ cuts, A$_{rest}$ cuts, $120 \leq Erd \leq 150$ MeV KM2PBOX, COS3D.
SETUP$_{PV}$	BAD_RUN, BAD_STC, TRIGGER, ICBIT, A$_{RD}$ cuts, A$_{recon}$ cuts, A$_{rest}$ cuts, $120 \leq Erd \leq 150$ MeV KM2PBOX, COS3D, $LAY < 21$.

Table 22: Setup cuts used in the $K_{\mu 2}$-based acceptance measurement shown in Table 22. PV(noBV) is the pass3 PV for all detector subsystems except for BV. KM2PBOX is a 2σ cut on the $K_{\mu 2}$ momentum.

9.2 $K_{\pi 2}$-based acceptance

The structure and results of $K_{\pi 2}$-based acceptance study are shown in Table 23. This acceptance accounts for the acceptance of the beam background and kinematic pathology cuts which involve track energy in the target. The $K_{\pi 2}(1)$ monitor sample is used for this measurement. The final $K_{\pi 2}$-based acceptance is

$$A_{K_{\pi 2}} = 0.8739 \pm 0.0028_{stat.}. \tag{11}$$

9.3 π_{scat}-based kinematic acceptance

The π_{scat}-based kinematic acceptance is measured from the π_{scat} monitor sample. It measures the acceptance of the kinematic pathology cuts that involve safety cuts, track energy and scattering in Range Stack. Because π_{scat} events typically have messy target pathologies resulting in uncertainties in target energy and range, systematic uncertainty is estimated by varying the size of the BOX cuts used in the setup. These BOX cuts are obtained by comparing π_{scat} and $K_{\pi 2}$ mass resolutions. Table 24 shows the corresponding structure and results. The final π_{scat}-based kinematic acceptance is

$$A_{piscat} = 0.6675 \pm 0.0070^{+0.1040}_{-0.0191}. \tag{12}$$

Where the systematic uncertainty contains two parts, one part is from the difference ± 0.0191 between the different box definitions. The other part is from the uncertinty due to the fixed scattering and safety cuts applied. Since the final open-the-box shows the same single event even if use the NN scatering method alone, a systematic uncertainty due to the possible

Cut	1998 (acceptance)
SETUP$_{ops}$	14882
OPSVETO	14563 (0.97856)
OPSVETO_LKB	14563 (1.00000)
A$_{ops}$	0.9786 ± 0.0012
SETUP$_{tgkin}$	14149
TGDEDX	13719 (0.96961)
TGER	13715 (0.99971)
TGLIKE	13405 (0.97740)
EPITG	13399 (0.99955)
EPIMAXK	13147 (0.98119)
TGEDGE	13115 (0.99757)
TGCCDPF	12970 (0.98894)
PHIVTX	12698 (0.97903)
PHIVTX2	12698 (1.00000)
DRP	12635 (0.99504)
A$_{tgkin}$	0.8930 ± 0.0026
A$_{K_{\pi2}}$	0.8739 ± 0.0028

Table 23: $K_{\pi2}$-based acceptances for the $\pi^+\nu\bar{\nu}$ analysis. OPSCUT_LKB is not applied to the 1995 data. SETUP$_{ops}$ includes BAD_RUN, BAD_STC, TRIGGER, pass1 reconstruction, beam and kinematic cuts (except those whose acceptances are being measured here), photon energy in BV+EC+RD> 200 MeV, all TD cuts except TDECON, TDVEL and those which require electron information ($K_{\pi2}(2)$ monitors do not have extended TD time information), and a 2σ cut on the $K_{\pi2}(2)$ range, energy and momentum. SETUP_tgkin is SETUP_ops plus OPSVETO, OPSVETO_LKB and TGPVCUT.

acceptance gain can be obtained from the difference between the acceptance given above and the acceptance 0.7697 from the NN scattering method, yielding a value +0.1022 which is added in the one from the first part of systematic uncertainty.

9.4 π_{scat}-based TD acceptance

The TD acceptance is measured using π_{scat} monitor sample. The structure and results are shown in Table 25. The FITPI acceptance is estimated using both the area and the counting method. In the area method, all pass1 cuts up to the FITPI cut (including FITPI cut) are applied to select the pion sample. And then the pion lifetime distribution is fitted with the formula (13)

$$N(t_\pi; N_A) = \frac{N_A}{t_\pi} e^{-\frac{t}{t_\pi}}. \tag{13}$$

Where t_π is the pion lifetime (in PDG 2000, it is 26.033 ns). N_A is the integrated number of events under a pion-lifetime fit to the events. Figure 31 shows the binned likelihood fitting results from a 1-parameter fit (range from 26 to 78 ns) and 2-parameter fit (range from 26 to 78 ns and t_π is included in the fit). Both fits are in good agreement and the 2-parameter fit yields (25.81 ± 0.17) ns for the pion lifetime which agrees with the PDG value. The final FITPI acceptance from the area method should be corrected as written in expression (15), taking into account of the situation with a $\pi \rightarrow \mu$ decay signature which fail FITPI for reasons other than being an early $\pi \rightarrow \mu$ decay and the fraction of muons ($\epsilon_{\mu escape}$) escaping the stopping counter.

$$A^{area}_{FITPI} = \frac{N_P}{N_A + \Delta N_A} \times \epsilon_{\mu escape}, \tag{14}$$

$$= 0.7205 \pm 0.0025_{stat.} \tag{15}$$

Where N_P is the number of events that pass FITPI. ΔN_A is the "hand-scan correction" for the problem of FITPI failure mentioned above. $\epsilon_{\mu escape}$ is estimated to be 0.982. The ratio of $\frac{\Delta N_A}{N_A}$ 0.072 is taken from 1996 and 1997 data analysis. The A^{area}_{FITPI} is consistent with the counting method given in Table 25. In this analysis, the FITPI acceptance is taken from the counting method as used in the 1995-1997 analysis. The final π_{scat}-based TD acceptance is

$$A_{TD} = 0.3941 \pm 0.0068_{stat.} \pm 0.0052_{sys.}. \tag{16}$$

9.5 μ-veto accidental loss

The $\pi\nu\bar{\nu}1$ trigger involves a muon veto in the form of $\overline{19_{ct} + 20_{ct} + 21_{ct}}$. This can result in acceptance loss when accidentals hit Range Stack layer 19+20+21 in an otherwise good $\pi\nu\bar{\nu}$ candidate event. This loss is measured by using $K_{\mu 2}(1)$ monitor sample. Events are counted with hits in Range Stack layer 19+20+21 in a 10 pre-prompt window in 12 adjacent sectors opposite the stopping sector in $K_{\mu 2}(1)$ monitor events which pass all cuts except PV(no BV) in Table 32. The result is given in Table 26. The acceptance due to μ-veto accidental loss is therefore

$$A^{acc}_{\bar{\mu}} = 0.9909 \pm 0.0001_{stat.}. \tag{17}$$

Cut	1998
SETUP$_{\pi_{scat}}$ large BOX	8417
PR_RF_AB	8292 (0.98504)
XYHIT	8181 (0.98661)
TWO-TRACK	8054 (0.98448)
RNGMOM	7940 (0.98585)
CHIMAX	7739 (0.97469)
CL_RSDEDX	6799 (0.87854)
RS_LIKE	6715 (0.98765)
PR_RF	6163 (0.91780)
PR_RFZ1	5830 (0.94597)
PR_RFZ2	5824 (0.99897)
NN CUT	5467 (0.93870)
A$_{large}$	0.6495 $\pm$ 0.0052
SETUP$_{\pi_{scat}}$ final BOX	4526
PR_RF_AB	4497 (0.99359)
XYHIT	4430 (0.98510)
TWO-TRACK	4364 (0.98510)
RNGMOM	4308 (0.98717)
CHIMAX	4216 (0.97864)
CL_RSDEDX	3709 (0.87974)
RS_LIKE	3680 (0.99218)
PR_RF	3381 (0.91875)
PR_RFZ1	3204 (0.94765)
PR_RFZ2	3199 (0.99844)
NN CUT	3021 (0.94436)
A$_{final}$	0.6675 $\pm$ 0.0070
SETUP$_{\pi_{scat}}$ small BOX	890
PR_RF_AB	882 (0.99022)
XYHIT	866 (0.98186)
TWO-TRACK	857 (0.98961)
RNGMOM	842 (0.98250)
CHIMAX	829 (0.98456)
CL_RSDEDX	730 (0.88058)
RS_LIKE	725 (0.99315)
PR_RF	678 (0.93517)
PR_RFZ1	643 (0.94838)
PR_RFZ2	641 (0.99689)
NN CUT	612 (0.95476)
A$_{small}$	0.6876 $\pm$ 0.0154
A$_{\pi_{scat}}$	0.6675 $\pm$ 0.0203

Table 24: π_{scat}-based kinematic acceptances for the $\pi\nu\bar{\nu}$ analysis. Acceptances from both fixed cuts and neutral network cut are presented. Errors are statistical only. SETUP_PISCAT includes BAD_RUN, BAD_STC, all pass1 cuts, b4abm2 < 1.3, $\mid t_\pi - t_{rs} \mid <$ 5 ns, ICBIT, $\mid t_{IC} - t_{RS} \mid <$ 5 ns, TARGF, DTGTTP, RTDIF, TGQUALT, TGZFOOL, BHTRS, CKTRS, CKTAIL, photon veto in the stack only, all TD cuts, cos3d and LAYV4. The final box is defined by Rdev > 2.7, range < 40 cm, Edev > 2.35, kinetic energy < 135 MeV Pdev > 2.5 and momentum < 229 MeV/c. "Small" box is defined by Rdev > 4.0, range < 38.8 cm, Edev > 3.0, kinetic energy < 131 MeV, Pdev > 5.0 and momentum $<$ 222.2 MeV/c. "Large" box is defined by Rdev > 2.0, range < 41.2 cm, Edev > 1.0, kinetic energy < 139 MeV, Pdev $> 0.$ and momentum < 235.8 MeV/c.

Cut	1998 (acceptance)
SETUP_TD_1	6129
FITPI (bad data)	5936 (0.96851)
FITPI (counting)	4343 (0.73164)
L1.1 and L1.2	3591 (0.82685)
TDCUT	3485 (0.97048)
RSHEX2	3485 (1.00000)
TDTCON	3485 (1.00000)
TDDFA	2977 (0.85423)
EV5	2793 (0.93819)
ELVETO	2792 (0.99964)
TDLIK	2384 (0.85387)
A_{TD1}	0.3890 ± 0.0061
SETUP_TD_2	4482
FITPI (bad data)	4356 (0.97189)
FITPI (counting)	3207 (0.73623)
L1.1 and L1.2	2666 (0.83131)
TDCUT	2592 (0.97224)
RSHEX2	2592 (1.00000)
TDTCON	2592 (1.00000)
TDDFA	2205 (0.85069)
EV5	2069 (0.93832)
ELVETO	2068 (0.99952)
TDLIK	1765 (0.85348)
A_{TD2}	0.3993 ± 0.0074
A_{TD}	0.3941 ± 0.0086

Table 25: π_{scat}-based TD acceptances for the $\pi^+\nu\bar{\nu}1$ analysis. A_TD is an average of A_TD_1 and A_TD_2, in which A_TD_2 is scaled by a factor of 1.014 to account for pion absorption and decay-in-flight. The final A_TD include statistical error (100% correlated) and systematic error (use the difference between A_TD_1 and A_TD_2 and divide it by two). The total TD acceptance includes the FITPI acceptance as calculated in the counting method. SETUP_TD_1 is the same as SETUP$_{\pi_{scat}}$ in Table 24, with BOX, LAYV4, RNGMOM, ZFRF, ZUTOUT LAYER14 and EICKIN, but without the TD cuts. SETUP_TD_2 is SETUP_TD_1 with CL_RSDEDX, CHIMAX PR_RF and PR_RFZ1 also applied.

N_{total}	N_{loss}	$A^{acc}_{\bar{\mu}}$
1180235	10844	0.9909 ± 0.0001

Table 26: Accidental induced acceptance of the trigger muon veto.

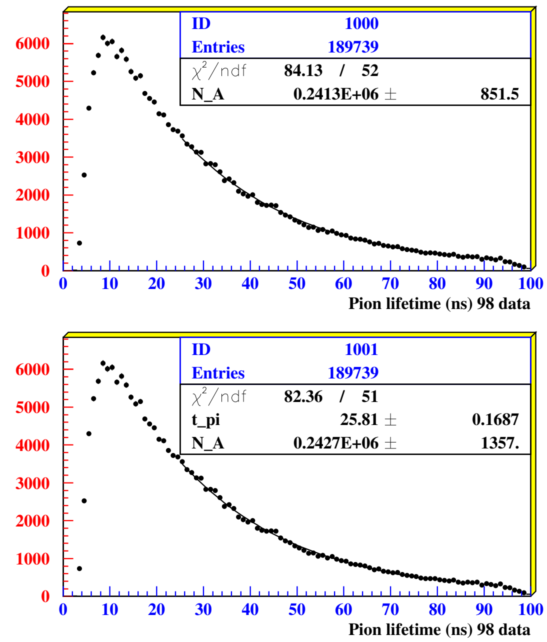

Figure 31: The pion lifetime spectrum. The fit is performed with 1-parameter N_A fit (top) and 2-parameter t_π and N_A fit (bottom) separately.

$\epsilon T\cdot 2(K_{\mu 2})$	$k(K_{\mu 2})$	$\epsilon T\cdot 2(K_{\pi 2})$	$k(K_{\pi 2})$	k	$\epsilon T\cdot 2(\pi^+\nu\bar{\nu})$	$\epsilon T\cdot 2(\pi^+ f)$
0.8650±0.0018	1.89	0.9014±0.0045	1.59	1.74	0.892 ±0.006	0.891±0.006

Table 27: $T\cdot 2$ efficiencies for $K_{\mu 2}$, $K_{\pi 2}$, $\pi^+\nu\bar{\nu}$ and $\pi^+ f$.

9.6 $T\cdot 2$ efficiency

$T\cdot 2$ efficiency indicates the detection ability of $T\cdot 2$ sector. Starting from 1995-1997 analysis, this efficiency is treated separately for different Kaon decay modes. $T\cdot 2$ efficiencies are measured using 1998 K_B monitor data, the values corresponding to $K_{\mu 2}$, $K_{\pi 2}$, $\pi^+\nu\bar{\nu}$ and $\pi^+ f$ are given below (see Table 27) by means of

$$\epsilon T\cdot 2 \;=\; 1 - 0.04 - e^{kE} \tag{18}$$

where E is the energy deposit in T-counter and k is the number of photon electrons per MeV. In computing the $T\cdot 2$ efficiency for $\pi^+\nu\bar{\nu}$ and $\pi^+ f$, the number of photon electrons per MeV is taken from the average of both $k(K_{\mu 2})$ and $k(K_{\pi 2})$. From Table 27, one can find the $T\cdot 2$ efficiencies for both $\pi^+\nu\bar{\nu}$ and $\pi^+ f$ are almost indentical. Therefore, single value given below will be used in the folloing analsysis

$$\epsilon T\cdot 2 = 0.892 \pm 0.006_{stat.}. \tag{19}$$

Cut	1998 (acceptance)
KT	50000
T·A	22646 (0.45292)
19ct+20ct+21ct	18996 (0.83882)
$A^{UMC}_{K_{\mu2},trig}$	0.37992 ± 0.00217
UTC/RANGE	18986 (0.99947)
UTCQUAL	18985 (0.99995)
TARGET	18963 (0.99884)
$A^{UMC}_{K_{\mu2},recon}$	0.99826 ± 0.00030
COS3D	18577 (0.97964)
RTOT40	18574 (0.99984)
$A^{UMC}_{K_{\mu2},kin}$	0.97949 ± 0.00103
$A^{UMC}_{K_{\mu2},K_{\mu2}}$	0.37148 ± 0.00216

Table 28: UMC $K_{\mu2}$ acceptance of cuts applied in the f_s analysis.

9.7 UMC based acceptance

The UMC based acceptances are estimated for $K_{\mu2}$ used for the f_s analysis, (see Table 28), $K_{\pi2}$ used for the $K_{\pi2}$ branching ratio analysis (see Table 29), $\pi^+\nu\bar{\nu}$ and $\pi^+ f$ (see Table 30 and Table 31), respectively. UMC verstion 6.0 is adopted with modification as decribed in Section Monte Calro simulation. In the trigger and the fiducial efficiencies for both $\pi^+\nu\bar{\nu}$ and $\pi^+ f$, the values are taken from those without nuclear interation simulation. The correction for nuclear interation effect is obtained from

$$A_{nidif} = \frac{A_{trig}(NIDIFon)}{A_{trig}(NIDIFoff)} \times \frac{A_{UMC}(NIDIFon)}{A_{UMC}(NIDIFoff)}, \quad (20)$$

$$= 0.5277 \pm 0.0082_{stat.} \qquad \text{for } \pi^+\nu\bar{\nu}, \quad (21)$$

$$= 0.4786 \pm 0.0057_{stat.} \qquad \text{for } \pi^+ f. \quad (22)$$

$$(23)$$

10 f_s measurement

To measured f_s, $K_{\mu2}(1)$ monitor sample is selected by the cuts shown in Table 32. The corresponding $K_{\mu2}(1)$ acceptance is also measured in Table 33. The f_s is then computed by

$$f_s = \frac{N_{K_{\mu2}}}{\epsilon T \cdot 2(K_{\mu2}) \cdot (K^{eff}_{Blive})_{K_{\mu2}} \cdot A_{K_{\mu2},f_s} \cdot A^{UMC}_{K_{\mu2},kin} \cdot A^{UMC}_{K_{\mu2},trig}} \times \frac{1}{0.6351} \quad (24)$$

$$= 0.7019 \pm 0.0049_{stat.} \quad (25)$$

The $N_{K_{\mu2}}$, $\epsilon T{\cdot}2(K_{\mu2})$, $(K^{eff}_{Blive})_{K_{\mu2}}$, $A_{K_{\mu2}}$, $A^{UMC}_{K_{\mu2},kin}$ and $A^{UMC}_{K_{\mu2},trig}$ are taken from Table 32, 27, 20, 33, 28.

Cut	1998 (acceptance)
KT	49995
T·A	23916 (0.47837)
Reach layer B	20326 (0.84989)
(19ct+20ct+21ct)bar	17694 (0.87051)
UFATE	15085 (0.85255)
USTMED	14337 (0.95041)
USTOP_HEX	13335 (0.93011)
$A^{UMC}_{K_{\pi2},trig}$	0.26673 ± 0.0019
UTC/RANGE	13185 (0.98875)
UTCQUAL	13183 (0.99985)
TARGET	13047 (0.98968)
$A^{UMC}_{K_{\pi2},recon}$	0.97840 ± 0.0012
KP2STOP	12406 (0.95087)
COS3D	11853 (0.95542)
KP2BOX	10718 (0.90424)
$A^{UMC}_{K_{\pi2},kin}$	0.82149 ± 0.00335
$A^{UMC}_{K_{\pi2}}$	0.21438 ± 0.00184

Table 29: UMC $K_{\pi2}$ acceptance of cuts applied in the $K_{\pi2}$ branching ratio analysis.

Trigger	$\pi\nu\bar{\nu}$ NIDIF on	$\pi\nu\bar{\nu}$ NIDIF off	πf NIDIF on	πf NIDIF off
KT	199999	150000	99998	60000
T·2	77633 (0.3882)	61311 (0.4087)	43666 (0.4367)	27215 (0.4536)
LayerB	54570 (0.7029)	50352 (0.8213)	36129 (0.8274)	27213 (0.9999)
DC	54570 (1.0000)	50352 (1.0000)	36129 (1.0000)	27213 (1.0000)
μ veto	54270 (0.9945)	50335 (0.9997)	35357 (0.9786)	27040 (0.9936)
BV	54179 (0.9983)	50335 (1.0000)	35244 (0.9968)	27040 (1.0000)
EC	54160 (0.9996)	50335 (1.0000)	35187 (0.9984)	27040 (1.0000)
HEX	54079 (0.9985)	50335 (1.0000)	35072 (0.9967)	27040 (1.0000)
Refined Range	23701 (0.4383)	26971 (0.5358)	24176 (0.6893)	23666 (0.8752)
A_{trig}	0.1185 ± 0.0007	0.1798 ± 0.0010	0.2416 ± 0.0014	0.3944 ± 0.0022

Table 30: The $\pi\nu\bar{\nu}$ and πf trigger acceptances in 1998 data.

Cuts	$\pi\nu\bar{\nu}$ NIDIF on	$\pi\nu\bar{\nu}$ NIDIF off	πf NIDIF on	πf NIDIF off
SETUP	23531	26949	23677	23646
UFATE	21141 (0.8984)	26949 (1.0000)	20949 (0.8848)	23646 (1.0000)
USTMED	20975 (0.9921)	26799 (0.9944)	20781 (0.9920)	23390 (0.9892)
USTOP_HEX	20936 (0.9981)	26799 (1.0000)	20736 (0.9978)	23390 (1.0000)
COS3D	20283 (0.9688)	25904 (0.9666)	19824 (0.9560)	22268 (0.9520)
LAYER14	20225 (0.9971)	25886 (0.9993)	19690 (0.9932)	22211 (0.9974)
ZFRF	18898 (0.9344)	24152 (0.9330)	18033 (0.9158)	20256 (0.9120)
ZUTOUT	18893 (0.9997)	24146 (0.9998)	18025 (0.9996)	20249 (0.9997)
BOX 1	18565 (0.9826)	23862 (0.9882)	12502 (0.6936)	15708 (0.7757)
BOX 2	6581 (0.3545)	9412 (0.3944)	10939 (0.8750)	13983 (0.8902)
A_{UMC}	0.2797 ± 0.0029	0.3493 ± 0.0029	0.4620 ± 0.0032	0.5913 ± 0.0032

Table 31: The $\pi\nu\bar{\nu}$ and πf fiducial acceptances in 1998 data. For $\pi\nu\bar{\nu}$, BOX 1 is defined as the upper BOX cut and BOX 2 is defined as the lower BOX cut. For πf, BOX 1 is defined as both lower and upper BOX cuts and BOX 2 is defined by requiring $35.5 \leq$ range ≤ 40 cm, $120 \leq$ kinetic energy ≤ 135 MeV and $221 \leq$ momentum ≤ 229 MeV.

11 Measurement of the $K_{\pi 2}$ branching ratio

To check the validity of f_s value, a measurement of the $K_{\pi 2}$ branching ratio is conducted using $K_{\pi 2}(1)$ monitor sample. Table 34 gives the number of events leftover up to the different cut. The corresponding acceptances are also given in Table 35 The UMC $K_{\pi 2}$ acceptance for relevant cuts are given in Table 29. The branching ratio of $K_{\pi 2}$ is given by

$$BR_{K_{\pi 2}} = \frac{N_{K_{\pi 2}}}{\epsilon T \cdot 2(K_{\pi 2}) \cdot (K_{Blive}^{eff})_{K_{\pi 2}} \cdot A_{K_{\pi 2},Br} \cdot A^{UMC}_{K_{\pi 2},kin} \cdot f_s \cdot A^{UMC}_{K_{\pi 2},trig}}, \tag{26}$$

$$= 0.6351 \frac{N_{K_{\pi 2}}}{N_{K_{\mu 2}}} \frac{\epsilon T \cdot 2(K_{\mu 2})}{\epsilon T \cdot 2(K_{\pi 2})} \frac{(K_{Blive}^{eff})_{K_{\mu 2}}}{(K_{Blive}^{eff})_{K_{\pi 2}}} \frac{A^{UMC}_{K_{\mu 2}}}{A^{UMC}_{K_{\pi 2}}} \frac{A_{PV,f_s}}{A_{FITPI} \cdot A^{acc}_{\bar{\mu}}} \frac{A_{bad}(K_{\mu 2})}{A_{bad}(K_{\pi 2})}, \tag{27}$$

$$= 0.217 \pm 0.003_{stat.}. \tag{28}$$

Where, the relevant inputs are taken from Table 32, 34, 27, 20, 28, 29, 33 and 35. In this analysis, A_{RD}, A_{recond} and A_{rest} given in Table 33 and Table 35 are assumed to be common and can be canceled out. Statictically, the value obtained above agrees with the PDG value 0.212 ± 0.001 with 2 sigmas.

12 Sensitivity of 1998 data

The sensitivity of 1998 data is given in Table 36 for $\pi^+\nu\bar{\nu}$ and $\pi^+ f$ separately.

Cut	1998
ALL	2553564
BAD_RUN	2527054
BAD_STC	2526464
TRIGGER	2523370
RD_TRK	2523370
TRKTIM	2521483
UTC/RANGE	2521483
UTCQUAL	2413319
TARGET	2398715
COS3D	2329411
B4DEDX	2283513
CPITRS	2267728
CPITAIL	2265773
ICBIT	2261631
TIC	2224466
TIMCON	2193135
TGCCD	2040858
DCBIT	1777962
DELCO	1544972
CKTRS	1529056
CKTAIL	1459308
BWTRS	1388567
BHTRS	1384039
TARGF	1330818
DTGTTP	1330574
RTDIF	1314604
TGQUALT	1314604
PIGAP	1300017
TGB4	1257306
KIC	1247797
TGGEO	1233671
B4EKZ	1199280
B4EKZ_IC	1199280
TGZFOOL	1199280
PV(noBV)	960527
RTOT40	960227
$N_{K_{\mu 2}}$	960227

Table 32: Cuts applied in the f_s analysis. RTOT40 requires range $>$ 40 cm to remove some $K_{\pi 2}$ and radiative $K_{\mu 2}$ not removed by PV(noBV).

Cut	1998 (acceptance)
$SETUP_{RD}$	1782053
RD_TRK	1782053 (1.00000)
TRKTIM	1780981 (0.99940)
A_{RD,f_s}	0.9994 ± 0.0000
$SETUP_{recon}$	903808
UTC/RANGE	903808 (1.00000)
UTCQUAL	878005 (0.97145)
TARGET	876143 (0.99788)
A_{recon,f_s}	0.9694 ± 0.0002
$SETUP_{rest}$	1077148 (0.00000)
ICBIT	1077148 (1.00000)
TIC	1068441 (0.99192)
TIMCON	1060353 (0.99243)
TGCCD	997170 (0.94041)
DCBIT	896899 (0.89944)
DELCO	788384 (0.87901)
CKTRS	783661 (0.99401)
CKTAIL	757567 (0.96670)
B4DEDX	746955 (0.98599)
CPITRS	745760 (0.99840)
CPITAIL	745537 (0.99970)
TARGF	720273 (0.96611)
DTGTTP	720206 (0.99991)
RTDIF	712706 (0.98959)
TGQUALT	712706 (1.00000)
PIGAP	705890 (0.99044)
TGB4	683858 (0.96879)
KIC	679542 (0.99369)
TGGEO	677482 (0.99697)
B4EKZ	662865 (0.97842)
B4EKZ_IC	662865 (1.00000)
TGZFOOL	662865 (1.00000)
BWTRS	649176 (0.97935)
BHTRS	647569 (0.99752)
A_{rest,f_s}	0.6012 ± 0.0005
$SETUP_{PV}$	397510
PV(noBV)	339345 (0.85368)
A_{PV,f_s}	0.8537 ± 0.0006
$SETUP_{BAD}$	2521559
BAD_RUN	2495460 (0.98965)
BAD_STC	2494880 (0.99977)
TRIGGER	2491817 (0.99877)
A_{BAD}	0.9882 ± 0.0001
$A_{K_{\mu 2},f_s}$	0.4914 ± 0.0005

Table 33: $K_{\mu 2}$-based acceptances of cuts applied in the f_s analysis. The SETUP cuts are defined in Table 22. SETUP_BAD is ICBIT.

Cut	# of events
ALL	262599
BAD_RUN	259889
BAD_STC	257734
TRIGGER	257734
RD_TRK	257734
TRKTIM	257734
UTC/RANGE	257734
UTCQUAL	248633
TARGET	246847
COS3D	234648
B4DEDX	228982
CPITRS	227346
CPITAIL	227164
ICBIT	226755
TIC	221899
TIMCON	218069
TGCCD	201110
DCBIT	172384
DELCO	150376
CKTRS	149146
CKTAIL	142432
BWTRS	136045
BHTRS	135656
TARGF	129520
DTGTTP	129493
RTDIF	127932
TGQUALT	127932
PIGAP	126306
TGB4	121609
KIC	120326
TGGEO	107115
B4EKZ	104082
B4EKZ_IC	104082
TGZFOOL	104082
FITPI	64484
KP2BOX	59515
KP2STOP	59388
$N_{K_{\pi 2}}$	59388

Table 34: Cuts applied in the $K_{\pi 2}$ BR analysis. KP2BOX is a 3σ cut on the KPI2 range, energy and momentum. KP2STOP requires the stopping layer to be between layers 8 and 15 inclusive.

Cut	1998 (acceptance)
$SETUP_{RD}$	80568 (0.00000)
RD_{TRK}	80568 (1.00000)
TRKTIM	80568 (1.00000)
$A_{RD,BR}$	1.00000 ± 0.00000
$SETUP_{recon}$	55941
UTC/RANGE	55941 (1.00000)
UTCQUAL	54659 (0.97708)
TARGET	54507 (0.99722)
$A_{recon,BR}$	0.97437 ± 0.00067
$SETUP_{rest}$	50742
ICBIT	50742 (1.00000)
TIC	50315 (0.99158)
TIMCON	49873 (0.99122)
TGCCD	43560 (0.87342)
DCBIT	40672 (0.93370)
DELCO	36224 (0.89064)
CKTRS	35957 (0.99263)
CKTAIL	34179 (0.95055)
B4DEDX	33698 (0.98593)
CPITRS	33456 (0.99282)
CPITAIL	33418 (0.99886)
TARGF	32129 (0.96143)
DTGTTP	32128 (0.99997)
RTDIF	31832 (0.99079)
TGQUALT	31832 (1.00000)
PIGAP	31451 (0.98803)
TGB4	30364 (0.96544)
KIC	30150 (0.99295)
TGGEO	28480 (0.94461)
B4EKZ	27768 (0.97500)
B4EKZ_IC	27768 (1.00000)
TGZFOOL	27768 (1.00000)
BWTRS	26481 (0.95365)
BHTRS	26409 (0.99728)
$A_{rest,BR}$	0.52046 ± 0.00222
$SETUP_{BAD}$	117697 (0.00000)
BAD_RUN	116499 (0.98982)
BAD_STC	115490 (0.99134)
TRIGGER	115490 (1.00000)
A_{BAD}	0.98125 ± 0.00040
A_{FITPI}	0.73470 ± 0.00490
A_{μ}^{acc}	0.99090 ± 0.00009
$A_{K_{\pi 2},Br}$	0.36233 ± 0.00288

Table 35: $K_{\pi 2}$-based acceptances of cuts applied in the Kp2 BR analysis. The FITPI acceptance is measured using piscat (counting method) similar to the pi nu nubar measurement of FITPI acceptance, except that here the piscat are selected using KP2BOX and KP2STOP instead of BOX and LAYV4. The SETUP are defined in Table 22, except that all SETUP here include the requirement of at least 200 MeV of photon energy in BV+EC; $120 \le erd \le 150$ MeV is replaced by $75 \le erd \le 105$ MeV; PV(noBV) is not applied; and KM2PBOX is replaced by KP2BOX, KP2STOP and FITPI. $SETUP_{bad}$ is ICBIT.

Decay mode	$\pi^+\nu\bar{\nu}$	$\pi^+ f$
A_{trig}	0.1798 ± 0.0010	0.3944 ± 0.0022
$A_{\bar{\mu}}^{acc}$	0.9909 ± 0.0001	0.9909 ± 0.0001
A_{UMC}	0.3493 ± 0.0029	0.5913 ± 0.0032
A_{nidif}	0.5277 ± 0.0082	0.4786 ± 0.0057
$A_{K\mu 2}$	0.4191 ± 0.0005	0.4191 ± 0.0005
$A_{K\pi 2}$	0.8739 ± 0.0028	0.8739 ± 0.0028
$A_{\pi_{scat}}$	$0.6675{\pm}0.0070_{stat}{}^{+0.1040}_{-0.0191 sys}$	$0.6675{\pm}0.0070_{stat}{}^{+0.1040}_{-0.0191 sys}$
A_{TD}	$0.3941{\pm}0.0068_{stat}{\pm}0.0052_{sys}$	$0.3941{\pm}0.0068_{stat}{\pm}0.0052_{sys}$
$\epsilon T \cdot 2$	0.882 ± 0.006	0.882 ± 0.006
f_s	0.7019 ± 0.0049	0.7019 ± 0.0049
$A\epsilon$	$0.00279{\pm}0.00007_{stat}{}^{+0.00044}_{-0.00009 sys}$	$0.00940{\pm}0.00024_{stat}{}^{+0.00147}_{-0.00020 sys}$
$A\epsilon \cdot f_s$	$0.00196{\pm}0.00005_{stat}{}^{+0.00031}_{-0.00006 sys}$	$0.00660{\pm}0.00014_{stat}{}^{+0.00103}_{-0.00021 sys}$
K_{Blive} (10^{12})	$2.70{\pm}0.02_{sys.}$	$2.70{\pm}0.02_{sys.}$
Sensitivity	$(1.89{\pm}0.05_{stat}{}^{+0.06}_{-0.30 sys})\ \times 10^{-10}$	$(0.56{\pm}0.01_{stat}{}^{+0.02}_{-0.09 sys})\ \times 10^{-10}$

Table 36: $\pi^+\nu\bar{\nu}$ and $\pi^+ f$ acceptance and sensitivity of the 1998 analysis.

13 $\pi^+\nu\bar{\nu}$ Acceptance for the paper

For the published paper, the definitions for the various acceptance categories are shown in Table 37. In order to make them to be comparable for 1995-97 data, the definitions are still the same as the previous ones. All individual acceptances are listed Table 37 respectively.

14 $K^+ \to \pi^+ f$ branching ratio

The search for kaon decays into a pion and a massless familon, $K^+ \to \pi^+ f$ is performed using all 1995-98 e787 data. Since the 1995-97 and 1998 analyses gives the 1/sensitivity $21.11{\times}10^{+9}$ and $17.86{\times}10^{+9}$ separately, the final E787 sensitivity for $K^+ \to \pi^+ f$ is $0.2566{\times}10^{-10}$. For a 90% confident level based on zero events observed in a $\pm 2\sigma$ region, a mean of the Possison distribution is 2.3026, yielding

$$Br(K^+ \to \pi^+ f) \ < \ 0.59 \times 10^{-10} \qquad (90\% \text{ C.L.}). \tag{29}$$

Category	Components	1995-1997	1998
K^+ stop efficiency	f_s	0.704	0.702
K^+ decay after 2 ns	DCBIT $(t_\pi - t_K) > 2$ ns	0.850	0.851
$K^+ \to \pi^+\nu\bar{\nu}$ phase space	A$_{trig}/T\cdot$ 2$(\pi^+ f)$ $\epsilon T\cdot$ 2 BOX	0.155	0.136
Solid angle acceptance	$T\cdot$ 2$(\pi^+ f)$ COS3D ZFRF ZUTOUT	0.407	0.409
π^+ nucl. interaction	A$_{nidif}$	0.513	0.527
Reconstruction efficiency	A$_{RD}$ A$_{recon}$	0.959	0.969
Other kinematic constraints	A$_{K_{\pi2}}$ RTDIF, PIGAP, TGB4 A$_{\pi_{scat}}$	0.665	0.554
$\pi^+ \to \mu^+ \to e^+$ decay acceptance	UFATE, USTMED USTOP_HEX, A$_{TD}$	0.306	0.392
Beam and target analysis	A$_{rest}$, excluding DCBIT, $(t_\pi - t_K) > 2$ ns RTDIF, PIGAP and TGB4	0.699	0.706
Accidental loss	A$_{PV}$ A$_{L14}$ A$_{\bar{\mu}}^{acc}$	0.785	0.751
Total acceptance	-	0.0021	0.00196

Table 37: Definitions for the acceptance categories for the paper.

15 Statistical Analysis of the $K^+ \to \pi^+ \nu\bar{\nu}$ Branching Ratio

There are 2 steps to the statistical analysis of the $K^+ \to \pi^+ \nu\bar{\nu}$ branching ratio:

1. Define a number of "cells" inside and outside the box of differing expected signal/noise, and calculate the expected signal/noise (dA/dN) using the individual N_{type} and A_{type} functions for each background type, and a simple model for their combination.

2. Examine the data to see if any events are observed these cells. Then, with

   - the expected background in each cell, based on the dN_i and the measured background level in the box;
   - the expected signal in each cell, based on the dA_i, the measured single-event-sensitivity in the box, and a given $K^+ \to \pi^+ \nu\bar{\nu}$ branching ratio;
   - the set of observed events $\{d_i\}$ in the M cells, $i = 1, M$,

   run Tom Junk's "ecl" code to loop over possible branching ratios and get the "confidence level" for each.

15.1 Definition of Signal/Noise Cells

For the purposes of combining the individual A and N functions into total expected signal and background in various regions inside and outside the box, we use 5 data points from each of the 7 individual background functions, at roughly $N = 0.2, 0.5, 1.0, 2.0, 5.0$ relative to the box cut positions (we only use 4 data points from the muon-band function, because if we cut too hard, we end up in the pion band). The 7 functions are the PV, $K_{\pi 2}$ kinematic, TD, $K_{\mu 2}$ range-tail kinematic, muon-band kinematic, single-beam, and double-beam functions. With 5 data points from 7 functions, there are potentially $5^7 = 78125$ different values of dA/dN. However, the kinematic functions all cut on the same variables (one or more of R, E, and P), so we actually expect about $3 \cdot 5^{7-2} = 9375$ different values, or regions, or "cells" of dA/dN space. The actual number that is calculated is 7500. 486 of these cells lie inside the box.

To simplify the calculation of expected background and signal in each cell, we make some assumptions:

- The rejections and acceptances of the PV, TD, single-beam, and double-beam functions are all completely independent.

- In the cell defined by the tightest $K_{\pi 2}$, $K_{\mu 2}$ range-tail, and muon-band kinematic cuts, the total kinematic acceptance is additive. That is, these 3 cuts remove mutually exclusive regions of the $K^+ \to \pi^+ \nu\bar{\nu}$ phase space.

- The $K_{\pi 2}$ background which passes the tightest $K_{\pi 2}$ kinematic cut position is distributed like signal in *ptot* and *rngmom_val*. That is, it is roughly flat in *ptot*, and falling in *rngmom_val* as *rngmom_val* increases away from 0. So the $K_{\pi 2}$ background which gets into the $K_{\mu 2}$ range tail and muon band is distributed like dA in these 2 kinematic functions.

- The $K_{\mu 2}$ range-tail background which passes the tightest $K_{\mu 2}$ range-tail kinematic cut position is distributed like signal in *ptot*, *etot*, *rtot*, and *rngmom_val*. That is, it is roughly flat in *ptot*, *etot*, and *rtot*, and falling in *rngmom_val* as *rngmom_val* increases away from 0. So the $K_{\mu 2}$ range-tail background which gets into the $K_{\pi 2}$ and muon-band regions is distributed like dA in these 2 kinematic functions.

- The muon-band background which passes the tightest muon-band kinematic cut position is distributed like signal in *ptot*, *etot*, and *rtot*. That is, it is roughly flat in *ptot*, *etot*, and *rtot*. So the muon-band background which gets into the $K_{\pi 2}$ and range-tail regions is distributed like dA in these 2 kinematic functions.

With these assumptions, the calculation of expected signal and background in each cell is performed separately for

1. the cell defined by the tightest $K_{\pi 2}$, $K_{\mu 2}$ range-tail, and muon-band kinematic cuts;

2. the cells defined by the tightest $K_{\mu 2}$ range-tail and muon-band kinematic cuts, and all $K_{\pi 2}$ kinematic cut positions except the tightest one;

3. the cells defined by the tightest $K_{\pi 2}$ and muon-band kinematic cuts, and all $K_{\mu 2}$ range-tail kinematic cut positions except the tightest one;

4. the cells defined by the tightest $K_{\pi 2}$ and $K_{\mu 2}$ range-tail kinematic cuts, and all muon-band kinematic cut positions except the tightest one.

The individual background functions consist of a list, $i = 1, 5$, of $N^{(i)}$ and $A^{(i)}$ values. $dN^{(i,j)}$ and $dA^{(i,j)}$ values then refer to the difference in consecutive $N^{(i)}$ and $A^{(i)}$ values, relative to the values at the final box cut position, N^{box} and A^{box}. For example, $dN_{PV}^{(1,2)} = (N_{PV}^{(1)} - N_{PV}^{(2)})/N_{PV}^{box})$.

For calculation (1), the individual background levels, dB_{type}, and the combined dN and dA values of this cell (where $\int dN = \int dA = 1$ over inside-the-box cells), are given by:

$$
\begin{aligned}
dB_{K_{\pi 2}} &= dN_{PV} \cdot dN_{K_{\pi 2}} \cdot dA_{TD} \cdot (dA_{Rtail} + dA_{\mu band} - 1) \cdot dA_{BM1} \cdot dA_{BM2} \cdot B_{K_{\pi 2}}^{box} && (30) \\
dB_{Rtail} &= dN_{TD} \cdot dN_{Rtail} \cdot dA_{PV} \cdot (dA_{K_{\pi 2}} + dA_{\mu band} - 1) \cdot dA_{BM1} \cdot dA_{BM2} \cdot B_{Rtail}^{box} && (31) \\
dB_{\mu band} &= dN_{TD} \cdot dN_{\mu band} \cdot dA_{PV} \cdot (dA_{K_{\pi 2}} + dA_{Rtail} - 1) \cdot dA_{BM1} \cdot dA_{BM2} \cdot B_{\mu band}^{box} && (32) \\
dB_{BM1} &= dN_{BM1} \cdot dA_{PV} \cdot dA_{TD} \cdot (dA_{K_{\pi 2}} + dA_{Rtail} + dA_{\mu band} - 2) \cdot dA_{BM2} \cdot B_{BM1}^{box} && (33) \\
dB_{BM2} &= dN_{BM2} \cdot dA_{PV} \cdot dA_{TD} \cdot (dA_{K_{\pi 2}} + dA_{Rtail} + dA_{\mu band} - 2) \cdot dA_{BM1} \cdot B_{BM2}^{box} && (34) \\
dN &= \frac{(dB_{K_{\pi 2}} + dB_{Rtail} + dB_{\mu band} + dB_{BM1} + dB_{BM2})}{(B_{K_{\pi 2}}^{box} + B_{Rtail}^{box} + B_{\mu band}^{box} + B_{BM1}^{box} + B_{BM2}^{box})} && (35) \\
dA &= dA_{PV} \cdot dA_{TD} \cdot (dA_{K_{\pi 2}} + dA_{Rtail} + dA_{\mu band} - 2) \cdot dA_{BM1} \cdot dA_{BM2} && (36)
\end{aligned}
$$

For calculation (2), the individual background levels, dB_{type}, and the combined dN and dA values of these cells (where $\int dN = \int dA = 1$ over inside-the-box cells), are given by:

$$
\begin{aligned}
dB_{K_{\pi 2}} &= dN_{PV} \cdot dN_{K_{\pi 2}} \cdot dA_{TD} \cdot dA_{BM1} \cdot dA_{BM2} \cdot B^{box}_{K_{\pi 2}} && (37)\\
dB_{Rtail} &= dN_{TD} \cdot dN_{Rtail} \cdot dA_{PV} \cdot dA_{K_{\pi 2}} \cdot dA_{BM1} \cdot dA_{BM2} \cdot B^{box}_{Rtail} && (38)\\
dB_{\mu band} &= dN_{TD} \cdot dN_{\mu band} \cdot dA_{PV} \cdot dA_{K_{\pi 2}} \cdot dA_{BM1} \cdot dA_{BM2} \cdot B^{box}_{\mu band} && (39)\\
dB_{BM1} &= dN_{BM1} \cdot dA_{PV} \cdot dA_{TD} \cdot dA_{K_{\pi 2}} \cdot dA_{BM2} \cdot B^{box}_{BM1} && (40)\\
dB_{BM2} &= dN_{BM2} \cdot dA_{PV} \cdot dA_{TD} \cdot dA_{K_{\pi 2}} \cdot dA_{BM1} \cdot B^{box}_{BM2} && (41)\\
dN &= \frac{(dB_{K_{\pi 2}} + dB_{Rtail} + dB_{\mu band} + dB_{BM1} + dB_{BM2})}{(B^{box}_{K_{\pi 2}} + B^{box}_{Rtail} + B^{box}_{\mu band} + B^{box}_{BM1} + B^{box}_{BM2})} && (42)\\
dA &= dA_{PV} \cdot dA_{TD} \cdot dA_{K_{\pi 2}} \cdot dA_{BM1} \cdot dA_{BM2} && (43)
\end{aligned}
$$

For calculation (3), the individual background levels, dB_{type}, and the combined dN and dA values of these cells (where $\int dN = \int dA = 1$ over inside-the-box cells), are given by:

$$
\begin{aligned}
dB_{K_{\pi 2}} &= dN_{PV} \cdot dN_{K_{\pi 2}} \cdot dA_{TD} \cdot dA_{Rtail} \cdot dA_{BM1} \cdot dA_{BM2} \cdot B^{box}_{K_{\pi 2}} && (44)\\
dB_{Rtail} &= dN_{TD} \cdot dN_{Rtail} \cdot dA_{PV} \cdot dA_{BM1} \cdot dA_{BM2} \cdot B^{box}_{Rtail} && (45)\\
dB_{\mu band} &= dN_{TD} \cdot dN_{\mu band} \cdot dA_{PV} \cdot dA_{Rtail} \cdot dA_{BM1} \cdot dA_{BM2} \cdot B^{box}_{\mu band} && (46)\\
dB_{BM1} &= dN_{BM1} \cdot dA_{PV} \cdot dA_{TD} \cdot dA_{Rtail} \cdot dA_{BM2} \cdot B^{box}_{BM1} && (47)\\
dB_{BM2} &= dN_{BM2} \cdot dA_{PV} \cdot dA_{TD} \cdot dA_{Rtail} \cdot dA_{BM1} \cdot B^{box}_{BM2} && (48)\\
dN &= \frac{(dB_{K_{\pi 2}} + dB_{Rtail} + dB_{\mu band} + dB_{BM1} + dB_{BM2})}{(B^{box}_{K_{\pi 2}} + B^{box}_{Rtail} + B^{box}_{\mu band} + B^{box}_{BM1} + B^{box}_{BM2})} && (49)\\
dA &= dA_{PV} \cdot dA_{TD} \cdot dA_{Rtail} \cdot dA_{BM1} \cdot dA_{BM2} && (50)
\end{aligned}
$$

For calculation (4), the individual background levels, dB_{type}, and the combined dN and dA values of these cells (where $\int dN = \int dA = 1$ over inside-the-box cells), are given by:

$$
\begin{aligned}
dB_{K_{\pi 2}} &= dN_{PV} \cdot dN_{K_{\pi 2}} \cdot dA_{TD} \cdot dA_{\mu band} \cdot dA_{BM1} \cdot dA_{BM2} \cdot B^{box}_{K_{\pi 2}} && (51)\\
dB_{Rtail} &= dN_{TD} \cdot dN_{Rtail} \cdot dA_{PV} \cdot dA_{\mu band} \cdot dA_{BM1} \cdot dA_{BM2} \cdot B^{box}_{Rtail} && (52)\\
dB_{\mu band} &= dN_{TD} \cdot dN_{\mu band} \cdot dA_{PV} \cdot dA_{BM1} \cdot dA_{BM2} \cdot B^{box}_{\mu band} && (53)\\
dB_{BM1} &= dN_{BM1} \cdot dA_{PV} \cdot dA_{TD} \cdot dA_{\mu band} \cdot dA_{BM2} \cdot B^{box}_{BM1} && (54)\\
dB_{BM2} &= dN_{BM2} \cdot dA_{PV} \cdot dA_{TD} \cdot dA_{\mu band} \cdot dA_{BM1} \cdot B^{box}_{BM2} && (55)\\
dN &= \frac{(dB_{K_{\pi 2}} + dB_{Rtail} + dB_{\mu band} + dB_{BM1} + dB_{BM2})}{(B^{box}_{K_{\pi 2}} + B^{box}_{Rtail} + B^{box}_{\mu band} + B^{box}_{BM1} + B^{box}_{BM2})} && (56)\\
dA &= dA_{PV} \cdot dA_{TD} \cdot dA_{\mu band} \cdot dA_{BM1} \cdot dA_{BM2} && (57)
\end{aligned}
$$

We now have dN and dA values for every cell, where dN and dA are those of the "combined" function. The cells are arranged in decreasing order of dA/dN (such that the "cleanest" cells with largest dA/dN are listed first), then a running sum is performed to define the integrated N and A values. So, every possible cut position correponding to a set of $\{N_{PV}, N_{K_{\pi 2}}, N_{TD}, N_{Rtail}, N_{\mu band}, N_{BM1}, N_{BM2}\}$ values now defines a cell with its own value of expected background, dN, expected signal, dA, as well as integrated N and A which have been used in the past to characterize the "cleanliness" of events inside and outside the box.

The total function gives dA/dN values ranging from 6.75 down to 0.023 for cells inside the 1998 box, where $dA/dN = 1$ corresponds to a cell with the same signal/noise ratio as that averaged over the entire box. If we expect 1 signal event and 0.0657 background events in the 1998 box, this means that there are very clean cells inside the box where we expect $6.75 \cdot 1/0.0657 = 103$ times more signal than background, and also dirty cells where we expect $0.023 \cdot 1/0.0657 = 0.35$ as much signal as background.

Note: Due to the simplicity of the model used to combine the individual background functions into a single combined function, it's possible for the tightest kinematic region to have smaller dA/dN than the 2nd-tightest region (typically by a small amount, maybe a few percent). This occurs in some cells bordered by the loosest PV and TD cut positions (i.e., where dA_{PV} and dA_{TD} are small). When this happens, we err on the conservative side, and force the dA/dN value of the 2nd tightest region to be marginally smaller than that of the tightest region.

15.2 Likelihood Estimator and Analysis

From section 15.1, we have broken up the region inside and just outside the 1998 box into many cells of different expected signal, dA_i, and expected background, dN_i, where $i = 1, 7500$. We can now calculate the probability of our 1998 result, assuming the presence of signal and/or background mechanisms. For the range of dA/dN space spanned by our combined function, our 1998 result consists of the observation of 3 events:

1. the "signal" event, run 37443, event 176348, which lies in an inside-the-box cell with $dA/dN = 0.596$, $N = 0.332$, $A = 0.837$
2. the "signal-like" or $bgtd = 3.1$ event, run 39180, event 56327, which lies in an outside-the-box cell with $dA/dN = 0.123$, $N = 1.635$, $A = 1.237$
3. the "L/R ambiguity" event, run 37761, event 142498, which lies in an outside-the-box cell with $dA/dN = 0.0122$, $N = 6.367$, $A = 1.470$

So we have 3 numbers each cell:

- an expected background, b_i, based on the dN_i and the measured background level in the box;
- an expected signal, s_i, based on the dA_i, the measured single-event-sensitivity in the box, and a given $K^+ \to \pi^+ \nu \bar{\nu}$ branching ratio;
- an observed number of events, d_i, which is 0 for all cells except the 3 listed above.

These 3 sets of numbers, $\{b_i\}, \{s_i\}, \{d_i\}$, are the inputs to the statistical analysis method of T. Junk, Nucl. Instrum. Meth. **A434** (1999), 435. This analysis also provides an easy way to combine the results of several data sets. For example, to combine the 1995-7 result with the 1998 result, we simply add 2 more cells to the 1998 cells: the 1995-7 "golden region" for which $dN = 0.1, dA = 0.55$, in which one event was observed; and the 1995-7 "non-golden region", for which $dN = 0.9, dA = 0.45$, and in which no events were observed. Both of these cells are "inside-the-box" cells.

Using these 3 inputs, Junk's analysis calculates 3 numbers for every possible experimental outcome (i.e., every possible set of $\{d_i\}$):

1. the value of a test statistic X;

2. the probability of getting the set $\{d_i\}$ assuming the presence of signal + background; and

3. the probability of getting the set $\{d_i\}$ assuming the presence of background only.

The answer to (1), for M cells, is

$$X = \prod_{i=1}^{M} X_i \tag{58}$$

where

$$X_i = \frac{e^{-(s_i+b_i)}(s_i + b_i)^{d_i}}{d_i!} / \frac{e^{-b_i} b_i^{d_i}}{d_i!} = e^{-s_i}\Big(1 + \frac{s_i}{b_i}\Big)^{d_i} \tag{59}$$

where the test statistic, X, has the properties that it optimally discriminates signal-like outcomes from background-like outcomes; it increases monotonically in each cell with the number of candidates, d_i; and the joint test statistic for the outcome of 2 cells is the product of the test statistics of the two cells separately.

The answer to (2) is

$$P_{s+b} = \prod_{i=1}^{M} P_{s+b}(d_i; s_i + b_i) = \prod_{i=1}^{M} \frac{e^{-(s_i+b_i)}(s_i + b_i)^{d_i}}{d_i!} \tag{60}$$

which does not increase monotonically with the $\{d_i\}$. Rather, its maximum value occurs when the $\{d_i\} = \{s_i + b_i\}$.

The answer to (3) is

$$P_b = \prod_{i=1}^{M} P_b(d_i; b_i) = \prod_{i=1}^{M} \frac{e^{-b_i} b_i^{d_i}}{d_i!} \tag{61}$$

which also does not increase monotonically with the $\{d_i\}$, but rather has a maximum value when the $\{d_i\} = \{b_i\}$.

These numbers are calculated for all possible sets of $\{d_i\}$, where each d_i is not allowed to exceed 100. Given our small numbers of expected signal, s_i, and background, b_i, in each cell, there's no need to go any higher in the d_i, because the probabilities of any larger numbers of events being observed in any given cell are vanishingly small. Once we have a Table of X, P_{s+b}, and P_b values for all significant sets of $\{d_i\}$, we do the following:

- Find all experimental outcomes (i.e., all sets of $\{d_i\}$) which give values of X less than or equal to the X for the $\{d_i\}$ which is actually observed, X_{obs}. We sum the probabilities of these experimental outcomes assuming the presence of signal+background (given by Eq. (60) above) to get a confidence level:

$$CL_{s+b} = P_{s+b}(X \leq X_{obs}). \tag{62}$$

- Again, we consider all experimental outcomes (i.e., sets of $\{d_i\}$) which give values of X less than or equal to X_{obs}. We sum the probabilities of these experimental outcomes assuming the presence of background alone (given by Eq. (61) above) to get a confidence level:

$$CL_b = P_b(X \leq X_{obs}). \tag{63}$$

- The confidence level at which the given $K^+ \to \pi^+\nu\bar{\nu}$ branching ratio is an upper limit is then given by the confidence level for signal alone, which is given by the ratio

$$CL_s = CL_{s+b}/CL_b \tag{64}$$

  In order to calculate confidence levels for lower limits of the $K^+ \to \pi^+\nu\bar{\nu}$ branching ratio, we replace the "$\leq$" signs by "$\geq$" signs in Eqs. (62) and (63).

Looping over $K^+ \to \pi^+\nu\bar{\nu}$ branching ratios between 0 and 10.5×10^{-10} gives values of CL_s between 1.0 and 0.0, which can then be used to find lower and upper limits of the $K^+ \to \pi^+\nu\bar{\nu}$ branching ratio in various confidence intervals. The central value of the $K^+ \to \pi^+\nu\bar{\nu}$ branching ratio is taken as the branching ratio which gives the maximum value of the likelihood estimator, X_{obs}. These results, for various combinations of observed 1995-7 and 1998 events, are shown in Tables 38 and 39. Note that values of $1 - CL_b$ in Table 39 are interpreted as the probabilities that background processes alone would give fewer than or equal to the number of candidates observed. The different combinations of observed events are described in Table 40. The background levels and single-event-sensitivities in the 1995-7 and 1998 boxes which were used for these calculations are shown in Tables 41 and 42.

	84% CL limits (68% CL interval)	90% CL limits (80% CL interval)	95% CL limits (90% CL interval)	99% CL limits (98% CL interval)
9597inside	[0.470,4.820]	[0.287,5.719]	[0.140,6.996]	[0.027,0.000]
9597insidelo	[0.451,4.568]	[0.273,5.424]	[0.133,6.640]	[0.026,9.338]
9597insidehi	[0.496,5.099]	[0.302,6.045]	[0.147,7.390]	[0.029,0.000]
98inside	[0.394,4.085]	[0.238,5.103]	[0.116,6.591]	[0.023,0.000]
98insidelo	[0.376,3.891]	[0.228,4.854]	[0.110,6.258]	[0.022,0.000]
98insidehi	[0.398,4.305]	[0.235,5.367]	[0.107,6.936]	[0.014,0.000]
98outside	[0.394,3.847]	[0.239,4.679]	[0.112,5.916]	[0.023,8.550]
98outside0	[0.346,3.218]	[0.223,3.945]	[0.109,5.003]	[0.023,7.415]
98total	[0.407,4.033]	[0.238,4.920]	[0.112,6.364]	[0.023,9.115]
9598inside	[0.749,3.323]	[0.560,3.886]	[0.366,4.694]	[0.132,6.452]
9598insidelo	[0.663,2.992]	[0.473,3.530]	[0.301,4.277]	[0.104,5.919]
9598insidehi	[0.775,3.509]	[0.579,4.116]	[0.378,4.932]	[0.042,6.791]
9598outside	[0.778,3.225]	[0.577,3.754]	[0.381,4.489]	[0.151,6.103]
9598outside0	[0.676,2.895]	[0.509,3.393]	[0.330,4.071]	[0.122,5.542]
9598total	[0.789,3.282]	[0.590,3.823]	[0.389,4.566]	[0.151,6.238]

Table 38: $K^+ \to \pi^+\nu\bar{\nu}$ branching ratio limits in different confidence level intervals. The various labels ("9597inside", etc.) are described in Table 40. The "insidelo" ("insidehi") label refers to the result obtained by fluctuating the expected signal and background in every cell upward (downward) by 1σ.

	BR central value (10^{-10})		
	median (50% CL)	max likelihood	1 - CLb
9597inside	1.816	1.476	0.010483
9597insidelo	1.726	1.400	0.013810
9597insidehi	1.719	1.551	0.007427
98inside	1.587	1.684	0.021526
98insidelo	1.502	1.476	0.036209
98insidehi	1.618	1.911	0.000866
98outside	1.602	1.987	0.004581
98outside0	1.312	1.060	0.039763
98total	1.632	2.270	0.001312
9598inside	1.757	1.570	0.000213
9598insidelo	1.543	1.419	0.001591
9598insidehi	1.847	1.722	0.000000
9598outside	1.753	1.722	0.000186
9598outside0	1.553	1.268	0.000186
9598total	1.778	1.835	0.000027

Table 39: $K^+ \to \pi^+\nu\bar{\nu}$ branching ratio central values, and probabilities that the observed events are due solely to background processes. The various labels ("9597inside", etc.) are described in Table 40. The "insidelo" ("insidehi") label refers to the result obtained by fluctuating the expected signal and background in every cell upward (downward) by 1σ.

label	events and dA/dN cells used to calculate BR	
9597inside	events:	1 (1995 inside-the-box event)
	cells:	2 (inside the 1995-7 box: "golden" + "non-golden")
98inside	events:	1 (1998 inside-the-box event)
	cells:	486 (inside the 1998 box)
98outside	events:	2 (1998 inside-the-box event + 1998 TD-failed event)
	cells:	7500 (inside and outside the 1998 box)
98outside0	events:	1 (1998 inside-the-box event)
	cells:	7500 (inside and outside the 1998 box)
98total	events:	3 (1998 inside-the-box event + 1998 Ntd=3.1 event + 1998 L/R amb. event)
	cells:	7500 (inside and outside the 1998 box)
9598inside	events:	2 (1995 and 1998 inside-the-box events)
	cells:	488 (2 inside the 1995-7 box, 486 inside the 1998 box)
9598outside	events:	3 (1995 and 1998 inside-the-box events + 1998 Ntd=3.1 event)
	cells:	7502 (2 inside the 1995-7 box, 7500 inside and outside the 1998 box)
9598outside0	events:	2 (1995 and 1998 inside-the-box events)
	cells:	7502 (2 inside the 1995-7 box, 7500 inside and outside the 1998 box)
9598total	events:	4 (1995 and 1998 inside-the-box events + 1998 Ntd=3.1 event + 1998 L/R amb. event)
	cells:	7502 (2 inside the 1995-7 box, 7500 inside and outside the 1998 box)

Table 40: Numbers of observed events and numbers of dA/dN cells used in various calculations of the $K^+ \to \pi^+\nu\bar{\nu}$ branching ratio.

	1995-7	1998
$K_{\pi 2}$	0.0216 ± 0.0050	$0.012 \pm 0.003^{+0.001}_{-0.003}$
$K_{\mu 2}$	0.0282 ± 0.0098	0.0092 ± 0.0067 (R-tail) 0.0245 ± 0.0155 (μ-band) $0.034 \pm 0.017^{+0.040}_{-0.017}$ (total)
BM1	0.0054 ± 0.0042	0.0039 ± 0.0012
BM2	0.0157 ± 0.0149	0.0004 ± 0.0001
CEX	0.0096 ± 0.0068	$0.0157 \pm 0.0030^{+0.0040}_{-0.0032}$
total	0.0804 ± 0.0201	$0.0657 \pm 0.0175^{+0.0402}_{-0.0176}$

Table 41: Number of background events expected in the $\pi^+\nu\bar{\nu}(1)$ signal region for the 1995-7 and 1998 data sets. The first quoted uncertainties are statistical, and any additional quoted uncertainties are systematic.

	1995-7	1998
1/s.e.s. (10^{-10})	$1.496 \pm 0.036 \pm 0.051$	$1.89 \pm 0.05 \pm 0.06$

Table 42: $K^+ \to \pi^+\nu\bar{\nu}$ single-event sensitivities of the 1995-7 and 1998 analyses. The first quoted uncertainties are statistical, and any additional quoted uncertainties are systematic.